Final Report
Regional carbon dioxide and water vapor exchange over heterogeneous terrain

Grant NAG5-11231

Larry Mahrt
Oregon State University

5 August 2005

ABSTRACT

In spite of setbacks due to forest fires, eviction after a change of landowners and unanticipated need to upgrade and replace much of the instrumentation, substantial progress has been made during the past three years, resulting in major new findings. Although most of the results are in manuscript form, three papers have been published and a fourth was recently submitted.

The data has been subjected to extensive quality control. Extra attention has been devoted to the influence of tilt rotation and flux-calculation method, particularly with respect to nocturnal fluxes.

A relatively complete canopy model (SPA) used in a data assimilation mode can successfully predict the CO2 budget and NEE by iteratively adjusting the data and model parameters (Chapter 1). To reduce uncertainty in data assimilation methods, long-term flux data are needed (both CO2 and water vapor exchange). The version of the data assimilation method that includes fluxes and state variables is suitable for application in a coupled vegetation-atmosphere regional model.

The SPA model forced by observed meteorological data indicates that in more semi-arid forests, interannual variability of precipitation exerts a strong influence on interannual variability of NEE, in contrast to moister regions (Chapter 2). These results re-enforce the need to construct a model that correctly couples water vapor exchange and CO2 exchange in canopy processes and feedbacks between vegetation and the atmosphere. We tested a way to improve the subcanopy moisture flux contribution at a boreal site that had a wetter environment (Chapter 3) and found that a representation of litter depth in the model could be used to improve subcanopy contributions to energy exchange with the atmosphere.

Existing canopy models suitable for mesoscale and regional models do not apply to sparse canopies because of the importance of daytime buoyancy-generation of mixing in the subcanopy and the controlling influence of subcanopy nocturnal inversions, which become much stronger than the stratification above the canopy (Chapter 4). A new canopy-mixing model has been developed to accommodate the important influence of subcanopy stability (Chapter 4), although further improvements are possible with data taken this year.

Many Fluxnet sites have reported loss of carbon dioxide inferentially attributed to advection and implying accumulation of CO2 somewhere downwind. The failure of towers to detect this advective accumulation suggests either fundamental observational problems or substantial bias in tower locations. The low-lying young pine site appears to accumulate carbon dioxide at night at a rate that exceeds the estimated respiration when mixing and u* are weak (Chapter 5), although more investigation is needed.

Existing techniques for estimating advection of CO2 are unreliable, partly due to the inability to estimate the mean vertical velocity with sonic anemometers and current flux correction methods (Chapter 6). Estimates of the mean vertical motion from the horizontal convergence using a small network of wind sensors appears to be more promising, but more expensive in terms of equipment and processing time. More extensive observations will be collected in summer 2005.

Previous/standard methods for calculating nocturnal fluxes with moderate and strong stability are inadequate and lead to large random fluxes errors for individual records, due partly to inadvertent inclusion of mesoscale motions that strongly contaminant the estimation of fluxes by weak turbulence. Such large errors are serious for process studies requiring carbon dioxide fluxes for individual records, but are substantially reduced when averaging fluxes over longer

periods as in calculation of annual NEE budgets. We have employed a superior method for estimating fluxes in stable conditions with a variable averaging width . Mesoscale fluxes are generally unimportant except for events and are generally not systematic or predictable. Mesoscale or regional models of our region are not able to reproduce important aspects of the diurnally varying wind field

At the writing of this final report, we are working on a short manuscript that re-examines the utility of the commonly used u* filter for eliminating records where the NEE is thought to be inadequately estimated due to incomplete mixing. We have found that the traditional flux calculation methods for nocturnal turbulence lead to some inaccuracies in the u*-filter method. In addition, u* is an incomplete indicator of the ability to assess the degree of mixing since it is influenced by pressure fluctuations that do not directly lead to mixing of scalars such as carbon dioxide. Use of the heat flux in concert with u* provides a better filter. The net result is that present methods underestimate nocturnal respiration.

PUBLICATIONS

Willliams, M., P. Schwartz, B. Law, J. Irvine and M. Kurpius, 2005: An improved analysis for forest carbon dynamics using data assimilation. Global Change Bio. **11**, 89-105.

Schwartz, P., B. Law, M. Willliams, J. Irviine, M. Kurpius and D. Moore, 2004. Climatic versus biotic constraints on carbon and water fluxes in seasonally drought-affected ponderosa pine ecosystems. Global Biogeochem. Cycles, **18**, GB4007.

Lee, Y.-H. and L. Mahrt, 2004: Comparison of heat and moisture fluxes from a modified soil-plant-atmosphere model with observations from BOREAS. J. Geophys. Res., **109**, D08103, doi: 10.1029/2003JD003949.

Lee, Y.-H. and L. Mahrt, 2005: Effect of stability on mixing in open canopies. submitted to Agric. Forest Meteorol.

Table of Contents

Chapter I

An improved analysis of forest carbon dynamics using data assimilation

Global Change Biology (2005) 11, 89–105, doi: 10.1111/j.1365-2486.2004.00891.x

An improved analysis of forest carbon dynamics using data assimilation

MATHEW WILLIAMS*, PAUL A. SCHWARZ†, BEVERLY E. LAW†, JAMES IRVINE† and MEREDITH R. KURPIUS†

School of GeoSciences and NERC Centre for Terrestrial Carbon Dynamics, Darwin Building, University of Edinburgh, Edinburgh EH9 3JU, UK, †College of Forestry, Oregon State University, Corvallis, OR 97331, USA

Abstract

There are two broad approaches to quantifying landscape C dynamics – by measuring changes in C stocks over time, or by measuring fluxes of C directly. However, these data may be patchy, and have gaps or biases. An alternative approach to generating C budgets has been to use process-based models, constructed to simulate the key processes involved in C exchange. However, the process of model building is arguably subjective, and parameters may be poorly defined. This paper demonstrates why data assimilation (DA) techniques – which combine stock and flux observations with a dynamic model – improve estimates of, and provide insights into, ecosystem carbon (C) exchanges. We use an ensemble Kalman filter (EnKF) to link a series of measurements with a simple box model of C transformations. Measurements were collected at a young ponderosa pine stand in central Oregon over a 3-year period, and include eddy flux and soil CO_2 efflux data, litterfall collections, stem surveys, root and soil cores, and leaf area index data. The simple C model is a mass balance model with nine unknown parameters, tracking changes in C storage among five pools; foliar, wood and fine root pools in vegetation, and also fresh litter and soil organic matter (SOM) plus coarse woody debris pools. We nested the EnKF within an optimization routine to generate estimates from the data of the unknown parameters and the five initial conditions for the pools. The efficacy of the DA process can be judged by comparing the probability distributions of estimates produced with the EnKF analysis vs. those produced with reduced data or model alone. Using the model alone, estimated net ecosystem exchange of C (NEE) = $-251 \pm 197\,g\,C\,m^{-2}$ over the 3 years, compared with an estimate of $-419 \pm 29\,g\,C\,m^{-2}$ when all observations were assimilated into the model. The uncertainty on daily measurements of NEE via eddy fluxes was estimated at $0.5\,g\,C\,m^{-2}\,day^{-1}$, but the uncertainty on assimilated estimates averaged $0.47\,g\,C\,m^{-2}\,day^{-1}$, and only exceeded $0.5\,g\,C\,m^{-2}\,day^{-1}$ on days where neither eddy flux nor soil efflux data were available. In generating C budgets, the assimilation process reduced the uncertainties associated with using data or model alone and the forecasts of NEE were statistically unbiased estimates. The results of the analysis emphasize the importance of time series as constraints. Occasional, rare measurements of stocks have limited use in constraining the estimates of other components of the C cycle. Long time series are particularly crucial for improving the analysis of pools with long time constants, such as SOM, woody biomass, and woody debris. Long-running forest stem surveys, and tree ring data, offer a rich resource that could be assimilated to provide an important constraint on C cycling of slow pools. For extending estimates of NEE across regions, DA can play a further important role, by assimilating remote-sensing data into the analysis of C cycles. We show, via sensitivity analysis, how assimilating an estimate of photosynthesis – which might be provided indirectly by remotely sensed data – improves the analysis of NEE.

Correspondence: Mathew Williams, fax + 44 131 662 0478,
e-mail: mat.williams@ed.ac.uk

2

estimates of ecosystem C stocks and fluxes, with reduced uncertainty compared with the original observations, or the model alone. The argument of this paper is that combining measurements and modelling through DA generates more precise estimates of C dynamics, and simultaneously highlights areas where model improvement is required.

Methods

The premise of DA is that neither models nor observations can perfectly describe a system, but an analysis that combines model and data will provide a better estimate of system dynamics than model or observations alone. DA is a process for the optimal combination of information about a system, which evolved from the engineering approaches to filtering and control theory applied in missile guidance and interception (Maybeck, 1979). DA has been applied in meteorology for forecasting (Lorenc, 1986), and extended into stream ecology (Cosby, 1984), oceanography (Eknes & Evensen, 2002), and soil science (Heuvelink & Webster, 2001) for time series analysis.

DA is the process of finding the model representation that is most consistent with observations (Lorenc, 1995). DA recognizes that there are never sufficient observations to represent the state of a system at any one time. For a detailed, complete picture, further information is required, such as knowledge of the behaviour and probable structure of the system. In DA, knowledge of system evolution in time is usually embodied in a model. In sequential assimilation, the approach we demonstrate here, the model organizes and propagates forward information from previous observations (Lorenc, 1995). When new information becomes available, the prediction, or forecast, of the model can be compared with these observations and corrected. A poor model will drift and will be frequently and heavily corrected; an effective model will require little reinitialization by observations. However, it is not simply a question of fitting the model to the new data, as the assimilation process must also conserve the information provided by the model itself and by previous observations.

The DA technique that we use here is the Kalman filter (KF) (Kalman, 1960), which has been widely used (Grewal, 1993), and, given various assumptions, has been shown to be an optimal, variance-minimizing analysis (Maybeck, 1979). The basic KF requires three assumptions: that a linear model can describe the system, and that the system and measurement noise are both white and Gaussian. Developments of the basic KF have provided means to deal with deficiencies in these assumptions (Grewal, 1993). The product of the KF is an estimate, or analysis, of the state variables that takes account of prior knowledge plus new observations to ensure that estimated errors are statistically minimized.

The KF generates a variance-minimizing analysis by combining the model forecast with the observations, weighted according to these prediction and measurement error covariances. If measurement noise is large, relatively less emphasis is placed on the current observation. If measurement noise is small, or the model estimation error is large, the corrected estimate approaches the observation. As inputs, the KF requires details on the covariances of both the model forecast and of the measurements. The error covariance of the measurements can be derived from knowledge of the accuracy of the techniques used to measure them. The error covariances for the model prediction are computed by solving an equation for the evolution in time of the error covariance matrix of the model state (Evensen, 2003).

The KF uses covariance matrices to store information on the uncertainty in the models, observations, and analysis. Storing, integrating, and inverting large covariance matrices is computationally expensive and the matrix operations required for the analysis are not always robust. Evensen (1994) suggested that, instead of storing a full covariance matrix, the same error statistics can be represented approximately using an appropriate ensemble of model states. The ensemble KF (EnKF, Evensen, 1994) uses a Markov Chain Monte Carlo method to solve the time evolution of the probability density of the model state. The probability density is represented by a large (ca. 100–1000) ensemble of model states, and these are integrated forward in time by a differential equation (i.e., the model) with a stochastic forcing term representing the model errors. Each ensemble member evolves in time according to

$$\psi_j^{k+1} = M(\psi_j^k) + dq_j^k, \tag{1}$$

where ψ is the state vector, j counts from 1 to N, where N denotes the number of model state ensemble members, k denotes time step, M is the model operator or transition matrix, and dq is the stochastic forcing representing model errors from a distribution with mean zero and covariance Q (Burgers *et al.*, 1998).

Similarly, observations are treated as random variables by generating an ensemble of observations from a distribution with the mean equal to the measured value and a covariance equal to the estimated measurement error (Burgers *et al.*, 1998). Thus, we define the new observations

$$d_j = d + \varepsilon_j, \tag{2}$$

where d are the observations, and ε are drawn from a distribution of zero mean and covariance equal to the

Keywords: carbon budget, ecosystem model, ensemble Kalman filter, net ecosystem exchange, primary production, uncertainty analysis

Received 4 February 2004; revised version received 12 July 2004; accepted 10 August 2004

Introduction

Quantifying the carbon (C) dynamics of the terrestrial biosphere is a current and major concern for earth system science. A major uncertainty concerns identifying whether regions or landscapes are sources or sinks for C. There are two broad approaches to quantifying landscape C dynamics – by measuring changes in C stocks over time, or by measuring fluxes of C directly. Stock inventories involve recording the mass of C in living biomass (leaves, stems, and roots), and in litter and soil pools, and quantifying the changes in pool sizes between sampling times (Turner *et al.*, 1995; Malhi *et al.*, 2002). The advantage of this approach is that measurements are generally cheap and simple, although labour intensive. The difficulty is that pools are spatially patchy (e.g., a large proportion of C can be in a few large tree stems), belowground pools (such as fine roots, root litter, soil C) are difficult to measure, and that monitoring is generally restricted to small plots by logistical constraints.

Direct determination of C fluxes has been revolutionized by the development of automated measurement systems of net carbon dioxide (CO_2) and water vapour exchange between land and atmosphere, via the eddy covariance technique (Baldocchi, 2003). Cuvettes and chamber measurements of soil effluxes, stem and foliage respiration, and leaf photosynthesis have enhanced the understanding of processes contributing to the eddy fluxes (Law *et al.*, 1999a, 2001a). Flux data can be generated somewhat continuously (e.g., half-hourly), and the instruments sample a 'footprint' of the surrounding landscape covering a few km^2. However, these data often have gaps, and filling these may introduce biases, and increase uncertainty. Also, night-time flux data can be biased when winds are light and intermittent (Goulden *et al.*, 1996), and complex terrain may jeopardize some of the assumptions of the approach (Finnigan *et al.*, 2003). Finally, the scale of measurement is often uncertain because the footprint varies depending on wind speed and direction (Schmid & Lloyd, 1999).

An alternative approach to generating C budgets has been to use process-based models, constructed to simulate the key processes involved in C exchange (Farquhar & von Caemmerer, 1982; Jarvis *et al.*, 1985; Parton *et al.*, 1988). The advantage of using models is that they can be extended across large spatial domains and into the future, given the relevant driving variables (Running *et al.*, 1999; White *et al.*, 2000; Rastetter *et al.*, 2003). Forecasts are possible because models incorporate a representation of the simulated system and its dynamics. Rules, such as the conservation of mass, can be enforced to guide system trajectories. The disadvantage of modelling is that the process of model construction is arguably subjective. Occam's razor – making models as simple as possible, but no simpler – is a useful guiding principle. But there is always a danger that the model's representation of the system is not accurate. Other problems include parametrization – setting the rate constants on fluxes in a compartment-flow model, for instance. Generally these parameters are unknown and have to be derived from data, somehow. There is always a danger that poorly defined parameters will be 'tuned' to give good output. When several parameters are tuned, the right answer may be generated for the wrong reason (Williams *et al.*, 2001a).

Generally, scientific papers on C budgets can be classified into stock (Phillips *et al.*, 1998), flux (Wofsy *et al.*, 1993), or model approaches (McGuire *et al.*, 1993), following the definitions given above. However, some papers do attempt to combine the methods. Ecological inventories are now being compared with micrometeorological data (Ehman *et al.*, 2002), and models are often corroborated against observations (Running, 1994; Williams *et al.*, 1996; Law *et al.*, 2003).

Models are generally parametrized with some subset of observational data, and tested against remaining data. Such tests are designed to show that the model can effectively describe the observed system by demonstrating a strong correlation, or a low mean error, between prediction and observation. This standard modelling approach assumes a primacy of the data over the model representation. But if this is the case, then the standard approach is inefficient. It would be much more worthwhile to use all the available data to improve the model and minimize confidence limits on predictions, rather than only a subset. Here we demonstrate the technique of data assimilation (DA), combining all available data with a model, to develop a full analysis of C cycling in a ponderosa pine forest.

Objectives

The objective of this paper is to demonstrate why the application of DA techniques results in improved

estimated measurement error. The analysis step of the EnKF updates each of the model state ensemble members using the following equation:

$$\psi_j^a = \psi_j^f + K_e(d_j - H\psi_j^f), \quad (3)$$

where ψ^f is the forecast state vector (i.e., the prediction) and ψ^a is the analysed estimate generated by the correction of the forecast. H is the observation operator, a matrix that relates the model state vector to the data, so that the true model state is related to the true observations by

$$d^t = H\psi^t. \quad (4)$$

K_e is the KF gain matrix, which determines the weighting applied to the correction (Burgers *et al.*, 1998).

We use the EnKF based on its ability to predict error statistics for strongly nonlinear systems and for its simplicity and numerical stability (Evensen, 2003). The analysis generated by the EnKF is a combination of the model forecast and a number of influence functions, one for each of the measurements (Allen *et al.*, 2002). These influence functions are computed from the ensemble statistics, and thus include cross-correlations between the different variables in the model. The influence functions summarize the correlations between model state variables that are determined from the ensemble of model runs. In effect, the ensemble serves as a large sensitivity analysis, quantifying how small changes in each state variable affect system dynamics. Changes to one variable resulting from a new observation are transmitted to other model variables according to the strength of these cross-correlations. This is a particularly powerful component of the EnKF – information on a single observation is transmitted to all state variables via the connections set out in the model. The FORTRAN code required to perform the EnKF is provided in Evensen (2003).

The study area

The Metolius young ponderosa pine site is located in a Research Natural Area (44°26′N, 121°34′W, elevation 1165 m) in the eastern Cascades, near Sisters, Oregon. The site was clear cut in 1978, and has regenerated naturally since then, with some recent thinning. In 2002, there were 431 trees ha^{-1}, with a mean diameter at breast height (DBH) of 11.3 cm. The understorey vegetation is sparse with patches of bitterbrush (*Purshia tridentata*) and bracken fern (*Pteridium aquilinum*), and a groundcover of strawberry (*Fragaria vesca*). The site is in a semiarid region that experiences warm, dry summers and wet, cool winters. While the flux tower samples a variable footprint, most of the remaining data were collected within a 100 m × 100 m plot located ~50 m upwind of the tower.

Flux measurements

A variety of flux data were used to generate daily estimates of specific C fluxes for use in the analysis. We made continuous eddy covariance measurements to determine half-hourly fluxes of CO_2 throughout 2000–2002 at 12 m height, ~9 m above the canopy (Law *et al.*, 1999a, b; Anthoni *et al.*, 2002). Data were screened to remove possible eddy covariance instrumentation and sampling problems (e.g., friction velocity, $u^* < 0.2\ m\ s^{-1}$), and fluxes were also rejected when unreasonably large CO_2 fluxes ($|F_c| > 25\ \mu mol\ m^{-2}\ s^{-1}$) were observed. CO_2 concentration was measured every 30 min at 1, 3, and 12 m above the ground. The buildup or release of CO_2 from within the canopy was quantified by determining the rate of change of CO_2 along the vertical profile. The total CO_2 flux was then calculated as the sum of CO_2 flux and this change in storage. Data gaps were filled based on seasonal empirical relationship with environmental variables (PAR, VPD) derived from valid flux data (Anthoni *et al.*, 1999). We generated daily net ecosystem exchange of CO_2 (NEE) data for days in which less than 25% of the 48 possible half-hour measurements were gap-filled; for the 3-year period of this study, this amounted to 684 daily NEE values.

Other periodic gas exchange measurements included foliage and stem respiration, and soil surface CO_2 fluxes (Law *et al.*, 1999b). Soil respiration was measured using six automated chambers installed in 1999 (Irvine & Law, 2002); total daily effluxes were recorded on 401 days during 2000–2002. Root contributions to soil C effluxes were measured by recording CO_2 efflux with a manual system, removing a 30 cm soil core, extracting the roots, and then measuring root CO_2 effluxes (methods in Law *et al.*, 2001a). These soil/root data were collected on 3 days in 2000 (days 153, 201, and 278), and 2 days in 2001 (115 and 227). Pine foliage respiration was determined using a temperature function fitted to 12 nights of cuvette data collected during 1999 and 2001 (Law *et al.*, 1999b); shrub foliage respiration rates were determined similarly using five nights of data (Law *et al.*, 2001a). Site-level estimates of total foliar respiration were determined from air temperature data, temperature response functions for trees and shrubs, and partitioning of estimated site leaf area index (LAI) between trees and shrubs. We estimated sapwood respiration at the *Y* site using a temperature response function developed from data at a nearby old-growth site, using sapwood volume estimates derived from tree rings at the young site

(Law *et al.*, 1999a, 2001a). Because sapwood of young trees has higher respiration rates than old trees, we likely underestimated the respiration loss from the system, but in the old forest, sapwood respiration accounted for only 10% of total ecosystem respiration (Law *et al.*, 1999a).

We limited estimates of total ecosystem respiration to those 401 days where soil measurements were available. Estimating foliar and stem respiration on these days required temperature and biomass data for each of these days. Errors will be dominated by uncertainty in the foliar biomass and sapwood volume estimates, although the latter should be relatively small. To estimate total autotrophic respiration, we combined estimates of the root fraction of soil effluxes with foliar and stem respiration measurements. Because there were no automated soil chamber data within 55 days of the root respiration measurement on day 115 in 2001, we discarded this data point. Thus, over the 3-year period there were 4 days when we were able to produce estimates of autotrophic respiration.

To provide independent estimates of gross primary production (GPP) (direct observations were lacking), we used the soil-plant-atmosphere (SPA) model (Williams *et al.*, 1996), which is based on the underlying biochemistry of carboxylation, of light interception, gaseous CO_2 exchange, and the impacts of soil moisture on stomatal conductance. The SPA model has multiple canopy layers and a 30 min time step, and has been previously parametrized and applied in ponderosa pine ecosystems (Williams *et al.*, 2001b), generating reasonable estimates of C fixation throughout the annual cycle. The SPA model requires as driving variables a daily phenology of LAI, foliar N, and root biomass, which we generated from interpolations of the limited data available over time. We used measured estimates of maximum carboxylation and electron transport rates on pine foliage at the site to parametrize the model (Law *et al.*, 2003), and time series of sap flow data to parametrize the hydraulic characteristics of the trees (Schwarz *et al.*, in press). The close correspondence of SPA predictions of daily transpiration with sap flow estimates (R^2 varied from 0.82 to 0.87 over the three years) means that we have confidence in the SPA predictions of stomatal opening (Schwarz *et al.*, 2004). The SPA model, in effect, translates sap flow observations into GPP estimates, which are then assimilated. This means that NEE data, respiration data, and GPP pseudo-observations can all be assimilated into the analysis and their consistency can be determined.

Stock measurements

We estimated LAI (one-sided LAI) from optical measurements with an LAI-2000 plant canopy analyzer (LI-COR, Lincoln, NE, USA), on a 10 m grid within the 100 m × 100 m plot. We also measured needle clumping within shoot, and clumping at scales larger than shoot to correct for these effects on LAI estimates. LAI data were collected at four times through the 3-year period of this study – once in 2000 and in 2001, and twice in 2002. Foliar mass was determined from LAI and direct measurements of C mass per unit leaf area on foliage samples.

On five 10 m radius subplots within the main plot, we recorded dimensions of all trees (stem height, and DBH, 1.37 m) and shrubs (length, width, height, and diameter at shrub base). Aboveground biomass and coarse root mass were then determined from allometric relationships derived from destructive harvest of five trees covering the range of sizes present (Law *et al.*, 2001b). Likewise, shrub biomass was determined from the destructive harvest of five to nine shrubs per species and scaled to the site by the number of shrubs per size class (Law *et al.*, 2001b). Dimensions were sampled at three times during the 3-year period of the study, once in 2000 and twice in 2002.

Litterfall production (<1 cm diameter) was determined from monthly collections of litterfall in 20 trays (0.13 m^2 each); litter was separated into foliage and woody material (Law *et al.*, 2001b). Litterfall was only collected during the latter half of each of the 3 years, when the majority of litterfall occurs, resulting in around 18 months of data over 3 years. We estimated daily litterfall for both foliage and woody material on the basis of a constant rate across the month.

Fine root (≤2 mm diameter) biomass was estimated from soil cores collected on 2 days during 2002 (days 134 and 219). On each occasion, cores were extracted from 18 different locations (six sampling points along three transects) using a 7.2 cm diameter corer. At each sampling location, samples were divided into three layers: 0–20, 20–50, and 50–100 cm depth. All samples were refrigerated until processed in the laboratory, at which time the roots were separated from the surrounding soil and sorted according to diameter class and then further separated into live and dead categories based on visual inspection of each root segment. Following the separation and sorting, the root samples were dried at 70 °C for 48 h and then weighed to measure biomass.

C storage in soil was determined from 27 soil cores to 1 m depth. Live vegetation and roots were removed and total C was determined to 1 m depth (Law *et al.*, 2003). Coarse woody debris (CWD) was measured in four 75 m line transects, and fine wood debris was recorded on four 15 m transects per subplot for all four subplots, following the protocol of Harmon & Sexton (1996). Six samples of forest floor fine litters

Table 1 Estimated errors associated with each component of the model and with each set of observations, and the total number of daily observations available

Symbol	Model error	Observational error	Number of observations	Pool/flux description
C_f	20%	10%	4	Foliar C mass
C_w	20%	10%	3	Wood C mass
C_r	20%	30%	2	Fine root C mass
C_{lit}	20%	30%	1	Fresh litter C mass
$C_{SOM/WD}$	20%	30%	1	Soil organic matter plus woody debris C mass
A_f	20%	N/A		Foliage allocation rate
A_w	20%	N/A		Wood allocation rate
A_r	20%	N/A		Fine root allocation rate
L_f	$0.5\,g\,C\,m^{-2}\,day^{-1}$	20%	18	Foliage litter production rate
L_w	$0.5\,g\,C\,m^{-2}\,day^{-1}$	20%	18	Wood litter production rate
L_r	$0.5\,g\,C\,m^{-2}\,day^{-1}$	N/A		Fine root litter production rate
D	20%	N/A		Decomposition rate of litter
G	20%	30%	1096	Gross primary production
R_{tot}		20%	401	Total respiration rate
R_a	20%	50%	4	Autotrophic respiration rate
R_{h1}	20%	N/A		Heterotrophic respiration rate of fresh litter
R_{h2}	20%	N/A		Heterotrophic respiration rate of SOM/WD
NEE	N/A	$0.5\,g\,C\,m^{-2}\,day^{-1}$	684	Net ecosystem exchange rate of C

For each time step, the predictive error on each pool and flux is drawn from a normal distribution of mean zero and with a standard deviation defined as a percentage of the mean pool or flux at that time. For modelled litter fluxes and observed net ecosystem exchange (NEE), an absolute and constant value is set instead (see text).

were collected to determine nonwoody litter mass (Law *et al.*, 2003).

Confidence limits on observations

Correct estimation of observational error is crucial to the quality of the analysis (Table 1), because the magnitude of observational errors determines to what extent the simulated fields will be corrected to match the observations. Observation error variances are best specified by knowledge of instrumental characteristics, and by comparing replicated samples. Observation error correlations are usually assumed to be zero – distinct measurements are assumed to be affected by physically independent errors. In most cases, we specify the standard deviation of model error as a percentage of the mean.

Errors in the total respiration estimates arise from the limited sampling of the automated soil chambers in space, and the use of empirical relationships to scale foliage and stem respiration in time. Because soil respiration is the largest component of ecosystem respiration, we set the coefficient of variation in total respiration in accordance with the reported values for the soil chamber data at the study site, ~ 0.2 (Irvine & Law, 2002). The uncertainty of autotrophic respiration estimates must be relatively larger than that of total respiration, because the autotrophy is estimated by a highly invasive approach, so errors are set to 50%. A detailed uncertainty analysis of modelling of GPP suggests errors of up to 30% (Williams *et al.*, 2001c), and this value was assigned to SPA model estimates of GPP. An analysis of the uncertainties in calculating daily NEE from eddy covariance (Anthoni *et al.*, 1999) suggests an error on daily estimates of 12%. The uncertainty because of potential advection at night and during early morning and late evening transition periods could not be assessed. In addition, recently discovered software error in the LI7500 flux instrument suggests that the flux estimates of NEE are biased high by about 20% (biased towards a stronger sink for CO_2; LI-COR Inc.). However, the nature of NEE (it can be positive or negative) means that defining errors by a coefficient of variation is unsuitable, so, instead, errors are set at $0.5\,g\,C\,m^{-2}\,day^{-1}$.

Errors on pool measurements (Table 1) were determined from the variation in replicated measurements. The coefficient of variation on LAI observations at the site was 10%, and stem sampling indicated a standard error on wood biomass equal to 10% of the mean (Law *et al.*, 2001b). Based on replicated soil cores, we estimate the error on fine root biomass at 30% (data not shown).

Models

Description of C dynamic model

We represent the C cycle with a simple box model of pools connected via fluxes (Fig. 1). There are five pools – C content of foliage (C_f), woody stems and coarse roots (C_w) and fine roots (C_r), and of fresh leaf and fine root litter (C_{litter}) and soil organic matter (SOM) plus WD ($C_{SOM/WD}$). There is one pseudopool, the daily accumulation of photosynthate (GPP) that is entirely utilized each day. The fluxes among pools are based on the following assumptions:

1. All C fixed during a day is either expended in autotrophic respiration or else allocated to one of three plant tissue pools – foliage, wood, or fine roots.
2. Autotrophic respiration is a fixed fraction of total photosynthetic fixation (Thornley & Cannell, 2000), and it is not directly temperature sensitive.
3. Plant allocation and litterfall are donor-controlled functions with no direct environmental influence and constant rate parameters.
4. Soil transformations are sensitive to temperature, with a Q_{10} of 2.0. Otherwise, the only environmental forcing in the C model is on GPP, via solar radiation, air temperature, and soil moisture.
5. All C losses are via mineralization; there is no dissolved loss term.

The aggregated canopy model (ACM) of photosynthesis (Williams *et al.*, 1997) provides the forecast estimate of daily C inputs to the system. The ACM is a big-leaf, daily time step model that estimates GPP as a function of LAI, foliar nitrogen, total daily irradiance, maximum and minimum daily temperature, day length, atmospheric CO_2 concentration, soil–plant water potential, and total soil–plant hydraulic resistance. The model has 10 parameters, and we use a local model calibration (see Appendix). Using measurements of leaf C mass per area (111 g C m^{-2} leaf area), estimates of LAI for the ACM are determined directly from the C_f pool. For simplicity we assume a constant value for foliar N concentration (2.7 g N m^{-2} leaf area). To characterize the changes in moisture limitation through the summer, we drive the ACM model with estimates of soil–leaf water potential difference and hydraulic resistance, both derived from a detailed ecophysiological study undertaken at the site using the SPA model (Schwarz *et al.*, 2004).

Initial conditions and rate constants

The C box model has nine unknown parameter constants (Table 2), and the initial values of the five C pools are also unknown (Table 3). To generate estimates of parameters and initial conditions, we nested the EnKF within an optimization routine. This routine varied the unknown parameters and initial conditions to find the

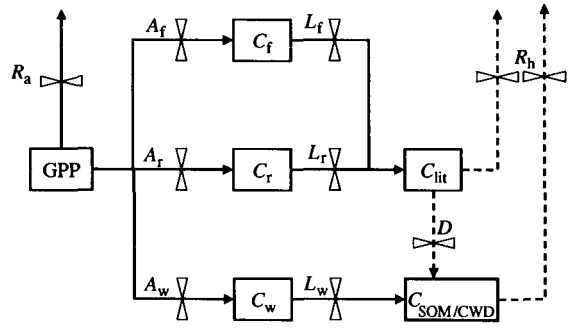

Fig. 1 C dynamic model, showing pools (boxes) and fluxes (arrows). Allocation fluxes are marked *A*, litterfall fluxes by *L*, and respiration by *R* (split between autotrophic (a) and heterotrophic (h)). *D* is a decomposition flux and GPP is gross primary production. Temperature-controlled fluxes are marked by dashed lines.

Table 2 Estimated values of the model parameters as calculated by the optimization routine

Parameter	Description	Model value	Low/high bounds
t_1	Decomposition rate constant	4.4×10^{-6}	$1 \times 10^{-6}/0.01$
t_2	Autotrophic respiration as a fraction of GPP	0.47	0.2/0.7
t_3	Fraction of NPP allocated to foliage	0.31	0.01/0.5
t_4	Fraction of NPP allocated to fine roots	0.43	0.01/0.5
t_5	Turnover rate of foliage	2.7×10^{-3}	$2 \times 10^{-4}/0.02$
t_6	Turnover rate of woody matter	2.06×10^{-6}	$2 \times 10^{-6}/0.02$
t_7	Turnover rate of fine roots	2.48×10^{-3}	$2 \times 10^{-4}/0.02$
t_8	Mineralization rate of fresh litter	2.28×10^{-2}	$5 \times 10^{-5}/0.5$
t_9	Mineralization rate of soil organic matter and woody debris	2.65×10^{-6}	$1 \times 10^{-6}/0.5$

Low and high bounds for each parameter, which define the search space are also shown.
NPP, net primary production; GPP, gross primary production.

Table 3 Estimated values of the initial conditions in each dynamic C pool

Symbol	C pool	Initial value ($g C m^{-2}$)	Low/high bounds
C_f	Foliage	58	30/70
C_w	Wood (stems and coarse roots)	770	750/900
C_r	Fine roots	102	50/300
C_{lit}	Fresh foliar and fine root litter	40	20/3000
$C_{SOM/WD}$	Soil organic matter plus woody debris	9897	6000/10 000

Low and high bounds for each pool, which define the search space.

values that minimized the sum-of-squared differences of the innovations (i.e., the difference between model forecast/prediction and observations) for all available observations (Table 1). This approach, in effect, undertakes numerous implementations of the EnKF with varied initial values and parameters, and identifies in which implementation the predictions require the minimum correction. This implementation is then assumed to have the optimal parameter set and initial conditions.

The optimization routine uses the quasi-Newton method and a finite difference gradient, UMINF, IMSL Math Library. We set specific bounds to the parameters and initial conditions to ensure realistic values (Tables 2 and 3). We used the optimized parameters in all the subsequent analyses, although we also undertook a sensitivity analysis to find how variation in parameters affected the analysis, and also affect model forecast bias.

Model error variances and ensemble size

The model errors determine how rapidly the uncertainty on the forecast of the state vector grows over time. The errors are determined by random disturbances to the system, errors in measured inputs (drivers), and the error inherent in representing a complex system as a simple model (Cosby *et al.*, 1984). The standard deviations of model error can be expressed as a fraction of mean values, and this is useful as it largely restricts the ensembles to positive, and thus meaningful, values when the mean of the particular ensemble is close to zero (e.g., GPP during winter). We set the model uncertainties to 20% (Table 1), and undertook sensitivity analyses to explore the implications of changes in these values. As an exception, we assigned a relatively large, constant error to litterfall simulations (Table 1). The modelling of litterfall uses a simple rate constant, and so does not simulate stochastic events, such as storms, or periodic events, such as leaf senescence, that cause pulses of litter. By setting a high and constant error on litterfall modelling, any available observations are used to form the majority of the analysis, and we are explicitly recognizing the weakness of our litterfall submodel.

The ensemble size of the EnKF is the number of model states that are concurrently predicted and analysed. The differences between the analyses form a statistical sample of analysis errors. We set ensemble size to 200, large enough to ensure the correct estimate of the error variances in the predicted model state (Allen *et al.*, 2002).

Results

Parameter estimates and initial conditions

The fitting process generated estimates of the nine model parameters and five initial conditions using all the available flux and stock data. The optimization estimated that 47% of GPP was respired by plants each day (Table 2), and 53% remained for net primary production (NPP). Of NPP, 31% was allocated to foliage each day, 43% to fine roots, and 25% to woody stems and coarse roots. The parametrized daily turnover rates of plant tissues (Table 2) suggest a leaf life span of 1.0 years, a fine root life span of 1.1 years, and a life span of woody materials of 1323 years. The parametrized estimate of fresh fine litter turnover, via mineralization and decomposition combined, was 0.1 years at a constant 10 °C. Parametrized turnover of SOM and WD was 1033 years, at a constant 10 °C.

The estimated initial conditions (Table 3) assigned a smaller C mass to foliage than to fine roots, but 83% of the initial vegetation C pool was allocated to woody biomass. The C mass of CWD and SOM are more than an order of magnitude greater than total plant C biomass.

Analysis of carbon ecosystem exchanges

Over the 3 years, 2000–2002, the analysis suggests a total NEE of $-419 \pm 29\,g C m^{-2}$ (i.e., a clear C sink) (Table 4). The total estimated GPP over the 3 years was $2172 \pm 18\,g C m^{-2}$, with 2002 being the most productive year (Table 4). The analysis suggests that autotrophic sources contributed to 58% of total respiration (Table 4)

Table 4 Analysis of annual C fluxes ($g C m^{-2} yr^{-1}$) for 3 years, and their sum total

Flux	2000	2001	2002	Total	SD	R^2	N	RMSE
Gross primary production	716	702	753	2172	18	0.95	1096	0.32
Total respiration	560	585	608	1753	33	0.95	401	0.23
Net ecosystem exchange	−156	−117	−145	−419	29	0.95	684	0.20
Net primary production	378	369	409	1156	20	N/A	N/A	N/A
Litter production	235	242	265	742	51	N/A	N/A	N/A
Autotrophic respiration	339	333	334	1016	18	N/A	N/A	N/A
Heterotrophic respiration	221	252	264	737	36	N/A	N/A	N/A

Standard deviation on the 3-year analysis in the ensemble of model runs (SD), the fraction of the daily variation of the observations explained by the analysis (R^2), the number of daily observations (N), and the root-mean-square error (RMSE) of the daily analysis over 3 years.

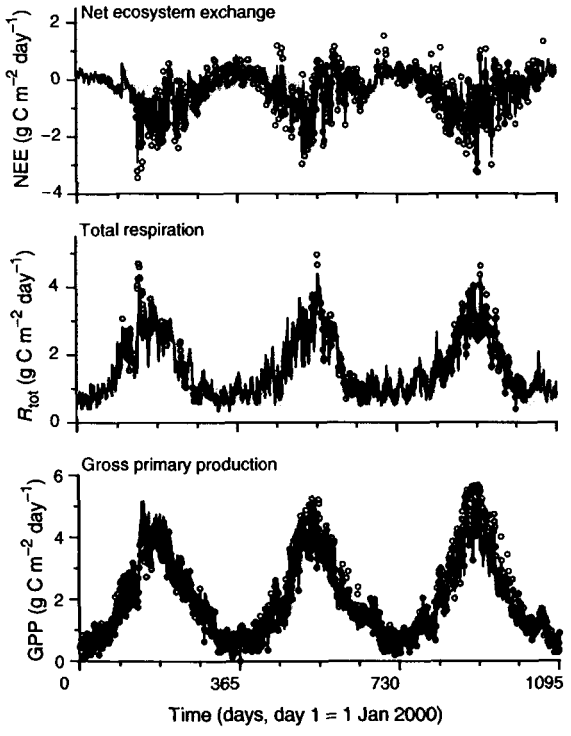

Fig. 2 Daily observations (∘) and analyses (lines) of net ecosystem exchange of CO_2 (NEE, negative flux = net ecosystem uptake), total respiration (R_{tot}), and gross primary production (GPP) for 3 years, 2000–2002. Grey vertical lines indicate the standard deviation around the mean of the ensembles, a measure of the confidence limits of the analysis.

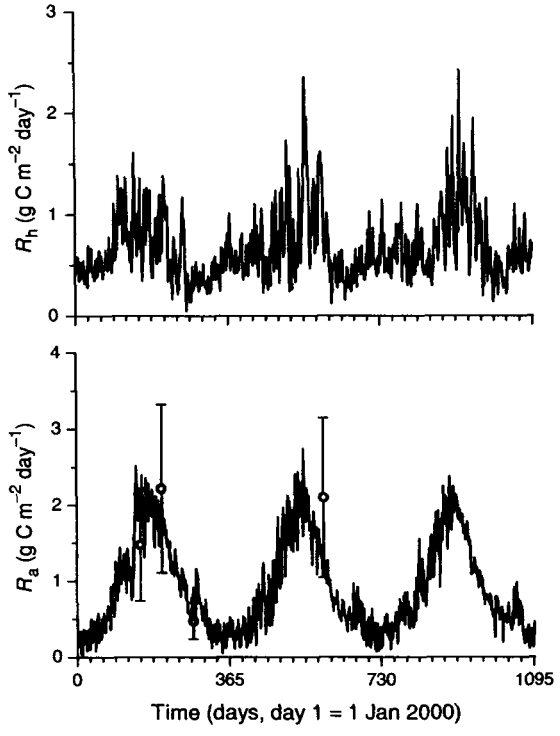

Fig. 3 Daily analysis of total heterotrophic respiration (R_h, top panel), and intermittent observations (symbols, **o**, with standard error bars) and complete analyses (lines) of autotrophic respiration (R_a, bottom panel) over 3 years, 2000–2002. Grey lines indicate the standard deviation around the mean of the ensembles.

and that litter production and heterotrophic respiration were of similar magnitude each year.

The daily analysis of NEE, GPP, and total respiration generally closely track their corresponding observations (Fig. 2) and have root-mean-square errors (RMSE) in the range 0.20–0.32 $g C m^{-2} day^{-1}$ (Table 4). Most of the NEE data lie within one standard deviation of the analysis of NEE (Fig. 2, top panel). Similarly, measurements of autotrophic respiration all lie within one standard deviation of the associated analysis (Fig. 3). Cosby *et al.* (1984) suggest tests for model adequacy (i.e., that all the component matrices of the KF, Eqns (1)–(4), are correctly specified). The tests analyse the innovation sequence specified by

$$d_j - H\psi_j^f$$

and require that the sequence has a zero mean and is serially uncorrelated. Innovations from the model forecast of NEE had a zero mean ($P>0.05$), but the innovations were serially correlated ($P<0.01$).

Analysis of C stock dynamics

The sparse nature of stock data means that the model forecast plays a greater role in the analysis, and observations correct the model for drift, particularly in slow cycling pools. The analysis of foliar C suggests a strong seasonal cycle (Fig. 4, top panel), and this is partly because of the direct link in the ACM model between foliar C (proportional to LAI) and GPP. The strong seasonal cycle in observed GPP is transmitted by the EnKF to the analysis of foliar C, and the high frequency of GPP data generates narrow confidence intervals on the analysis of foliar C, compared with intervals on the analyses of root or wood C. In three out of the four cases, the observed LAI lie within the uncertainty of the forecast. The analysis of wood C mass indicates a slow gain over 3 years. Each of the three observations of wood C lies close to or within one standard deviation of the forecast of the previous time step (Fig. 4). After an observation is assimilated, the uncertainty on the analysis is reduced, and then grows slowly with time. The analysis of fine root C suggests that mass doubles over the 3 years, and shows how reductions in uncertainty when observations are assimilated are less than for wood C (Fig. 4), because measurement uncertainty on fine roots is larger (Table 1). For fresh litter, no observations were available, but the analysis suggested an annual cycle varying between 10 and 60 g C m^{-2}, with a peak in early spring and a minimum in late summer (data not shown). For SOM and woody litter, only a single observation was available, so the analysis is primarily governed by the model forecast (data not shown). The model suggests an increase in the SOM/WD over the 3 years. However, the limited data mean that confidence limits on the analyses for the litter pools are broad.

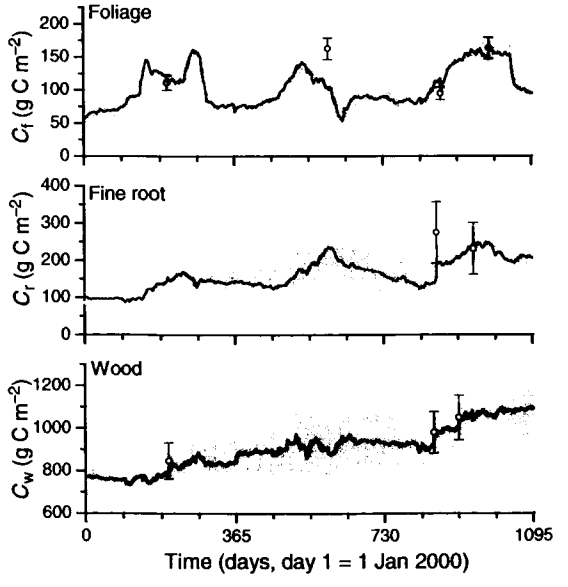

Fig. 4 Daily analysis (lines) and intermittent observations (symbols) of selected C stocks. Grey lines indicate one standard deviation around the mean of the ensembles. Errors bars (one standard error) are also given for each observation.

Analysis of litterfall

The analysis suggests that the total production of litter over 3 years is 742 g C m^{-2} (Table 4), with fine root litter dominating this flux (436 g C m^{-2}). Because the litterfall model is governed by simple turnover rates, and the uncertainty on the model was set high, the analyses of foliar and woody litterfall are dominated by the observations (Fig. 5) and have relatively broad confidence intervals (Table 4). Lacking any observations,

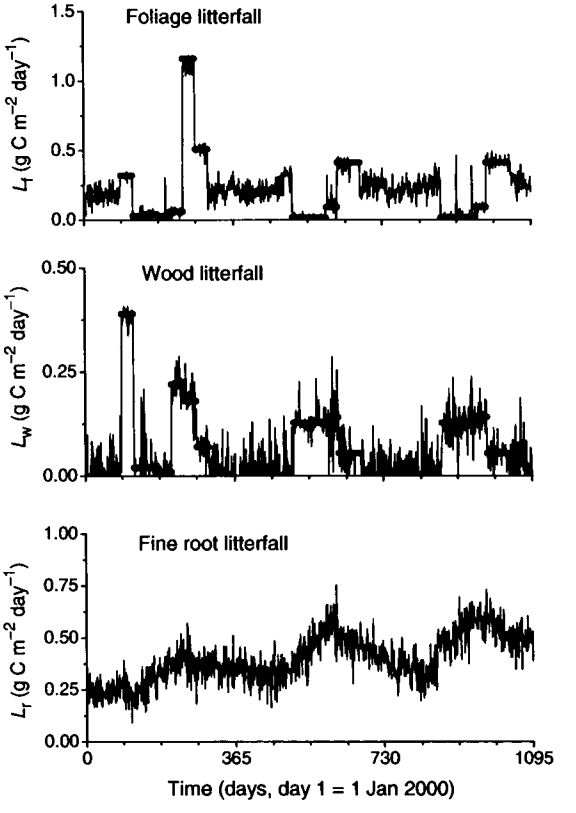

Fig. 5 Daily analysis (lines) and intermittent observations (symbols) of litterfall. For clarity, errors bars are omitted.

the analysis of fine root litter production is driven largely by the model, and is, thus, less seasonal.

Sensitivity analysis

We explored the sensitivity of the analysis to three different factors: (1) the number of time series observations assimilated; (2) variation in model error covariance; and (3) variation in model parameters.

We explored the sensitivity to the number of assimilated time series by reanalysis using the following: (a) the model without any DA, so that model forecasts are never corrected with data; (b) assimilating only GPP data into the model forecasts; and (c) assimilating GPP data and total respiration data only into the forecast (Fig. 6). Without any DA, the model forecasts were of NEE were poor (mean of the innovations was significantly different from zero, $P > 0.05$), and the total NEE prediction over 3 years was $-251 \pm 197\,\mathrm{g\,C\,m^{-2}}$. The NEE prediction was a clear underestimate of observed summer sink strength. The confidence interval of one standard deviation encompasses most of the observations (Fig. 6a), suggesting that the model error estimate is reasonable. Once GPP data were assimilated into the forecast (Fig. 6b), the analysis was significantly improved. The estimate of NEE over 3 years was $-413 \pm 107\,\mathrm{g\,C\,m^{-2}}$, and the mean forecast innovations were not significantly different from zero ($P < 0.05$). The analysis reproduced the seasonal pattern of NEE, but was poorer at predicting the high-frequency variation. When both GPP and total respiration data were assimilated (Fig. 6c), forecasts of NEE remained unbiased ($P < 0.05$), and there was a further reduction in the uncertainty on the NEE estimates (over 3 years $-472 \pm 56\,\mathrm{g\,C\,m^{-2}}$).

We made changes to the values of the model and observational error covariances to explore the sensitivity of NEE analyses to these parameters (Table 5). A halving or a doubling of model error had little impact on the analysis. An order of magnitude reduction in model error slightly increased sink strength, reduced the estimated analysis error, and almost doubled the size of the RMSE of analysed NEE vs. observed NEE (RMSE). A tripling of model error resulted in a small reduction in sink strength and the RMSE. A halving or doubling of observational error had only a minor impact on NEE predictions and on the comparison of analysed with observed NEE. Reducing observational error to 10% of the nominal value decreased sink strength by only $19\,\mathrm{g\,C\,m^{-2}}$ over 3 years. Tripling observational error increased sink strength by just $6\,\mathrm{g\,C\,m^{-2}}$ over 3 years. The sensitivity analyses suggest

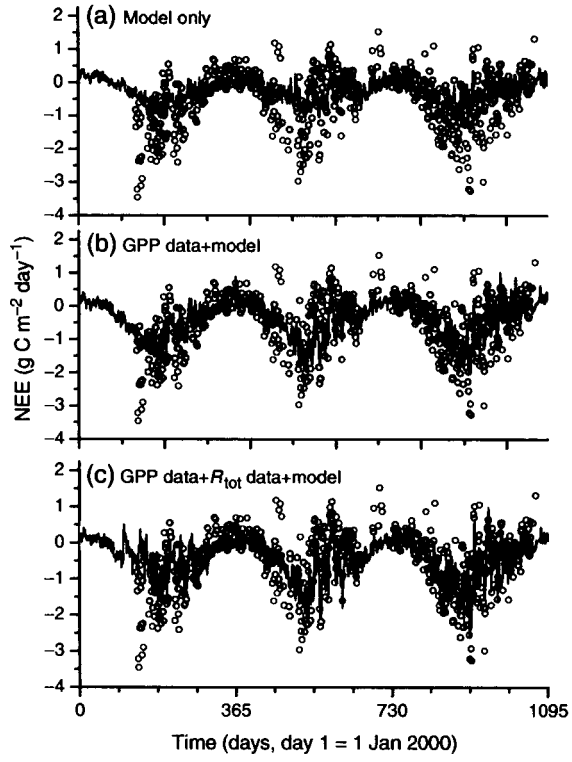

Fig. 6 Daily analysis (lines) of net ecosystem exchange (NEE) generated using (a) model only, no observations; (b) model plus gross primary production (GPP) data only; and (c) model plus GPP and total respiration data (R_{tot}). NEE observations are shown as open circles. Grey vertical lines indicate the standard deviation around the mean of the ensembles.

that there is little sensitivity in the NEE analysis to variations in estimated model and observational errors.

The nominal parameters and initial conditions used in the model (Tables 2 and 3) are not unique, and it is important to quantify how uncertainty in these values affects the analysis. We used a Monte Carlo technique to select alternative parameter sets and initial conditions, and used these in a multidimensional sensitivity analysis. For the model parameters ($N = 9$) and initial conditions ($N = 5$), we first generated, for each, distributions with means equal to the nominal values and variances equal to 20% or 50% of the mean. All parameters and initial conditions were sampled randomly from these distributions to generate 400 new, unique sets of parameters and initial conditions. We generated a new analysis with each of these unique parameter sets and initial conditions, and determined whether NEE forecasts were unbiased (innovations have a zero mean, $P > 0.05$), using the innovation test outlined in Results. Of the 400 analyses generated with

Table 5 Sensitivity analyses quantifying the impact of changes in estimated model and observation error covariances

Model error (% of nominal)	Observation error (% of nominal)	NEE (± SD)	R^2	RMSE
100	100	−419 ± 29	0.95	0.20
10	100	−440 ± 18	0.81	0.41
50	100	−423 ± 24	0.93	0.25
150	100	−417 ± 33	0.96	0.19
300	100	−414 ± 43	0.96	0.17
100	10	−400 ± 23	0.96	0.17
100	50	−414 ± 26	0.96	0.17
100	150	−422 ± 32	0.94	0.23
100	300	−425 ± 38	0.91	0.29

Changes were made to either all observational or all model errors, using a percentage adjustment to the nominal values (see Table 1). The table shows the predicted mean net ecosystem exchange (NEE) over 3 years ($g C m^{-2}$) ± 1 standard deviation of the ensemble. The R^2 and root-mean-square-error (RMSE) ($g C m^{-2}$), are for the comparison of the analysis with the NEE observations. The first case is the default analysis.

20% variance, 189 had unbiased estimates of NEE, and, for the analyses with 50% variance, 75 were valid. For the 20% variance analyses, the mean NEE was $-421 \pm 17 g C m^{-2}$, and for the 50% variance analyses the mean NEE was $-449 \pm 60 g C m^{-2}$. Inspection of the 50% variance cases at the extremes of the range of NEE estimation revealed that, while NEE forecasts were unbiased, analyses of C stocks (e.g., wood C) were poor. The tests of bias and the analyses of NEE were most sensitive to changes in the parameter t_2, the parameter that determines autotrophic respiration as a fraction of GPP.

Discussion

The quality of the analysis

The tests on the innovations show that the model forecast is an unbiased predictor of NEE, although autocorrelations in the innovations show that the errors are not white. These autocorrelations suggest that Eqns (1)–(4) are not perfectly specified, although this might be expected given the extreme simplicity of the C model we used. Iterative improvements to the model should be undertaken in the light of these statistical tests of adequacy. For the current analysis, and carefully avoiding any prediction into the future, the lack of bias in the forecasts means that the results should still provide a valid basis for discussion.

The sensitivity analysis shows how the addition of extra data sets, particularly time series of photosynthesis and ecosystem respiration, improves the estimates of NEE (compare top panel of Fig. 2 with Fig. 6). The confidence interval is approximately halved with the assimilation of each additional flux time series. With model alone the uncertainty is $196 g C m^{-2}$; the uncertainty drops to $109 g C m^{-2}$ once GPP data are assimilated, to $56 g C m^{-2}$ with the assimilation of respiration data, and to $29 g C m^{-2}$ with the assimilation of NEE data. DA improves on the estimates generated by observations alone. The uncertainty on daily measurements of NEE was estimated at $0.5 g C m^{-2} day^{-1}$, but the uncertainty on assimilated estimates average $0.47 g C m^{-2} day^{-1}$, and vary depending on whether NEE data were available for assimilation (Fig. 7). Higher uncertainties occurred on days when neither NEE nor R_{tot} observations were available for assimilation.

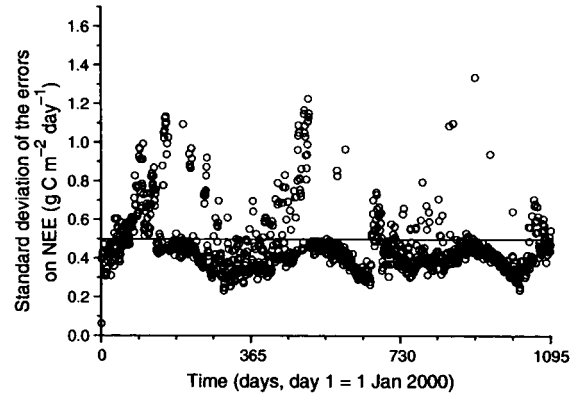

Fig. 7 Daily variation in the standard deviation around the mean of the ensembles on net ecosystem exchange (NEE). Symbols show the error on the assimilated estimate, and the line indicates the uncertainty assigned to measurement data.

The assimilation process improves the quality of the estimates of C dynamics, but the calculated uncertainty needs to take account of the full range of uncertainties in the model, which can be challenging to quantify. Our approach was to use an ensemble of analyses to explore how uncertainty in the parameters and initial conditions of the model affected the quality of the analysis. We found that, if all parameters and initial conditions were sampled from a normal distribution around their nominal values, with a variance set to 20% of the nominal values, the mean of the NEE analyses over 3 years for unbiased models ($-421 \pm 17 g C m^{-2}$) was little different from the nominal analysis ($-419 \pm 29 g C m^{-2}$). Increasing the variance to 50% broadened the confidence interval to $\pm 60 g C m^{-2}$, but this level of uncertainty in all the model parameters and initial conditions is unlikely. Overall, sensitivity analysis indicated that the uncertainty in model error

estimates, and in model parameter estimates, caused minor modifications to the analysis. This low sensitivity to model errors is important because these errors are generally poorly defined.

For simplicity, we used a daily model and assimilated daily data. However, generation of daily data was problematical, because flux data are rarely available in continuous time series. For NEE data, some hourly gap-filling was generally required, and this process necessarily introduced further uncertainty into the estimate, and potentially increased any inherent bias.

Ecological insights

The estimates of NEE from our analysis (a net sink) differ from those generated for 2001 using more conventional approaches for combining flux data (Law *et al.*, 2003), which suggested that the forest was a small net source of C. NPP estimates from this and previous studies are similar, but the analysis of heterotrophic respiration for 2001 ($184\,C\,m^{-2}\,yr^{-1}$) is less than that derived from a more direct estimate based on the same automated chamber measurements of soil respiration ($505\,C\,m^{-2}\,yr^{-1}$; Irvine & Law, 2002) and heterotrophic fractions of soil respiration plus woody detritus decomposition (detritus, $67\,C\,m^{-2}\,yr^{-1}$; total, $301\,C\,m^{-2}\,yr^{-1}$). This difference is large enough to determine whether the forest is a source or sink.

The strength of the KF approach is that it combines a mass balance model with all available data, and thus provides a more precise assessment of C exchange than pure budget approaches. However, the EnKF relies on the model being an unbiased representation of the system, and on the data being unbiased. For example, the analysis may be degraded by bias in the NEE data, because of unreliable night-time measurements. One way to remove the night-time bias of eddy flux data would be to assimilate hourly data from well-mixed periods only. This approach would also avoid the problem of using gap-filling to generate daily NEE, but would require a model complex model. DA can also identify bias, by using the model and other data sources to reveal inconsistencies in the analysis. For instance, a bias in NEE data would necessarily alter the GPP and respiration analyses. Through the interconnections in the model, the NEE bias would be transmitted into the analyses of GPP and respiration. The transmission of bias will thereby increase the differences between the analyses of GPP and respiration and the unbiased observations of these data. The analysis presented here indicates a high degree of consistency among all flux data (see R^2 estimates in Table 4), which argues against a significant bias. Systematic bias through all observations will cause greater problems, as this may conceal any inconsistencies. In any DA exercise a careful investigation for evidence of bias is vital.

The model representation of litterfall and turnover is oversimplified, and the scarcity of data relating to CWD/SOM pools and their turnover means that the analysis of these processes is problematical. The difference between the EnFK estimate of R_h and that provided by mass balance suggests that process understanding and measurement capability remain weak in this area. Time series data describing the dynamics of the soil C and WD pools must be a critical part of any C study, so that this area of uncertainty is minimized. The broad confidence limits on the modelling of litter ensured that the observations determined the values of litter fluxes in the analysis. The current model formulation is valid for diagnosis, but, until an improved litter model is incorporated, it is less suitable for prognosis.

The parameter-fitting exercise suggests an NPP/GPP ratio of 53%, slightly larger than the range suggested by a survey of multiple forest types (Waring *et al.*, 1998), where NPP/GPP = 0.47 ± 0.04. The parameterized estimates of leaf life span are reasonable (1.0 years), as the site is a mix of pine, ferns, and deciduous shrubs. The model estimate of fine root life span (1.1 years) is close to that suggested by mini-rhizotron data, 1.7 years (Law *et al.*, 2001b). However, the turnover rates of woody stems (1330 years) and SOM/WD (1033 years) are unrealistically large, as a result of the relatively long time constants on the dynamics of these pools, compared with the length of the observational period in this study, and also because of the aggrading nature of the forest stand.

A comparison of NEE estimated by fluxes against the overall change in C stocks revealed that the assimilation process can break the strict mass balance of the model forecast. The analysis suggested that C stocks increased by $1990 \pm 436\,g\,C\,m^{-2}$, a larger, more uncertain sink than suggested by summing daily NEE ($419 \pm 19\,g\,C\,m^{-2}$). The poor match arose because of a gradual, but significant accumulation of C in the SOM pool, which is poorly constrained and acts as a noise sink. We found that increasing the model confidence in the SOM prediction improved the mass balance, and reduced the accumulation of C in the SOM pool. While the mismatch identified here would be problematical over very long model runs, in this analysis the SOM pool has such a slow turnover that these mass changes have no noticeable impact on the predictions of fluxes. For prognostic applications, an improved model parametrization is required, and decadal data on woody biomass, from inventories and tree ring studies, should be assimilated to improve predictions of wood turnover. Field manipulation studies on soil processes will

provide insights and constraints into their rates of change.

Operating the model without assimilation, so that predictions are uncorrected throughout the 3 years (Fig. 6a), led to a reduced estimate of the strength of the C sink. The model-only simulations revealed a bias in NEE forecasts compared with observations. The bias largely resulted from the constant, low allocation to foliage that leads to a low GPP over the summer months. The cumulative effect becomes significant. When the model is linked to data via assimilation, the GPP and LAI observations ensure a boost of allocation to foliage in spring, increased GPP, and a stronger summer sink. To improve the prognostic capability of the simple model, a detailed leaf phenological model with temporal variation in C allocation is required. A more effective phenological model should ensure a better forecast of maximum LAI in 2001 (Fig. 4).

The future of DA in ecosystem studies

Our study has demonstrated why DA provides a powerful tool for analysing ecosystem processes, such as C cycling. Data alone are often insufficient for this task, or at least problematical, because of gaps in time series, or methodological uncertainties. Gap-filling techniques are generally highly statistical, and fail to take account of related data sets or process-based models. A conventional modelling approach to ecosystem analysis can also be problematical. Models are often tuned to fit a single data set, and that means the model provides little extra information. And if models have large numbers of parameters, there may be several different combinations of these parameters that can be tuned to match the data. Finally, many models fail to provide meaningful confidence limits around predictions.

Model DA, as we have demonstrated here with the EnKF, solves many of these problems. Assigning uncertainties to all observations determines the relative importance of data in forming the analysis. All predictions have associated confidence limits. The EnKF uses a model to generate complete time series, so gaps are eliminated. But the gap-filling makes use of all other available data at that time, and a modelled estimate embodying all prior information from the data set that is to be filled. Any increase in uncertainty for gap-filled estimates is explicitly calculated. DA makes use of all available data sets, so none are wasted in model parametrization. In our application here, we have estimated the key components of the C cycle from a combination of respiration data from chambers, NEE data from an eddy flux tower, C mass changes in vegetation and soil pools, a detailed model of photosynthesis calibrated from sap flow data, and a mass balance model of C dynamics. By attaching error estimates to all model components and data sets, the KF produces a statistically optimal estimate of NEE (and, of course, each state variable in the model). The process is an efficient and ordered way of dealing with so much data.

Arguably, the subjective component of the assimilation process is in choosing the predictive model. By keeping this model simple, and by generating the model parameters directly from the available data sets, with their associated uncertainties, we keep the model construction process transparent and reproducible. The DA process and the statistical analysis of innovations offer the potential to compare alternative models, which would improve objectivity. For example, it would be intriguing to test a model that predicted autotrophic respiration based on the kinetics of metabolic reaction, rather than indirectly through GPP. Examining the analysis to locate when and where major corrections occur provides information on model reliability. The model we have used here clearly oversimplifies seasonal dynamics in litter turnover, and foliar and root phenology (Figs 4 and 5), and improvements to the model in these areas would be worth investigating. Using more detailed models in place of the simple model used here should provide enhanced analyses. The DA framework provides a means of quantifying any such improvement.

DA offers another important service, the determination of minimum data sets required to achieve specified confidence levels. The assimilation procedure can quantify how changes in the frequency of eddy flux data, chamber data, or measures of C pools affect the confidence limits on NEE predictions, for example. The very dense data collected at the young ponderosa pine site are not easily or rapidly reproducible or extensible. But it is not currently clear to what degree measurements could be reduced while still providing a reasonable estimate of NEE. DA offers the capability to make this determination, and thus play an important role in designing efficient regional ecological monitoring systems. The results of this initial analysis emphasize the importance of time series as constraints. Occasional, rare measurements of stocks, such as SOM or CWD pools, have limited use in constraining the estimates of other components of the C cycle. Long time series are particularly crucial for improving the analysis of pools with long time constants, such as SOM, woody biomass, and WD. Long-running forest stem surveys, and tree ring data, offer a rich resource that could be assimilated to provide an important constraint on C cycling of slow pools. Detailed time series of belowground processes are more challenging to obtain. But

both on-line mass spectrometry, to determine continuously C isotopes of soil CO_2 effluxes, and tunable diode laser technology, for monitoring whole ecosystem isotopic signatures, may provide powerful sets of dynamic data that can be assimilated into models. And for extending estimates of NEE across regions, DA can play a further important role, by assimilating remote-sensing data into the analysis of C cycles. We have shown, via sensitivity analysis, how assimilating an estimate of photosynthesis – which might be provided indirectly by remotely sensed data – improves the analysis of NEE. Long-term remote-sensing data sets (from the past 30 years) could provide estimates of disturbance that could also be assimilated into a model.

Acknowledgements

This project was funded by NASA (NAG5-11 231) and DOE (Grant # FG0300ER63 014). Thanks are due to Darrin J. Moore, Osbert Sun, Steve Van Tuyl, Adam Pfleeger, and Aaron Domingues for their field and laboratory assistance. Thanks are also due to Ed Rastetter for comments on the manuscript.

References

Allen JI, Eknes M, Evensen G (2002) An Ensemble Kalman Filter with a complex marine ecosystem model: hindcasting phytoplankton in the Cretan Sea. *Annales Geophysicae*, **20**, 1–13.

Anthoni PM, Law BE, Unsworth MH (1999) Carbon and water vapor exchange of an open-canopied ponderosa pine ecosystem. *Agricultural and Forest Meteorology*, **95**, 115–168.

Anthoni PM, Unsworth MH, Law BE *et al.* (2002) Seasonal differences in carbon and water vapor exchange in young and old-growth ponderosa pine ecosystems. *Agricultural and Forest Meteorology*, **111**, 203–222.

Baldocchi DD (2003) Assessing the eddy covariance technique for evaluating carbon dioxide exchange rates of ecosystems: past, present and future. *Global Change Biology*, **9**, 479–492.

Burgers G, van Leeuwen PJ, Evensen G *et al.* (1998) On the analysis scheme in the ensemble Kalman filter. *Monthly Weather Review*, **126**, 1719–1724.

Cosby BJ (1984) Dissolved oxygen dynamics of a stream: model discrimination and estimation of parameter variability using an extended Kalman filter. *Water Science and Technology*, **16**, 561–569.

Cosby BJ, Hornberger GM, Kelly MG *et al.* (1984) Identification of photosynthesis – light models for aquatic systems. II. Application to a macrophyte dominated stream. *Ecological Modelling*, **23**, 25–51.

Ehman JL, Schmid HP, Grimmond CSB *et al.* (2002) An initial inter-comparison of micrometeorological and ecological inventory estimates of carbon exchange in a mid-latitude deciduous forest. *Global Change Biology*, **8**, 575–589.

Eknes M, Evensen G (2002) An ensemble Kalman filter with a 1-D marine ecosystem model. *Journal of Marine Science*, **36**, 75–100.

Evensen G (1994) Sequential data assimilation with a nonlinear quasi-geostrophic model using Monte Carlo methods to forecast error statistics. *Journal of Geophysical Research*, **99**, 10143–10162.

Evensen G (2003) The ensemble Kalman filter: theoretical formulation and practical implementation. *Ocean Dynamics*, **53**, 343–367.

Farquhar GD, von Caemmerer S (1982) Modelling of photosynthetic response to the environment. In: *Physiological Plant Ecology II. Encyclopedia of plant physiology, New Series*, **Vol. 12B** (eds Lange OL, Nobel PS, Osmond CB, Ziegler H), pp. 549–587. Springer-Verlag, Berlin.

Finnigan JJ, Clement R, Malhi Y *et al.* (2003) A re-evaluation of long-term flux measurement techniques – part I: averaging and coordinate rotation. *Boundary Layer Meteorology*, **107**, 1–48.

Goulden ML, Munger JW, Fan S-M *et al.* (1996) Measurements of carbon storage by long-term eddy correlation: methods and a critical evaluation of accuracy. *Global change biology*, **2**, 169–182.

Grewal MS (1993) *Kalman Filtering: Theory and Practice*. Prentice-Hall, Englewood Cliffs, NJ.

Harmon ME, Sexton J (1996) *Guidelines for measurement of woody detritus in forest ecosystems*. 20. US LTER Network Office, University of Washington, Seattle.

Heuvelink GBM, Webster R (2001) Modelling soil variation: past, present, and future. *Geoderma*, **100**, 269–301.

Irvine J, Law BE (2002) Contrasting soil respiration in young and old-growth ponderosa pine forests. *Global Change Biology*, **8**, 1183–1194.

Jarvis PG, Miranda HS, Muetzenfeldt RI (1985) Modelling canopy exchanges of water vapour and carbon dioxide in coniferous forest plantations. In: *The Forest–Atmosphere Interaction* (eds Hutchison BA, Hicks BB), pp. 521–542. D. Reidel, Dordrecht.

Kalman RE (1960) A new approach to linear filtering and prediction problems. *Transactions of the ASME – Journal of Basic Engineering*, **82**, 35–45.

Law BE, Baldocchi DD, Anthoni PM *et al.* (1999a) Below-canopy and soil CO2 fluxes in a ponderosa pine forest. *Agricultural and Forest Meteorology*, **94**, 171–188.

Law BE, Kelliher F, Baldocchi DD *et al.* (2001a) Spatial and temporal variation in respiration in a young ponderosa pine forest during summer drought. *Agricultural and Forest Meteorology*, **110**, 27–43.

Law BE, Ryan MG, Anthoni PM *et al.* (1999b) Seasonal and annual respiration of a ponderosa pine ecosystem. *Global Change Biology*, **5**, 169–182.

Law BE, Sun OJ, Campbell J *et al.* (2003) Changes in carbon storage and fluxes in a chronosequence of ponderosa pine. *Global Change Biology*, **9**, 510–524.

Law BE, Thornton P, Irvine J *et al.* (2001b) Carbon storage and fluxes in ponderosa pine forests at different developmental stages. *Global Change Biology*, **7**, 755–777.

Lorenc A (1986) Analysis methods for numerical weather prediction. *Quarterly Journal of the Royal Meteorological Society*, **112**, 1177–1194.

Lorenc AC (1995) *Atmospheric data assimilation*. Scientific Paper No. 34, Meteorological Office, Bracknell.

Malhi Y, Phillips OL, Lloyd J *et al.* (2002) An international network to monitor the structure, composition and dynamics of Amazonian forests (RAINFOR). *Journal of Vegetation Science*, **13**, 439–450.

Maybeck PS (1979) *Stochastic Models, Estimation and Control*, **Vol. 1**. Academic Press, New York.

McGuire AD, Joyce LA, Kicklighter DW *et al.* (1993) Productivity response of climax temperate forests to elevated temperature and carbon dioxide: a North American comparison between two global models. *Climatic Change*, **24**, 287–310.

Parton WJ, Stewart JWB, Cole CV *et al.* (1988) Dynamics of C, N, P and S in grassland soils: a model. *Biogeochemistry*, **5**, 109–131.

Phillips OL, Malhi Y, Higuchi N *et al.* (1998) Changes in carbon balance of tropical forests: evidence from long-term plots. *Science*, **282**, 439–442.

Rastetter EB, Aber JD, Peters DPC *et al.* (2003) Using mechanistic models to scale ecological processes across space and time. *Bioscience*, **53**, 68–76.

Running SW (1994) Testing forest – BGC ecosystem process simulations across a climatic gradient in Oregon. *Ecological Applications*, **4**, 238–247.

Running SW, Baldocchi DD, Turner DP *et al.* (1999) A global terrestrial monitoring network integrating tower fluxes, flask sampling, ecosystem modelling and EOS satellite data. *Remote Sensing of Environment*, **70**, 108–127.

Schmid HP, Lloyd CR (1999) Spatial representatives and the location bias of flux footprints over inhomogeneous areas. *Agricultural and Forest Meterology*, **93**, 195–209.

Schwarz PA, Law BE, Williams M *et al.* (2004) Climatic vs. biotic constraints on carbon and water fluxes in seasonally drought-affected ponderosa pine ecosystems. *Global Biogeochemical Cycles*, **18**, GB4006, doi: 10.1029/2004GB002227.

Thornley JHM, Cannell MGR (2000) Modelling the components of plant respiration: representation and realism. *Annals of Botany*, **85**, 55–67.

Turner DP, Koerper GJ, Harmon ME *et al.* (1995) A carbon budget for the forests of the conterminous United States. *Ecological Applications*, **5**, 421–436.

Waring RH, Landsberg JJ, Williams M *et al.* (1998) Net primary production of forests: a constant fraction of gross primary production? *Tree Physiology*, **18**, 129–134.

White MA, Thornton PE, Running SW *et al.* (2000) Parameterization and sensitivity analysis of the BIOME-BGC terrestrial ecosystem model: net primary production controls. *Earth Interactions*, **4**, 1–85.

Williams M, Bond BJ, Ryan MG *et al.* (2001a) Evaluating different soil and plant hydraulic constraints on tree function using a model and sap flow data from ponderosa pine. *Plant, Cell and Environment*, **24**, 679–690.

Williams M, Law BE, Anthoni PM *et al.* (2001b) Use of a simulation model and ecosystem flux data to examine carbon–water interactions in ponderosa pine. *Tree Physiology*, **21**, 287–298.

Williams M, Rastetter EB, Fernandes DN *et al.* (1996) Modelling the soil–plant–atmosphere continuum in a *Quercus-Acer* stand at Harvard Forest: the regulation of stomatal conductance by light, nitrogen and soil/plant hydraulic properties. *Plant, Cell and Environment*, **19**, 911–927.

Williams M, Rastetter EB, Fernandes DN *et al.* (1997) Predicting gross primary productivity in terrestrial ecosystems. *Ecological Applications*, **7**, 882–894.

Williams M, Rastetter EB, Shaver GR *et al.* (2001c) Primary production in an arctic watershed: an uncertainty analysis. *Ecological applications*, **11**, 1800–1816.

Wofsy SC, Goulden ML, Munger JW *et al.* (1993) Net exchange of CO_2 in a mid-latitude forest. *Science*, **260**, 1314–1317.

Appendix

Carbon dynamic model equations. T is a temperature-sensitive rate parameter.

Fluxes:

For G, see ACM model below

$R_a = t_2 G$

$A_f = (1-t_2)\ t_3 G$

$A_w = (1-t_2)(1-t_3-t_4)G$

$A_r = (1-t_2)t_4 G$

$L_f = t_5 C_f$

$L_w = t_6 C_w$

$L_r = t_7 C_r$

$R_{h1} = t_8 C_{lit} T$

$R_{h2} = t_9 C_{SOM} T$

$D = t_1 C_{lit} T$

Pools:

$\Delta C_f = A_f - L_f$

$\Delta C_w = A_w - L_w$

$\Delta C_r = A_r - L_r$

$\Delta C_{lit} = L_f + L_w + L_r - R_{h1} - D$

$\Delta C_{SOM/WD} = D - R_{h2}$

$T = 0.5 \times \exp(0.0693A)$ (equivalent to a curve with $Q_{10} = 2$, $T = 1$ when $A = 10$)

where A is the mean daily air temperature (°C).

ACM equations to estimate G

$$g_c = \frac{|\psi_d|^{a_{10}}}{0.5T_r + a_6 R_{tot}}, \tag{A1}$$

where ψ_d is the maximum soil–leaf water potential difference (MPa), T_r is the daily temperature range (°C), and R_{tot} is the total plant–soil hydraulic resistance (MPa m^2 s $mmol^{-1}$).

$$p = \frac{a_1 NL}{g_c} \exp(T_{max} a_8), \tag{A2}$$

where N is the average foliar N (g N m^{-2} leaf area), L is the LAI, estimated by $L = C_f/111$, T_{max} is the maximum daily temperature

$$q = a_3 - a_4, \tag{A3}$$

$$C_i = \frac{1}{2}\Big[C_a + q - p + \sqrt{(C_a + q - p)^2 - 4(C_a q - p a_3)}\Big], \quad \text{(A4)}$$

$$e_0 = \frac{a_7 L^2}{L^2 + a_9}, \quad \text{(A5)}$$

$$\delta = -0.408 \cos\left(\frac{360(D+10)}{365}\frac{\pi}{180}\right), \quad \text{(A6)}$$

where δ is the solar declination (radians) and D the day of year.

$$s = 24\cos^{-1}(-\tan(\Delta)\tan(\delta))/\pi, \quad \text{(A7)}$$

where s is the day length in hours. If $\tan(\Delta)\tan(\delta) \geq 1$ then $s = 24$, Δ the latitude (radians)

$$G = \frac{e_0 I g_c (C_a - C_i)}{e_0 I + g_c (C_a - C_i)}(a_2 s + a_5), \quad \text{(A8)}$$

where G is the GPP in $\mathrm{g\,C\,m^{-2}\,day^{-1}}$, I the irradiance ($\mathrm{MJ\,m^{-2}\,day^{-1}}$).

Parameters valid for Ponderosa pine GPP predictions in ACM model (calibrated from SPA model predictions at the young site, Schwarz *et al.*, 2004)

Parameter	Value
a_1	2.155
a_2	0.0142
a_3	217.9
a_4	0.980
a_5	0.155
a_6	2.653
a_7	4.309
a_8	0.060
a_9	1.062
a_{10}	0.0006

Chapter II

Climatic versus biotic constraints on carbon and water fluxes in seasonally drought-affected ponderosa pine ecosystems

Climatic versus biotic constraints on carbon and water fluxes in seasonally drought-affected ponderosa pine ecosystems

P. A. Schwarz,[1] B. E. Law,[1] M. Williams,[2] J. Irvine,[1] M. Kurpius,[3] and D. Moore[1]

Received 5 February 2004; revised 28 June 2004; accepted 26 July 2004; published 15 October 2004.

[1] We investigated the relative importance of climatic versus biotic controls on gross primary production (GPP) and water vapor fluxes in seasonally drought-affected ponderosa pine forests. The study was conducted in young (YS), mature (MS), and old stands (OS) over 4 years at the AmeriFlux Metolius sites. Model simulations showed that interannual variation of GPP did not follow the same trends as precipitation, and effects of climatic variation were smallest at the OS (<10%), largest at the MS (>50%), and intermediate at the YS (<20%). In the young, developing stand, interannual variation in leaf area has larger effects on fluxes than climate, although leaf area is a function of climate in that climate can interact with age-related shifts in carbon allocation and affect whole-tree hydraulic conductance. Older forests, with well-established root systems, appear to be better buffered from effects of seasonal drought and interannual climatic variation. Interannual variation of net ecosystem exchange (NEE) was also lowest at the OS, where NEE is controlled more by interannual variation of ecosystem respiration, 70% of which is from soil, than by the variation of GPP, whereas variation in GPP is the primary reason for interannual changes in NEE at the YS and MS. Across spatially heterogeneous landscapes with high frequency of younger stands resulting from natural and anthropogenic disturbances, interannual climatic variation and change in leaf area are likely to result in large interannual variation in GPP and NEE. *INDEX TERMS:* 0315 Atmospheric Composition and Structure: Biosphere/atmosphere interactions; 1615 Global Change: Biogeochemical processes (4805); 1851 Hydrology: Plant ecology; 3210 Mathematical Geophysics: Modeling; *KEYWORDS:* gross primary production, net ecosystem CO_2 exchange, interannual variation, climatic variation, drought, ponderosa pine

Citation: Schwarz, P. A., B. E. Law, M. Williams, J. Irvine, M. Kurpius, and D. Moore (2004), Climatic versus biotic constraints on carbon and water fluxes in seasonally drought-affected ponderosa pine ecosystems, *Global Biogeochem. Cycles*, *18*, GB4007, doi:10.1029/2004GB002234.

1. Introduction

[2] Temperate forests are an important component of the terrestrial carbon cycle, and it is generally believed that these forests are net sinks for atmospheric carbon [*Myneni et al.*, 2001; *Goodale et al.*, 2002]. Both climate [e.g., *Schimel et al.*, 2000, 2001; *Schaefer et al.*, 2002] and time since stand-replacing disturbance [e.g., *Turner et al.*, 1995; *Caspersen et al.*, 2000; *Law et al.*, 2001b, 2003] have been identified as important controls on the net ecosystem exchange of CO_2. Even within a single forest type, disturbances such as wildfire and timber harvesting have resulted in spatially heterogeneous landscapes in the western United States [*Cohen et al.*, 1996]. Consequently, many western landscapes are mosaics of forest stands in different stages of development (Figure 1) with a range of carbon stocks and fluxes [*Law et al.*, 2003, 2004].

[3] Detailed, process-based simulation models provide an approach for integrating knowledge of ecophysiological processes and scaling these processes to stand and ecosystem levels [*Landsberg and Gower*, 1997; *Ryan*, 2002]. Previously, we evaluated the detailed process model, Soil-Plant-Atmosphere (SPA), in an old-growth ponderosa pine forest (*Pinus ponderosa* var. ponderosa) in Central Oregon, using eddy covariance estimates of whole ecosystem gross photosynthesis (GPP) and water vapor exchange [*Law et al.*, 2000], and made subsequent modifications of the model treatment of root access to soil water [*Williams et al.*, 2001b].

[4] In this study, we took advantage of a unique collection of data collected at AmeriFlux sites in young (YS) 20-, mature (MS) 90-, and old (OS) >200-year-old stands of ponderosa pine in the Metolius River area in central Oregon (Figure 1). At these sites, in addition to stand-level data on CO_2 and water vapor exchange, the structure, physiological

[1]College of Forestry, Oregon State University, Corvallis, Oregon, USA.
[2]School of GeoSciences, University of Edinburgh, Edinburgh, UK.
[3]College of Oceanic and Atmospheric Sciences, Oregon State University, Corvallis, Oregon, USA.

0886-6236/04/2004GB002234$12.00

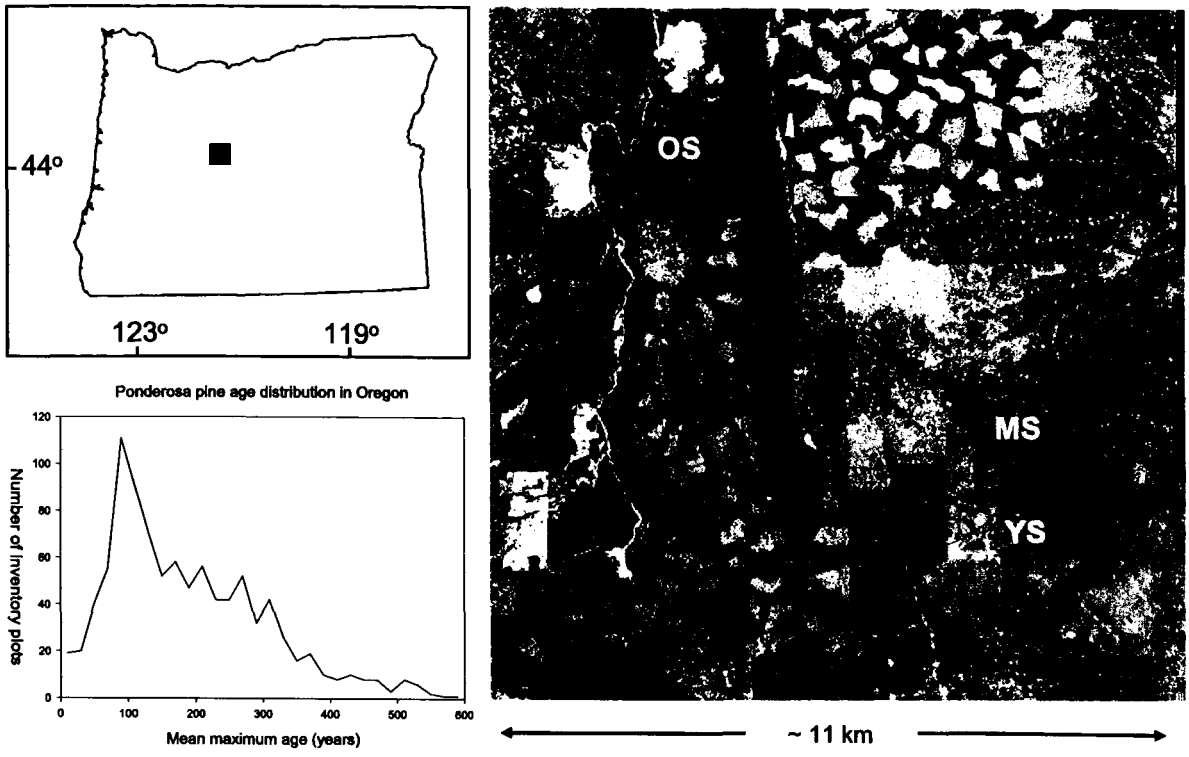

Figure 1. IKONOS image of the Metolius River area of central Oregon showing the locations of the young site (YS), mature site (MS), and old site (OS) and the spatial heterogeneity of stand structure and development stages. The distribution of stand ages is shown in the lower left.

characteristics, and soil properties were measured to explain variation in ecosystem fluxes in this semi-arid region subject to summer drought.

[5] The goal of this study was to investigate systematically the relative importance of climatic versus biotic controls on GPP and water vapor exchange over a 4-year period. Our objectives were (1) to parameterize the SPA model for three ponderosa pine stands with differing age structure and stand characteristics but otherwise growing under similar climate and environmental conditions and then to compare, for each of the three stands, simulated and field-measured estimates of tree transpiration, total latent energy (LE) fluxes, and GPP derived from eddy covariance data; (2) to carry out a sequence of simulations designed to evaluate the potential relative importance of climate, climatic variation over 4 years, and stand-related biotic factors such as leaf area and hydraulic conductance as controls on interannual variation of GPP; and (3) to examine the implications of interannual variation of GPP and ecosystem respiration on net ecosystem exchange of CO_2 (NEE). This is the first time we have used such a large amount of site-specific data to parameterize the SPA model for different age stands and for several years of different climate. We hypothesized that interannual variation of GPP at these sites was controlled primarily by climatic factors, such as precipitation, but that the magnitude of the interannual variation was determined by site-specific biotic factors.

2. Methods

2.1. Study Sites

[6] The three sites selected for this study are in the eastern Cascade Mountains near Sisters, Oregon, and are located within 8 km of one another. The Metolius sites are part of the AmeriFlux network [*Hargrove et al.*, 2003]. All three sites have an exclusive overstory of ponderosa pine trees but

Table 1. Selected Site and Stand Characteristics for the Young Site (YS), Mature Site (MS), and Old Site (OS), Which are Located in the Metolius Area of Central Oregon

	YS	MS	OS
Latitude	44.437	44.451	44.498
Longitude	−121.568	−121.558	−121.625
Elevation, m	1165	1232	895
Mean tree height, m	4.3	14.0	38.9
Stand age, years	23	89	190
Foliar nitrogen, g m^{-2}	2.1–2.9	2.1–2.9	2.0–3.6
Sand, %	54–69	59–67	63–67
Clay, %	5–11	8–11	10–11
Soil organic matter, %	2.2	3.0	3.0
Soil porosity, %	54–59	53–61	54–61

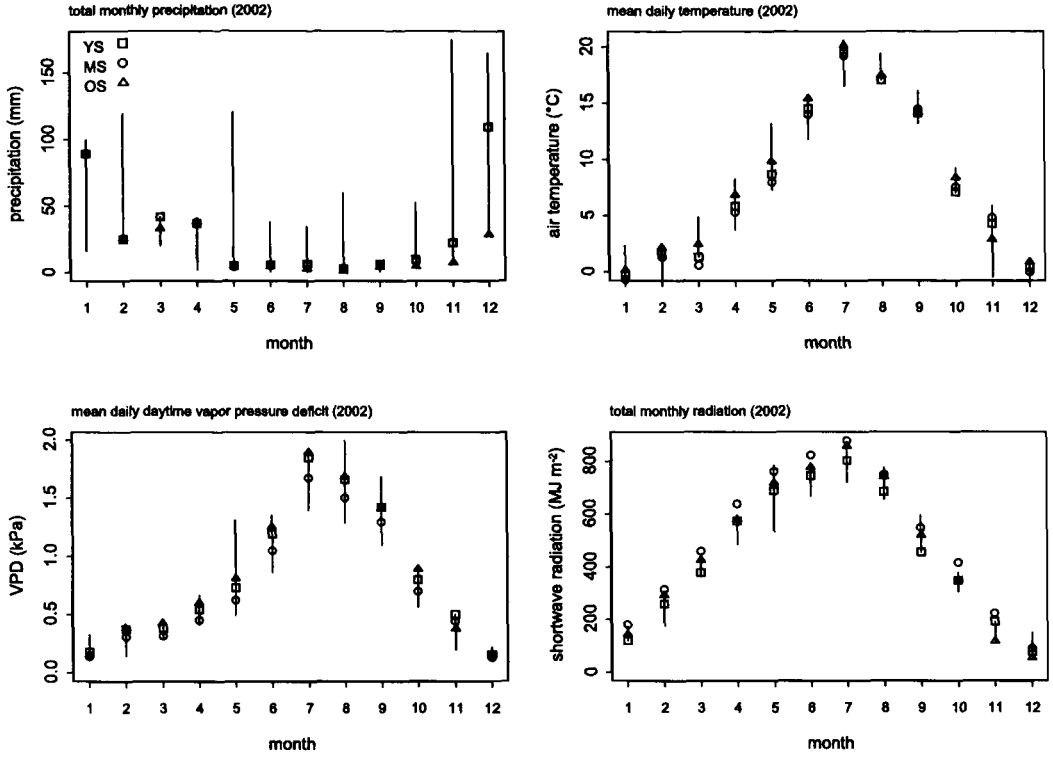

Figure 2. Monthly climate data for each site during 2002 showing seasonal trends. Vertical bars show the range of variation in the monthly values during the 4 years of the study, 1999–2002.

differ in their age structure and understory composition (Table 1). The young pine site (YS) was clear-cut in 1978 and then allowed to regenerate naturally, and understory shrubs account for approximately 40% of the site's leaf area index [*Law et al.*, 2001a]. The mature site (MS) was also clear-cut and allowed to regenerate naturally, and the average tree age is now about 90 years. The old-growth site (OS) site has never been logged and consists of old (250 years), young (60–70 years), and mixed-age patches of ponderosa pine. All three sites are nearly level, with sandy, well-drained soils with relatively little organic matter and little evidence of surface runoff (Table 1). Details regarding site conditions and soils are described by *Law et al.* [2001c, 2003].

2.2. Climatic Characteristics

[7] The three sites have similar climate typical of the semi-arid region of central Oregon: warm, dry summers and cool, wet winters. Four years of meteorological data (1999–2002) were available for the YS and OS, whereas only 1 year of data (2002) was available for the MS. The YS and MS are about 2 km apart and several hundred meters higher in elevation than the OS and are ~0.5–1.0 degrees cooler (Figure 2). At the sites, annual precipitation varies between 300 and 600 mm, with the majority falling between November and April as both rain and snow. The winter snowpack generally sustains these forests through summer drought, and rain on snow events can increase runoff to streams, limiting summer water availability to trees. During the 4 years of the study, mid-summer rainfall (June 1 to September 30) accounted for less than 15% of total annual precipitation. The 30-year mean annual precipitation, based on data from the Sisters Ranger Station (~15 km east of the study sites), is 360 mm yr^{-1}. Although precipitation patterns are highly variable from year to year, they are generally synchronous among the three sites. Other meteorological conditions are similar among the three sites and have substantially less interannual variation than precipitation.

2.3. Environmental Measurements

[8] In 2002, rates of soil water depletion across different soil horizons were estimated from calibrated, periodic time domain reflectometry (TDR) measurements in three soil pits at each site. Continuous environmental measurements at each site included meteorological conditions as well as eddy flux measurements of net carbon exchange (F_c) and whole-ecosystem water fluxes. Meteorological and micrometeorological instruments were installed at a height of 47 m at the OS (14 m above the forest canopy), 31 m at the MS (15 m above the canopy), and 12 m at the YS (9 m above the canopy). Meteorological variables measured at each site

22

consisted of half-hour means calculated from measurements at the top of the instrument tower at each of the sites and included air temperature, vapor pressure deficit, wind speed and direction, global shortwave solar radiation, photosynthetically active radiation (PAR), net radiation, and precipitation. After data screening and gap filling, these data were used to drive the SPA model.

[9] NEE and total LE fluxes were computed from the micrometeorological data using the eddy covariance technique. At the YS, eddy covariance measurements have been made continuously since the beginning of April 2000 [*Anthoni et al.*, 2002], and similar measurements have been made at the OS from 1996 until the instruments were moved to the MS at the end of 2001 [*Anthoni et al.*, 1999; *Law et al.*, 1999a, 1999b]. Full details of the instrumentation and sampling methodology for the OS and YS are described by *Anthoni et al.* [2002] and by M. R. Kurpius et al. (Annual carbon exchange along a ponderosa pine chronosequence, submitted to *Journal of Geophysical Research*, 2004) (hereinafter referred to as Kurpius et al., submitted manuscript, 2004) for the MS. All flux data were summarized and stored at half-hour intervals, screened, and filtered based on a friction velocity threshold for wind speed (described below) prior to being made available for further analysis [*Anthoni et al.*, 2002]. Data collected on rainy days were excluded from the final data set for comparison with the SPA model because of the effects of rain droplets on the sonic anemometers and open-path infrared gas analyzers.

[10] Flux-based estimates of gross primary production (GPP) were calculated as the sum of NEE and ecosystem respiration (R_e), the latter of which was calculated from nighttime net carbon exchange from the eddy covariance system and an empirical, Arrhenius-type function of temperature [*Anthoni et al.*, 2002]. The parameters of the function were estimated seasonally and thus implicitly accounted for gross changes in soil moisture. On the basis of examination of F_c versus $\underline{u}^*$ at night and comparison of R_e calculated from nighttime F_c ($R_{e.ec}$) versus R_e, calculated from summed soil, foliage, and sapwood respiration fluxes ($R_s + R_f + R_w$), we determined that local topography affects F_c under conditions of low turbulence at all three sites. We found a dependence of F_c on u^* when $u^* < 0.2$ m s^{-1} at YS and OS and $u^* < 0.35$ m s^{-1} at MS. Following the removal of F_c data below the u^* threshold and subsequent gap filling using the regression method outlined by *Falge et al.* [2001], we achieved good agreement between $R_{e.ec}$ and $R_s + R_f + R_w$ [*Anthoni et al.*, 2002, Kurpius et al., submitted manuscript, 2004]. Additional research is being conducted to further understand the role of local topography on nighttime F_c.

2.4. Structural and Physiological Measurements

[11] Leaf area index (LAI) was estimated at the YS and OS in 1999, 2001, and 2002, and at the MS in 2001 and 2002 using the optical approach described by *Law et al.* [2001a]. At each site, light transmittance was measured at 39 predetermined locations using an LAI-2000 Plant Canopy Analyzer (Li-Cor, Inc., Lincoln, Nebraska). Mean LAI was calculated and then corrected for wood interception and for clumping of shoots and needles within shoots according to methods outlined by *Law et al.* [2001a]. In 2002, LAI was measured in early spring, prior to the expansion of current year needles, and again in late summer during maximum seasonal leaf area to estimate the seasonal changes in leaf area. In 1999 and 2001, LAI was measured at the seasonal maximum. Examination of the measurements of maximum seasonal LAI suggested that leaf area at the YS was increasing by about 17% per year over the 4-year period, whereas maximum seasonal leaf area at the OS and MS were essentially constant.

[12] Fine root biomass (live roots $\leq$2 mm diameter) was measured in 2002 to a depth of 1 m by extracting soil cores at 18 locations within each site [*Law et al.*, 2003; *Sun et al.*, 2004]. In the laboratory, roots from the cores were sorted into live and dead fractions according to size class. These data were used to estimate surface root density (F_{max}), total root biomass (F_{total}), and rooting depth (D_{max}), all required parameters for the model (described below).

[13] Tree transpiration was estimated by measuring sap flux density continuously between April and November at each site using a heat dissipation technique [*Granier*, 1987]. Three years of data (2000–2002) were available for the OS and YS and one full year of data (2002) was available for the MS. Site-level estimates of tree transpiration were calculated by scaling the sap flux measurements using sapwood area relationships and stand density information. Details regarding the methodology and site-level scaling of tree transpiration are provided by *Irvine et al.* [2002].

[14] Net assimilation ($A-C_i$ curves with an LI-6400; LICOR, Lincoln, Nebraska) and foliar nitrogen were measured seasonally on shoots from trees and on shrubs. Predawn leaf water potential was also measured seasonally, and midday water potentials were made in mid-summer to estimate the critical water potential threshold required by the model.

2.5. SPA Model

[15] The soil-plant-atmosphere (SPA) model is a process model that simulates ecosystem photosynthesis, energy balance, and water transport. The model was designed for direct comparisons with eddy covariance estimates of carbon and water fluxes and has been successfully implemented in temperate [*Williams et al.*, 1996, 2001b], tropical [*Williams et al.*, 1998], and arctic ecosystems [*Williams et al.*, 2000]. The model uses 10 canopy layers to partition vertical structure of the forest canopy and uses a detailed radiative transfer scheme that calculates sunlit and shaded fractions of the foliage in each layer [*Williams et al.*, 2001b]. The model also has 20 soil layers into which fine root biomass is distributed that are used to simulate the transfer and uptake of soil water received from precipitation events. Detailed descriptions of the fundamental equations, model logic, algorithms, and the development history of the SPA model are given by *Williams et al.* [1996, 2001b].

2.6. Model Parameterization and Calibration

[16] For each site, measured net assimilation in relation to leaf internal CO_2 concentrations were used to derive estimates of maximum carboxylation (V_{cmax}) and electron transport (J_{max}) rates [*Farquhar and von Caemmerer*, 1982], which are required parameters of the model (Table 2). The

Table 2. Key Parameter Values for the Soil-Plant-Atmosphere (SPA) Model Determined From Structural and Physiological Measurements at Each of the Study Sites

Parameter Description	Units	YS	MS	OS
Critical leaf water potential prior to cavitation	MPa	−1.7	−1.7	−1.7
Daily foliar nitrogen concentration	g N m^{-2}	2.1–2.9	2.1–2.9	1.95–3.6
Maximum carboxylation capacity (V_{cmax})	μmol m^{-2} s^{-1}	48.9	48.9	48.9
Maximum electron transport rate (J_{max})	μmol m^{-2} s^{-1}	131.6	131.6	131.6
V_{cmax} per unit leaf nitrogen	μmol g N^{-1} s^{-1}	17.5	19.6	14.4
J_{max} per unit leaf nitrogen	μmol g N^{-1} s^{-1}	47.0	52.6	38.7
Daily leaf area index (LAI) in 2002	m^2 m^{-2a}	0.86–1.46	2.77–3.44	2.19–2.74
Stem-specific hydraulic conductivity	mmol m^{-1} s^{-1} MPa^{-1}	14	6	10
Root resistivity	MPa s g $mmol^{-1}$	12	3	10
Rooting depth	m	0.9–1.0	1.1	1.8
Maximum root biomass per unit volume (F_{max})	g m^{-3}	3800	1500	1400
Total fine root biomass (F_{total}), min–max	g m^{-2}	450–650	715	400

[a]Denotes m^2 half-surface area of foliage per m^2 ground.

two optical estimates of LAI during 2002 and measurements of foliar nitrogen along with observations of seasonal phenology (bud break, needle elongation, and senescence) at the sites were used to derive, via linear interpolation, daily estimates of LAI and foliar nitrogen for both the understory and the trees. Understory leaf area was assigned to the lowest canopy layer of the model, and the leaf area of the trees was distributed among the upper canopy layers. For the YS, additional years of daily LAI and foliar nitrogen were prepared in accordance with the observed rate of increase of LAI at the site.

[17] Using field measurements of fine root biomass (F_{total}) in the top meter of soil, we estimated numerically the parameters (F_{max}, D_{max}) of the exponential function that describes the vertical distribution of roots in the model [*Williams et al.*, 2001b]. The model also uses depth-specific estimates of soil texture to calculate the soil hydraulic conductivity and the energy balance at the soil surface. These data were available from previous studies for YS and OS [*Law et al.*, 2001c] and for the MS [*Law et al.*, 2003]. In addition, empirical, site-specific regressions of approximate soil water potential as a function of soil water content were estimated from TDR measurements and calculated effective soil water potential from predawn leaf water potential measurements. The remaining model parameters were as specified by *Williams et al.* [2001b].

[18] Stand hydraulic parameters were calibrated using measured estimates of daily tree transpiration derived from sap flux density data. We iteratively adjusted the values of the two parameters that determine aboveground and belowground hydraulic resistance in the simulated soil-plant-atmosphere continuum to determine the combination that produced the best agreement between simulated and measured tree transpiration. Parameter values were constrained based on field measurements of leaf specific conductance [*Irvine et al.*, 2004], and final values were selected based on the criteria of minimum root mean square error (RMSE) and highest coefficient of determination (R^2) calculated from regressions with measured data. In addition, we calculated relative error rates (in comparison with mean measured fluxes) and partitioned the mean squared error (MSE) into systematic and unsystematic fractions as recommended by *Wallach and Goffinet* [1987, 1989] as cited by *Kramer et al.* [2002].

[19] In summary, sap flux data from each site were used to parameterize the SPA model hydraulics, and a single set of parameters was determined for each site. Eddy flux data were used to evaluate model predictions of total LE and GPP. Three years of sap flux data and eddy flux data (2000–2002) were available for the YS. For the OS, 3 years of sap flux data (2000–2002) were available, but only 2 years of eddy flux data (2000–2001). For the MS, the model was parameterized and evaluated against sap flux and eddy flux data for 2002.

2.7. Simulations

[20] To separate relative effects of climatic variation from changes in stand structure, for example, LAI and physiology (plant water relations), we used the model to perform a series of simulations as computational experiments. A base case and three experimental scenarios were simulated (Table 3). Each scenario was applied to the three sites using the 4 years of site-specific climate data (1999–2002), and all 4 years were simulated consecutively for a total of 1461 days. These 4 years represented a 150–200% range of variation of winter precipitation (November–April), 300–600% variation of summer precipitation (May–October), and over 50% variation of annual precipitation (Figure 2). Other climatic vari-

Table 3. Summary Descriptions of the Four Simulation Scenarios That Investigate Potential Effects of Climatic Variation Versus Stand Development and Structure on Forest Carbon and Water Fluxes[a]

Scenario	Description	Daily Leaf Area Phenology	Model Parameters	Soil Moisture Limitation
1	base case	site-specific leaf area	site-specific parameters	yes
2	no drought stress	site-specific leaf area	site-specific parameters	no
3	identical LAI and aboveground structure	MS leaf area	MS parameters	yes
4	identical aboveground structure and no drought stress	MS leaf area	MS parameters	no

[a]See section 2.7.

24

ables showed a range of variation over the 4 years of about 10–20%. Given the close geographic proximity of the YS and MS (~2 km) and the similarity of the climate between the two sites, the YS climate data for 1999–2001 (in addition to the MS 2002 data) were used for MS simulations.

2.7.1. Effects of Climate and Climatic Variation on Carbon and Water Fluxes

[21] The base case (or first) scenario simulated the effects of interannual variation of climate over the 4 years at each of the three sites using site-specific LAI, stand structure, and hydraulic parameters. The second scenario (no drought stress) simulated the removal of soil moisture limitations by resetting soil moisture levels to field capacity (~0.3 m^3 m^{-3}) while using the same leaf area, stand structure, and hydraulic parameters as the base case scenario. For the YS, these two scenarios were simulated assuming both constant LAI (using the 2002 LAI data) and annually increasing LAI to investigate the added effects of annually increasing leaf area on simulated carbon and water fluxes during the 4 years. Differences between the base case and no drought stress scenarios were used to distinguish the effects of soil moisture limitations (i.e., precipitation) from other climatic effects on carbon and water fluxes.

2.7.2. Effects of Aboveground Stand Structure and Canopy Physiology on Fluxes

[22] Scenario 3 (identical aboveground stand structure and physiology) simulated the effects of replacing the entire aboveground structure of the YS and OS with the aboveground structure (LAI, tree heights, vertical distribution of LAI) and physiology (canopy hydraulic conductance) of the MS. Differences between the base case (scenario 1) and scenario 3 were used to help determine the effects of aboveground stand structure and canopy physiology on carbon and water fluxes. Variations of this scenario were used to distinguish the effects of LAI from other components of stand structure and physiology.

2.7.3. Effects of Root Density and Rooting Depth on Fluxes

[23] Scenario 4 (identical aboveground stand structure and no drought stress) was identical to scenario 3 except that soil moisture limitations were removed (like scenario 2). Under this scenario, virtually unlimited access to soil water effectively minimizes differences in the rooting characteristics among the sites. Thus, differences between scenario 3 and scenario 4 were used to assess effects of differences in soil properties and differences in root density and distribution among the sites.

[24] The scenarios are summarized in Table 3. For scenarios 2–4, the MS was selected as the reference site because it represents the upper limit of LAI and productivity among stands in the region [*Law et al.*, 2003]. Consequently, comparisons with the MS under these scenarios show the maximum potential effect of these simulated changes in stand structure on carbon uptake and water vapor exchange.

2.8. Annual Estimates of NEE

[25] Annual estimates of NEE were calculated as the difference between total annual GPP (from the simulations) and annual estimates of R_e. Estimates of R_e for each site were calculated as the sum of R_s, determined from automated chamber measurements [*Irvine and Law*, 2002], and empirically modeled estimates of R_f and R_w [*Law et al.*, 1999b], plus site-specific estimates of mean annual fine and coarse woody debris decomposition [*Law et al.*, 2003]. Four years of sapwood volume data were used to calculate R_w at the YS. In the absence of similar data for the MS and OS, R_w was assumed constant over the 4 years of the study. Previous studies at the YS and OS indicate that R_w is small fraction of R_e (≤6%) [*Law et al.*, 1999b, 2001c], and this assumption had little impact on the annual estimates of R_e.

3. Results and Discussion

3.1. Model Parameterization

[26] We were able to identify a single pair of hydraulic parameters for each site that was held constant during the multiyear simulations. In contrast, site-specific LAI and total foliar nitrogen varied seasonally. On the basis of the 2002 measurements, total (overstory plus understory) LAI ranged from 0.86 to 1.46 m^2 half-surface area of foliage per m^2 ground at the YS, 2.19 to 2.74 m^2 m^{-2} at the OS, and 2.77 to 3.44 m^2 m^{-2} at the MS (Table 2). The parameterizations indicated that rooting was deepest at the OS (1.8 m) and shallowest at the YS (1.0 m). However, fine root biomass in the top meter of soil was highest at the MS and lowest at the OS. Rooting depth and root biomass were assumed constant at the MS and OS during the simulations, but at the YS, because of its stage of development, fine root biomass increased over the 4 years from 450 to 650 g m^{-2}, and rooting depth increased from 0.9 to 1.0 m. In terms of water transport, the most conductive stems were at the YS, and the least conductive stems were at the MS. The most resistive roots were at the YS, and the least resistive were at the MS. Leaf specific conductance, which combines the stem and root hydraulic parameters, at the top of the forest canopy was 1.70, 0.28, and 0.20 mmol s^{-1} m^{-2} MPa^{-1} at the YS, MS, and OS, respectively.

3.2. Model Comparison With Sap Flux Measurements

[27] Simulations of the YS, MS, and OS indicate that the SPA model can accurately predict seasonal patterns of tree transpiration estimated from measured sap flux using simple parameterizations (Table 4). The SPA model explained 76% to 87% of the daily variation of tree transpiration for years 2000 through 2002 across the three sites. RMSE varied little (0.11–0.20 mm d^{-1}) among the seven site-year simulations, suggesting that it may be difficult to resolve model-data discrepancies of less than about 0.1 mm d^{-1}. The average relative error (calculated as RMSE/mean daily measured sap flux) between simulated and measured transpiration was 24% (±0.14 mm d^{-1}). Furthermore, after partitioning the mean square error into systematic and unsystematic fractions, on average more than half (57%) of the model-measurement discrepancies can be attributed to unsystematic (or random) errors, suggesting that the model is accurately capturing the daily dynamics of tree transpiration (Figure 3).

3.3. Model Comparison With Latent Energy Fluxes

[28] Comparisons between simulations of total daily latent energy (LE) fluxes at each of the three sites and

Table 4. Comparisons of Daily Estimates of Simulated Tree Transpiration, Total Latent Energy Exchange (Total LE), and Gross Primary Production (GPP) With Measured Values Derived From Sap Flow and Eddy Covariance Measurements[a]

		Tree Transpiration				Total LE				GPP			
Site	Year	R^2	RMSE, mm d^{-1}	Rel. Error, %	Bias, %	R^2	RMSE, mm d^{-1}	Rel. Error, %	Bias, %	R^2	RMSE, g C m^{-2} d^{-1}	Rel. Error, %	Bias, %
YS	2000	0.82	0.14	28	17	0.79	0.36	30	42	0.90	0.73	24	85
	2001	0.87	0.13	27	13	0.81	0.32	32	17	0.86	0.56	23	48
	2002	0.86	0.20	30	48	0.80	0.38	33	24	0.90	0.49	17	19
	Avg	0.85	0.16	28	26	0.80	0.35	32	28	0.89	0.59	21	51
MS	2002	0.84	0.15	19	32	0.50	0.62	50	67	0.46	0.74	12	20
OS	2000	0.85	0.11	19	54	0.62	0.51	36	81	0.40	0.56	13	38
	2001	0.87	0.11	23	65	0.64	0.36	31	49	0.67	1.13	22	91
	2002	0.76	0.14	22	67	-	-	-	-	-	-	-	-
	Avg	0.83	0.12	21	62	0.63	0.44	34	65	0.53	0.84	18	64
Overall Avg		0.84	0.14	24	43	0.70	0.42	35	47	0.70	0.70	19	52

[a]RMSE is root mean square error, and the relative error (Rel. Error) is the RMSE as a percentage of the daily mean value determined from field measurements. Bias is the fraction of the mean square error that can be attributed to systematic (as opposed to random) deviations from the measured values. Dashes indicate no data available.

eddy covariance measurements indicate that the model was able to explain 50% (MS) to 81% (YS) of the daily variation of total measured LE among the six site-year combinations with eddy flux data (Table 4). The average relative error between the model and the flux measurements was about 35%, and the overall average RMSE was ±0.42 mm d^{-1}. Relative error rates as well as the proportion of the error attributed to systematic differences were smallest at the YS and higher at the MS and OS. Eddy covariance-based estimates of integrated total LE at the YS and MS during non-rain days were higher than simulated estimates (Table 5), although the simulated estimates were within the uncertainty limits for the YS. Because tree transpiration was the largest component of total LE (>50% at each site), the higher relative error rates compared with tree transpiration were most likely associated with other components of total LE such as shrub transpiration, wet canopy evaporation, or soil evaporation.

[29] Because the same model hydraulic parameters were applied to both the understory and overstory canopy layers, we would have expected larger discrepancies between the model and field measurements at the YS (understory LAI 40% of total). However, relative error rates (or discrepancies) for total LE at the YS were smaller than the corresponding relative error rates at either the OS or MS, contrary to our expectations (Table 4). Thus it is unlikely that shrub transpiration, alone, could explain the discrepancies in simulated versus measured total LE, especially at the OS and MS.

[30] Evaporation from soil surfaces could also be contributing to the discrepancies between the flux measure-

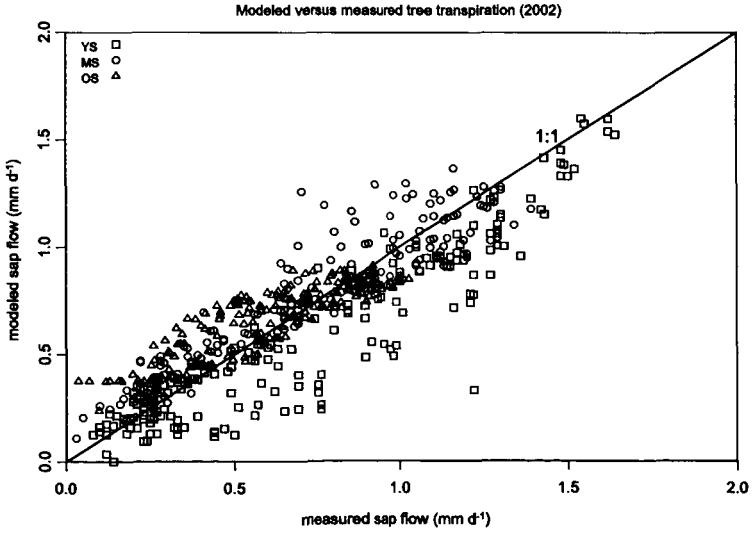

Figure 3. Simulated versus measured tree transpiration during 2002, the only year with measured sap flux data for each site. The 1:1 line indicates that the simulated values are relatively unbiased.

Table 5. Integrated Water Vapor Fluxes and Annual Carbon Fluxes Derived Eddy Covariance Measurements and Simulations[a]

	LE,[b] mm		GPP (g C m^{-2} yr^{-1})		NEE,[c] g C m^{-2} yr^{-1}	
Site (Year)	Measured	Modeled	Measured	Modeled	Measured	Modeled
YS (2001)	224 ± 36	199	704 ± 168	674	45 ± 6	48
YS (2002)	269 ± 43	234	809 ± 193	828	113 ± 15	192
MS (2002)	296 ± 51	241	1360 ± 333	1539	371 ± 53	516

[a]For the OS, insufficient eddy flux data were available for 2001 to estimate annual fluxes, and no eddy flux data were available for 2002.
[b]Rain days were excluded from the integrated estimates of LE because of the effects of rain droplets on the eddy covariance instrumentation. Thus the LE estimates are not true annual estimates.
[c]Modeled estimates of NEE are determined from simulated estimates of GPP plus empirical estimates of ecosystem respiration derived from measurements of soil CO_2 efflux, foliage respiration, sapwood respiration, and woody litter decomposition (see section 2.8).

ments and the model. *Williams et al.* [2001b] reported good agreement between the SPA model and measurements of soil evaporation at the OS during August 1997. In the current study, however, we utilized field measurements of tree transpiration and expanded the number of sites and the number of years of data used for the model-measurement comparison. The largest discrepancies between the eddy covariance-based estimates of total LE and the model occurred usually during June and July, when the model underestimated total LE by ~1 mm d^{-1} or >40% at the MS. Simulated soil evaporation at the MS during the summer months was relatively constant and averaged ~0.2–0.3 mm d^{-1}. Although simulated soil evaporation compared favorably with LE fluxes measured by a subcanopy eddy covariance system installed at the MS during August–September 2002, no measurements were available from earlier in the summer when measurement-model discrepancies were larger. Thus, to further improve the model's capability to simulate soil evaporation at these sites, additional measurements of soil evaporation will be needed that span the growing season.

[31] Another possible source for discrepancies between simulated and measured total LE is differences in the sampling footprint used to calculate tree transpiration from sap flow measurements and the sampling footprint for the eddy covariance measurements, even though a rigorous approach was used to scale the sap flow measurements to site [*Irvine et al.*, 2002]. Scaled estimates of transpiration are sensitive to the measured basal area and sapwood area relationships in the field plots, and although the field plots were chosen to be representative of each site, structural characteristics of the plots may not match those of the area being integrated by the eddy covariance technique. Other recent studies have also reported difficulties in reconciling sap flow measurements with latent energy flux measurements using the eddy covariance technique [*Wilson et al.*, 2001; *Meiresonne et al.*, 2003], and we submit that the footprint issue requires further investigation.

3.4. Model Comparison With GPP Estimates Derived From Eddy Flux Data

[32] The average relative error between modeled and measured estimates of daily GPP among the three sites was 19%, and RMSE varied by about a factor of 2 from 0.49 g C m^{-2} d^{-1} to 1.13 g C m^{-2} d^{-1} (Table 4). Simulations of the YS, though, explained considerably more day-to-day variation in GPP than at either the MS or OS, and roughly half of the mean square error could be attributed to systematic differences between the modeled and measured values. Although the overall relative error between the eddy covariance-based estimates and simulated estimates of GPP was generally good (19%, Table 4), the lower R^2 values and higher bias indicate that the model misses some of the day-to-day variation associated with the carbon dynamics of the sites. In general, though, as time series data are aggregated over longer periods, discrepancies between predicted and measured values are substantially reduced because differences due to unsystematic (or random) variation tend to cancel one another [*Goulden et al.*, 1996; *Moncrieff et al.*, 1996].

[33] Annual estimates of simulated GPP were well within the uncertainty limits of the flux measurements (Table 5). Simulated estimates were higher than the measured estimates in 2002 but lower than the measured estimate for the YS in 2001. Thus, although the model may be underestimating total LE at the study sites, the model appears suitable for simulating seasonal and annual responses of transpiration and GPP to changes in climate and climatic variation.

3.5. Simulation Scenarios

3.5.1. Effects of Climate and Climatic Variation

[34] Precipitation at the sites varied ~55% over the 4 years: 1999 was the wettest year followed by 2001, 2000, and 2002 was the driest year. When LAI at the YS was held constant over the 4 years to separate effects of climatic variation from changes in leaf area, GPP was highest during 1999 and lowest in 2002, following interannual trends in total annual precipitation. At the MS and OS, however, annual GPP was highest in 1999 and lowest in 2001, which mirrored the interannual pattern of soil water recharge from winter precipitation.

[35] Despite similar climate across the three sites, the base case simulations (scenario 1) showed that interannual variation of GPP differed by site in response to climatic variation over the 4-year period (Table 6, Figure 4, base case). Annual GPP in the base case simulations varied <10% per year at the OS to >50% per year at the MS across the 4 years, implying that interannual variation of GPP among the 4 years was highest at the MS and lowest at the OS. Under the base case scenario with constant LAI, interannual variation of GPP at the YS across the 4 years was 19%. The interannual variation of GPP at the MS was similar to the interannual variation of precipitation, and the interannual variation of GPP at the YS was comparable to that of the MS when simulations increased the LAI at the

Table 6. Annual Summaries of the Simulated Carbon and Water Vapor Fluxes From the Simulations[a]

Scenario		Total LE, mm yr^{-1}			Tree Transpiration, mm yr^{-1}			GPP, g C m^{-2} y^{-1}		
		YS	MS	OS	YS	MS	OS	YS	MS	OS
Base case	mean	309 | 279	304	299	136 | 115	171	161	801 | 679	1401	1098
	std dev	31 | 17	37	13	13 | 16	34	9	55 | 93	219	30
	percent variation	33 | 17	40	13	28 | 38	77	17	19 | 45	53	7
No drought stress	mean	434 | 385	442	327	241 | 204	309	187	1013 | 846	1886	1168
	std dev	18 | 32	20	14	4 | 32	11	6	8 | 132	49	15
	percent variation	11 | 17	12	11	5 | 52	10	9	2 | 55	7	3
	percent change	40 | −11	45	9	78 | −15	80	16	26 | −17	35	6
Identical LAI and aboveground structure	mean	305	304	369	191	171	227	1413	1401	1648
	std dev	25	37	20	23	34	22	100	219	83
	percent variation	23	40	16	37	77	31	21	53	14
	percent change	−1	-	23	40	-	42	76	-	50
Identical aboveground structure and no drought stress	mean	392	442	438	283	309	289	1686	1886	1816
	std dev	20	20	10	9	11	10	24	49	30
	percent variation	14	12	5	9	10	10	4	7	4
	percent change	27	45	46	108	80	27	110	35	65

Percent variation describes the relative range of variation over the four simulated years, 1999–2002.
[a]Percent change describes the relative difference between a given scenario and the base case scenario. Dashes indicate not applicable. The vertical bars for the YS separate the results for the constant LAI simulations on the left from the annually adjusted LAI simulations on the right.

YS to match the measured LAI. In contrast, the interannual variation of GPP at the OS was much less than the interannual variation of precipitation. Interchanging climate driver data among the sites had little effect on mean annual GPP at either the OS or MS and reduced mean GPP at the YS by no more than 5%.

[36] Seasonally, interannual variation of GPP at the MS was most pronounced during July–September, while variation at the YS was most noticeable earlier during May–July (Figure 4, base case). At the OS, the interannual variation appeared uniformly distributed throughout the year.

[37] Base case simulations (scenario 1) of tree transpiration and total LE showed noticeably more interannual variation than GPP because of larger interannual variation in LE and precipitation earlier in the year (Table 6, Figure 5, base case). Among-site differences in transpiration were substantially smaller than the corresponding differences in GPP (Table 6): about 25% for mean annual tree transpiration (assuming constant LAI at the YS) and less than 5% for mean annual total LE.

[38] Increased soil water availability at the MS and YS, under scenario 2 (no drought stress), resulted in large increases in mean annual tree transpiration of >75% and increased total annual LE by ≥40% (Table 6). Moreover, the increased tree transpiration and total LE were most evident during the period of otherwise maximum drought stress (Figure 5). The simulations suggest that increased soil moisture from precipitation during the growing season would probably have a greater effect on carbon and water fluxes in these forests than increased precipitation at other times of the year [*Goldstein et al.*, 2000; *Xu and Baldocchi*, 2004]. Mean simulated tree transpiration and total LE at the OS, on the other hand, increased only by about 16% and 9%, respectively, reflecting a smaller effect of increased soil moisture in the upper soil layers at this site. These results are consistent with those of *Irvine et al.* [2004], who determined that approximately 79% of water used during the summer months of 2002 at the YS was extracted from a depth of 80 cm or less, whereas almost half (47%) of the water extracted at the OS during the same months came from below 80 cm depth.

[39] Simulations that increased soil water availability and eliminated seasonal drought stress (scenario 2) increased mean annual GPP at the YS and MS by 26% and 35%, respectively (Table 6). Furthermore, simulations clearly show that the increased GPP occurs during the late summer and early fall months when drought stress would normally be experienced (Figure 4). In contrast, the simulated response of the OS was small: Mean annual GPP increased by 6%, and the seasonal pattern of GPP was similar to that of the base case scenario. Therefore the benefits of increased soil water availability had a much bigger effect at the YS and MS than at the OS.

[40] Increased soil water availability subsequently reduced interannual variation of GPP to similarly low levels at all three sites (2–7%, Table 6). Hence the simulations confirm that interannual variation of precipitation is an important causal factor controlling GPP and probably accounts for most of the interannual variability of GPP in these forests. Under scenario 2, though, after removing the variation of rainfall, the dominant sources of interannual climatic variation were radiation inputs and temperature, and the interannual variation of radiation probably had a larger effect on the interannual variation of GPP at the MS (7%) because it had highest LAI among the three sites. In contrast, the YS experienced the least interannual variation of GPP (2%, assuming constant LAI), and although the interannual variation of solar radiation was higher at the YS compared to the OS, even during the year with the lowest solar radiation inputs (2001), there was sufficient radiation to effectively saturate the lower LAI canopy of the YS.

[41] Other studies reached similar conclusions regarding effects of interannual variation of climate on carbon uptake in forests. For example, *Barford et al.* [2001], in a 9-year study of eddy covariance data from a deciduous hardwoods stand in Massachusetts, attributed interannual variation of carbon uptake and net carbon exchange to the variation of climatic characteristics such as cloudiness and low temper-

28

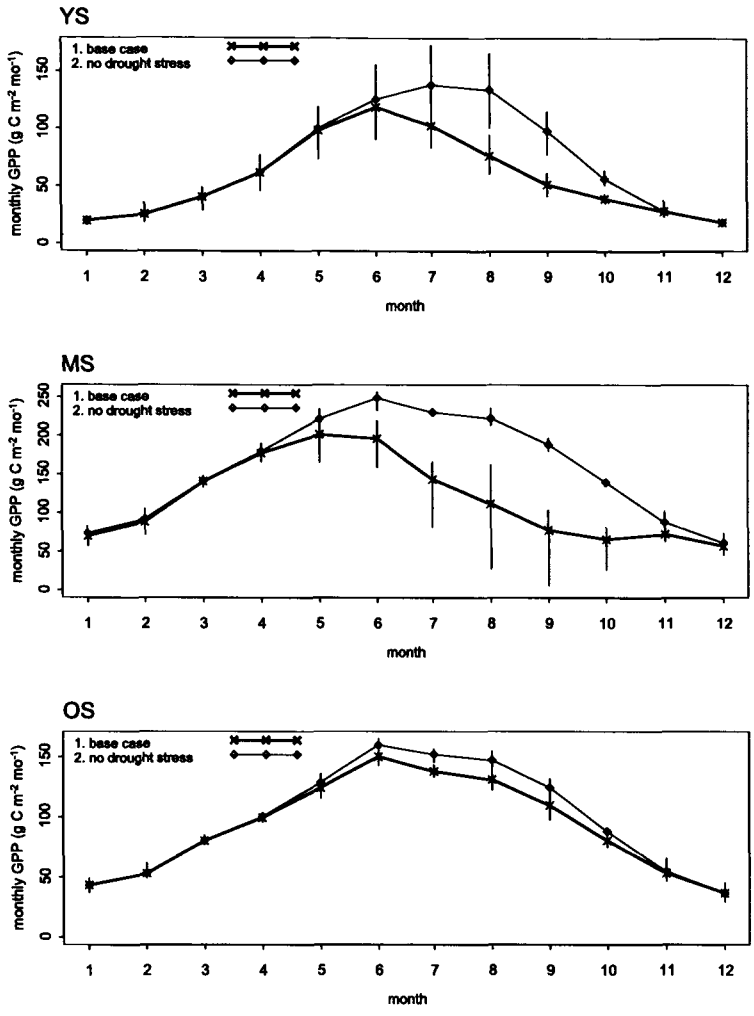

Figure 4. Monthly GPP under the base case and no drought stress scenarios showing effects of seasonal drought at the sites. Differences between the two curves are an estimate of the reduction in GPP caused by drought. Vertical bars show the range of variation over the four simulated years, 1999–2002.

atures, which influenced growing-season length. *Griffis et al.* [2003], based on 6 years of eddy covariance data, associated higher GPP with warmer climatic conditions at an aspen site in Saskatchewan, Canada. However, to our knowledge, our study is the first to suggest that gross carbon uptake of nearby stands of the same forest type, with largely similar climate, can have substantially different sensitivities to interannual variation of climate.

3.5.2. Effects of Aboveground Stand Structure and Canopy Physiology

[42] Mean annual simulated GPP during 1999–2002 was highest at the MS and lowest at the YS, consistent with the rank differences in LAI among the sites (Table 2). Mean annual GPP was 1401, 1098, and 679 g C m^{-2} yr^{-1} at the MS, OS, and YS, respectively (Table 6, base case). When LAI was held constant at the YS (using the 2002 LAI), mean annual GPP increased by ~18% to 801 g C m^{-2} yr^{-1}.

[43] Increasing the LAI at the YS to match interannual changes in measured values during the base case simulations produced higher interannual variation of the fluxes of carbon and water vapor (Table 6). For GPP, interannual variation increased from 19% to 45%, and the pattern of GPP relative to the pattern of annual precipitation was reversed. GPP was highest in 2002 and lowest in 1999, which reflected the importance of stand leaf area in determining gross carbon uptake. Similar responses to increasing LAI during the 4-year simulations were also noted for tree transpiration and total LE. Under scenario 2 (no drought stress), the interannual variation of GPP over the 4-year period increased despite the stabilizing effect of increased soil water availability (Table 6). Thus the simulations suggest that increases in leaf area, alone, may have a tendency to increase the sensitivity of a stand to interannual variation of climate, at least in low LAI systems like our

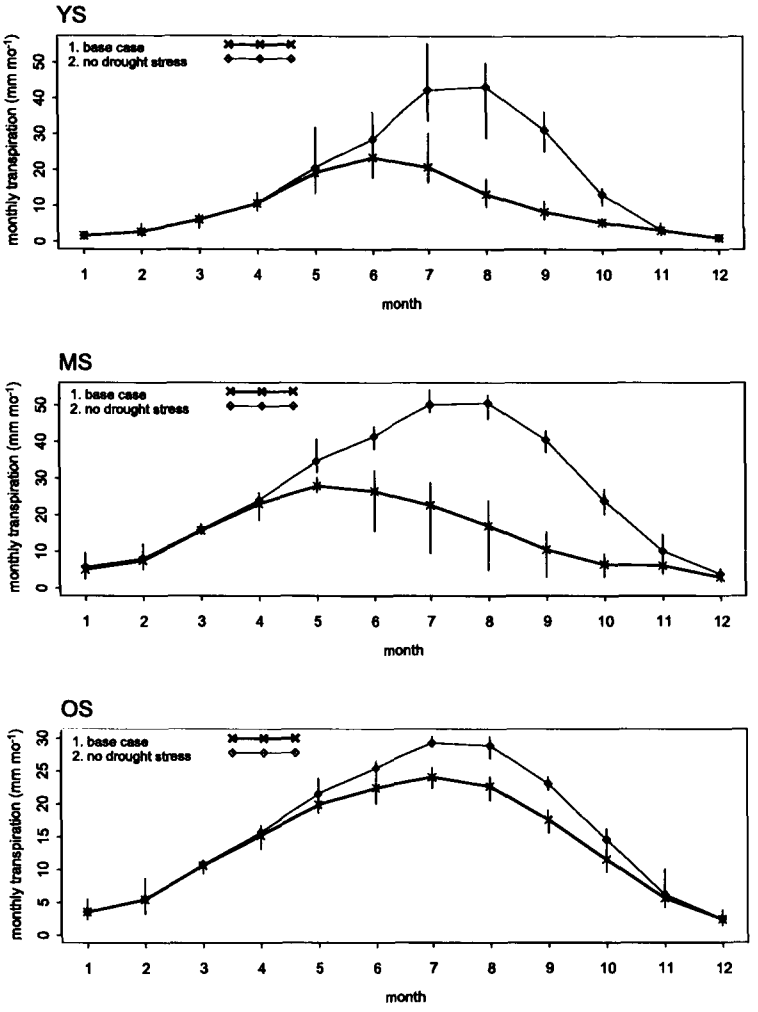

Figure 5. Monthly tree transpiration under the base case and no drought stress scenarios, showing effects of seasonal drought at the sites. Differences between the two curves are an estimate of the reduction in GPP caused by drought. Vertical bars show the range of variation over the four simulated years, 1999–2002.

sites. In stands with higher LAI, though, changes in leaf area could produce feedbacks in other components of the stand's overall energy balance.

[44] Scenario 3 (identical aboveground structure and physiology) replaced the aboveground structure of the YS and OS with the LAI, foliage distribution, and canopy hydraulic conductance of the MS. Most of among-site differences in GPP can be explained by differences in stand structure and canopy physiology (Figure 6, third plot). Compared to the base case, mean annual GPP increased 76% and 50%, respectively, at the YS and OS, and differences in mean annual GPP among the three sites were reduced to 18% (Table 6). Additional simulations at the OS, which separated the effects of LAI, hydraulic conductance, and vertical canopy structure, revealed that 16% of the 50% increase in mean GPP could be attributed to the increased LAI, and most of the remainder was caused more by the simulated changes in height and vertical distribution of foliage rather than the simulated changes in hydraulic properties of the sites. In contrast, at the YS, 61% of the 76% increase in mean GPP was related to the increased LAI, with most of the remainder being attributed the simulated changes in height and vertical distribution of foliage, which increased absorption of radiation by the plant canopies.

[45] Simulated responses of tree transpiration and total LE to changes in aboveground stand structure under scenario 3 differed somewhat from those of GPP (Table 6, Figure 7). Mean annual tree transpiration at the YS and OS increased by ~40% relative to the base case scenario, but in contrast with simulated GPP, differences among the sites in mean annual transpiration increased as well, suggest-

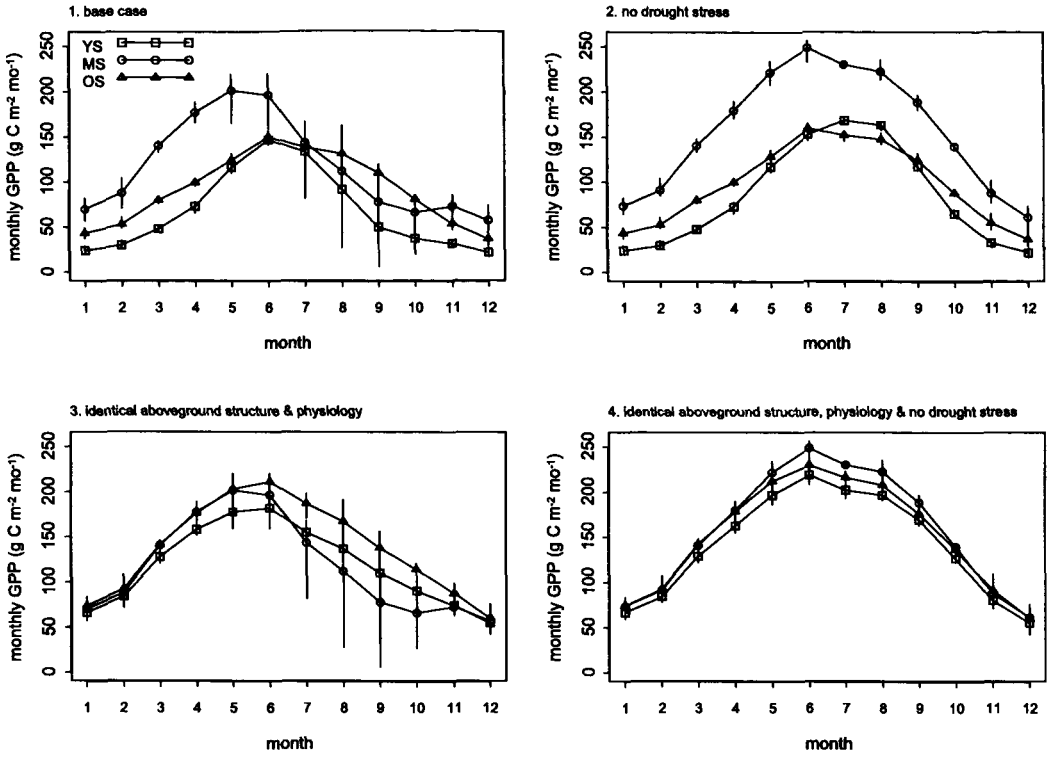

Figure 6. Comparisons of monthly GPP among the four simulated scenarios for each of the three sites. Vertical bars show the range of variation over the four simulated years, 1999–2002. The simulations for the YS assume that LAI was constant over the 4 years.

ing that belowground differences were contributing among-site differences.

[46] Most of the seasonal variation of the fluxes of carbon and water vapor was evident during the months of July–October (Figures 6 and 7), similar to the base case scenario. Furthermore, despite identical aboveground structure at each of the sites, there were still distinct differences in the interannual variation of GPP among the sites, which were 53%, 21%, and 14% at the MS, YS, and OS, respectively (Table 6), further suggesting that belowground site differences were responsible for the pattern of interannual variation. Similarly, the same pattern of interannual variation among the three sites was evident for tree transpiration and total LE.

[47] Other simulated changes in aboveground structure besides LAI influenced the hydraulic properties of both stands but had a bigger relative impact on GPP at the OS than at the YS. The net effect of altering the tree heights and hydraulic conductance increased overall canopy hydraulic conductance at the OS but decreased canopy conductance at the YS. Hydraulic limitations have been proposed as an explanation for reduced productivity in older trees [e.g., *Yoder et al.*, 1994; *Ryan and Yoder*, 1997], but see *Ryan et al.* [2004]. The effects of these simulated changes are a logical extension of previous research on hydraulic limitations [e.g., *Waring and Running*, 1978; *Zimmermann*, 1983; *Yoder et al.*, 1994; *Ryan and Yoder*, 1997] and have been discussed previously by *Williams et al.* [2001a].

[48] Our simulations also suggest that rapidly developing stands, such as the YS, may be prone to higher interannual variation of GPP than stands with stable LAI (Table 6, base case). Moreover, the interannual variability of GPP increased in the simulations that removed soil moisture limitations at the YS (no drought stress scenario). In the absence of water limitations, GPP is constrained on an annual basis mostly by the amount of PAR intercepted by the foliage, and over the 4-year simulation, the fraction of absorbed PAR at the YS increased by about 40%, which explains most of the increased variability of GPP despite the otherwise stabilizing effect of increased soil water availability. After accounting for the increase in LAI, the remaining variation (15%) was similar to the variation of the base case scenario with stable LAI (19%) and can be attributed to interannual climatic variation. In general, though, our results suggest that following disturbance, young, rapidly developing stands may be more sensitive to variations in climatic conditions than stands with more stable LAI, which, in turn, could cause these stands to shift, on an annual basis, from net sources or net sinks of carbon, assuming that the interannual variation of GPP is larger than the interannual variation of ecosystem respiration [*Law et al.*, 2001c, 2003]. This possibility is discussed in more detail below.

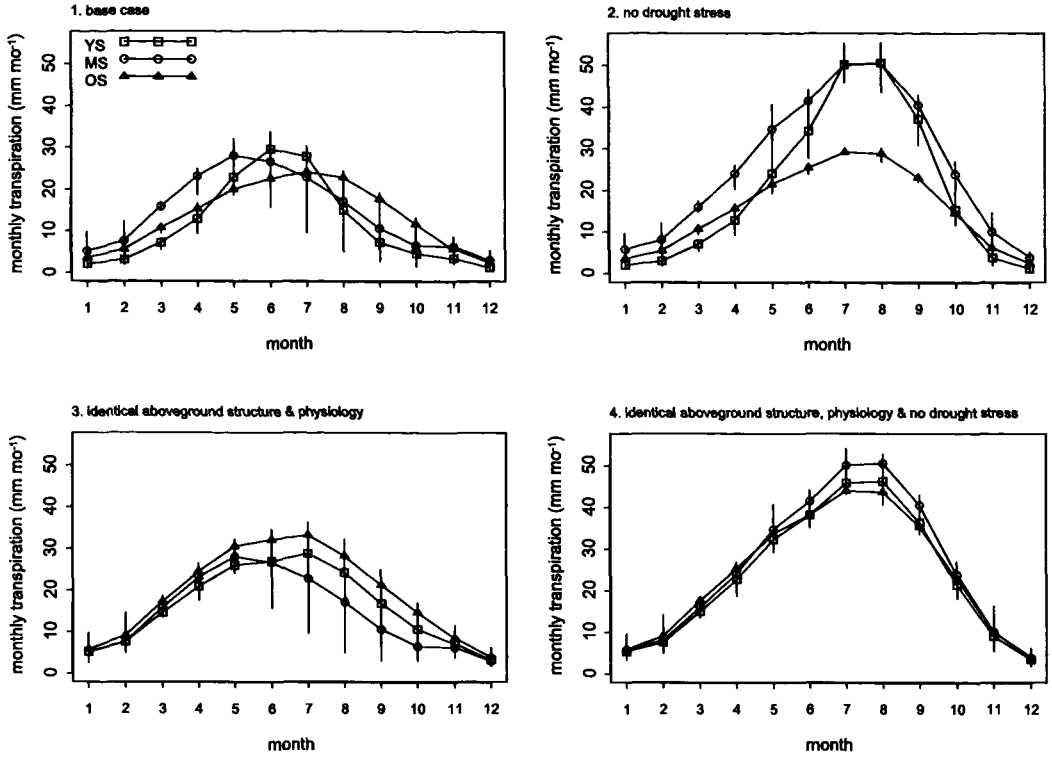

Figure 7. Comparisons of monthly tree transpiration among the four simulated scenarios for each of the three sites. Vertical bars show the range of variation over the four simulated years, 1999–2002. The simulations for the YS assume that LAI was constant over the 4 years.

[49] Our purpose for simulating changes in stand structure, though, was to investigate possible explanations for the differential response and sensitivity among the sites to increased precipitation and interannual climatic variation, and although the simulated changes in aboveground stand structure and physiology had a large impact on GPP at the sites, they had little effect on the interannual variation of GPP. The range of interannual variation among the sites (with identical aboveground structure) was similar to the range of variation under the base case scenario, and the rank differences among the three sites were the same (Figure 6, Table 6). Hence we concluded that differences in aboveground stand structure and physiology, alone, could not explain the site-specific differences in sensitivity to interannual climatic variation.

3.5.3. Effects of Root Density and Rooting Depth

[50] Under scenario 3 (identical aboveground structure and physiology), the only differences between the sites were those differences related to belowground structure (fine root density and distribution) and to physical soil properties, which were minor (Table 1), and the simulations under scenario 4 (identical aboveground structure and no drought stress) effectively minimized differences in carbon uptake and water vapor exchange among the three sites (Figure 6). Virtually unlimited soil water availability increased mean annual GPP at the YS and OS by 19% and 10%, respectively, compared with the previous scenario, and the variation of mean annual GPP among the three sites was reduced to 12% (Table 6). Furthermore, the interannual variation of GPP was similar among the sites and ranged from 4 to 7%. Hence the simulated increase in soil water availability compensated for differences in belowground structure among the sites and effectively eliminated differences in root density and distribution. Additional simulations using identical climate data for each site (rather than site-specific data) produced virtually identical interannual variation, 7.5–7.7% among the three sites. Thus most of the differences in interannual variation of GPP among the sites, evident in the previous simulations, could be attributed to site-specific differences in fine root density and root distribution. Therefore the smaller interannual variation of GPP at the OS evident in the base case simulations (Figure 6) can be explained by root systems at the site that can access water deeper in the soil profile.

[51] The effects of scenario 4 on tree transpiration and total LE were similar to those of GPP. Mean annual fluxes increased and differences among the sites decreased (Figure 7). Differences in interannual variation of transpiration and total LE among the sites were also reduced (Table 6), and although most of the among-site differences of total LE were related to differences in tree transpiration, some of the differences were also related to soil evaporation.

[52] An alternative explanation for lower interannual variation of GPP at the OS and the site's modest response

to simulated increased soil water availability could be that soil moisture levels at the OS were higher than at either the YS or MS. Precipitation, though, at the three sites was similar (Figure 2), and measurements of soil water content during the growing season in the topmost meter of soil indicated that soil moisture was also similar among the three sites (J. Irvine, unpublished data, 2002). Furthermore, measured and simulated soil water content values were also comparable. However, predawn foliage water potential measurements during the 1999–2002 growing seasons showed that the OS had higher levels of available soil water than either the YS or MS, which suggested that OS experienced less drought stress than the other two sites [*Irvine et al.*, 2004]. Consequently, among-site differences in soil characteristics and soil water content in the top meter of soil were minor and do not explain the sites' differential response to interannual climatic variation or a simulated increase in precipitation.

[53] Simulation scenarios 3 and 4 provide compelling evidence that the most likely explanation for both the modest reduction in GPP at the OS in response to drought as well as the site's lower interannual variation of GPP is that tree roots at the site are able to access soil water from deeper in the profile, whereas tree roots at the YS and MS cannot. In addition to the simulation results, there are some empirical data that support the conclusion of a greater rooting depth at the OS. *Irvine et al.* [2002] concluded that a deeper rooting depth at the OS (compared to the YS) was the most likely explanation for less negative soil water potentials at the OS in an empirical study of sap flux measurements and soil CO_2 fluxes at the YS and OS. Furthermore, analyses of stable oxygen isotope data, although not conclusive, indicated that the $\delta^{18}O$ signature of xylem water in trees at the OS was more similar to that of nearby spring water than the corresponding isotope signature of soil water in the surface layers, which also supports the argument that trees at the OS have access to and are using water from deeper in the soil profile [*Bowling et al.*, 2003].

[54] A comparatively shallower rooting depth parameter value for the YS is reasonable given the site's stage of development following disturbance [*Law et al.*, 2001c]. A similarly shallow rooting depth parameter value, though, for the MS raises questions regarding whether the root system has had adequate time to develop or whether there are site factors that could be limiting root system development. Ordinarily, individual ponderosa pine trees would be expected to establish their root systems within a few years, and pure stands would have fully developed root systems within a few decades [*Oliver and Ryker*, 1990; *Stone and Kalisz*, 1991]. An analysis of empirical height-age relationships similar to that used to develop site index curves for forestry applications [e.g., *Meyer*, 1938] suggests that both the MS and YS may be poorer quality sites compared to the OS, which might reflect possible differences in rooting depths at the sites. However, these site differences are probably not nutrient related. Recently, *Kelliher et al.* [2004] reported that concentrations of total carbon (C), total nitrogen (N), and mineral N in the top 10 cm of soil, where most fine roots are located, were similar at YS and OS. At deeper depths, though, the YS had higher concentrations of total C and total N but not mineral N. Nitrogen mineralization rates at the two sites were also similar, and they concluded that mineralization rates of both soil and litter C at the sites was limited more by the availability of water than by N [*Kelliher et al.*, 2004]. It is possible, though, that some physical obstruction, perhaps related to site geology or topography, may be restricting root system development at the MS.

[55] In general, our simulations support the view that older forest stands, with well-established root systems, are better able to buffer effects of intra-annual and interannual variation of climate than younger stands with less-developed root systems that grow in semi-arid regions like central Oregon. One concern of a potential change in climate is that there will be increased variation in individual extreme precipitation events as well as increased variation in total annual precipitation [*Easterling et al.*, 2000]. Our simulations suggest that younger forests, under circumstances of increased climatic variability, would be subject to higher interannual variation of gross carbon uptake and be more susceptible to climatic extremes. In a recent review, *Weltzin et al.* [2003] voiced similar concerns about the potential effects of changes in precipitation regimes on ecological systems. In addition, much of the western United States (including semi-arid regions with ponderosa pine) is subject to both natural (e.g., wildfire) and human-caused (e.g., logging) disturbances, which have a direct impact upon the stage of development and structure of forested ecosystems. Thus, in addition to the ecological implications of our results for ecosystem functioning, our simulation results may have further implications for forest management policies.

3.6. Implications for Net Ecosystem Exchange

[56] The model-based annual estimate of NEE for the YS in 2001 compared favorably with the estimates derived from eddy flux data (Table 5). However, for 2002, modeled NEE was considerably larger than the flux-based estimates. At the MS, the larger modeled NEE (compared with measured) is related to the much higher simulated GPP at the site. At the YS, it is unclear why modeled NEE was higher than measured NEE in 2002, but it may be related to a higher estimate of foliage respiration (R_f) in 2002 than 2001, although R_e is similar between the two years (Table 7).

[57] At the OS, NEE was lowest in 2000 and highest in 1999, but among the 4 years, the site was a consistent and stable net carbon sink (Table 7). In contrast, NEE at the YS varied widely. In 1999, the site was a small net carbon source but was a net sink for carbon thereafter. Similarly, the 2 years of available data for the MS suggest that NEE at the site was highly variable and that the site was a net sink for carbon. Across the 4 years, interannual variation of CO_2 fluxes from the soil surface (R_s) was similar among the three sites and accounted for >70% of annual R_e at the YS and OS and ~64% at the MS. Consequently, interannual variation of R_e at the sites was controlled mostly by interannual variation of R_s. At the YS, the variation of R_e was also controlled in part by interannual variation of R_f as leaf area increased. Because GPP at the OS was stable over the

33

Table 7. Annual Estimates of Net Ecosystem Exchange (NEE) Determined From Simulations of GPP and Annual Estimates of Respiration Derived From Measurements at Each of the Study Sites[a]

	YS					MS					OS				
	R_s	R_f	R_e	GPP	NEE	R_s	R_f	R_e	GPP	NEE	R_s	R_f	R_e	GPP	NEE
1999	453	111	590	573	−17	-	-	-	1565	-	497	141	69	1126	436
2000	377	142	545	643	98	-	-	-	1472	-	587	142	781	1101	320
2001	452	147	626	674	48	575	-	925	1026	101	488	148	688	1049	361
2002	430	180	636	828	192	673	268	1023	1539	516	519	147	718	1117	399
Mean	428	145	599	679	80	624	-	974	1401	309	523	144	719	1098	379
Std dev	36	28	41	108	88	69	-	69	253	293	45	3	44	35	50
Percent variation	20	62	17	45	n.a.	17	-	11	53	410	20	5	14	7	36

[a]Units are g C m^{-2} yr^{-1}. R_s, CO_2 efflux from the soil surface; R_f, foliage maintenance respiration; R_e, whole ecosystem respiration, $R_e = R_s + R_f +$ sapwood respiration (R_w) + annual decomposition of woody material (see section 2.8). NEE = GPP − R_e. Dashes indicate no data available.

4 years, interannual variation of NEE at the site was determined mostly by the interannual variation of R_e, whereas the interannual variation of GPP probably had a much bigger effect on the interannual variation of NEE at the YS and MS (Table 7).

[58] Determining the sign, magnitude, and interannual variation of NEE in various ecosystems is critical to developing a better understanding of global carbon budgets [*Schimel et al.*, 2001]. Our results suggest that the controls on the interannual variation of NEE in ponderosa pine forests, even with similar climate, are not simple and consistent across age classes but may differ according to development stage. Although the robustness of the NEE calculations using our approach is unclear, the apparent transition of the YS from a net carbon source to a net carbon sink highlights the importance of forest recovery following disturbance in determining terrestrial carbon balances [*Law et al.*, 2001c; *Schimel et al.*, 2001; *Goodale et al.*, 2002].

[59] Our results contribute to the debate regarding the relative importance of R_e versus GPP in controlling the interannual variation of NEE. Some studies of forests suggest that R_e varies more than GPP on an annual basis [*Valentini et al.*, 2000; *Janssens et al.*, 2001; *Valentini et al.*, 2003]. Other studies indicate that GPP varies more than R_e [*Arain et al.*, 2002; *Aubinet et al.*, 2002], while other studies show that the interannual variation of R_e and GPP is roughly the same [*Barford et al.*, 2001; *Suni et al.*, 2003; *Wang et al.*, 2004]. Our results are important because they suggest that in forests with similar climate, the relative importance of R_e and GPP may depend upon the development stage of the forest.

4. Conclusions

[60] Meteorological data collected at the study sites indicated that precipitation was the dominant source of climatic variation over the 4-year period, 1999–2002, and that the variation in annual precipitation exceeded 50%, while summer precipitation varied more than six-fold. Model simulations at the three sites suggested that interannual variation of GPP over the 4 years ranged from 7% (OS) to >50% (MS). Simulations that assessed the effects of seasonal drought at the sites suggested that the YS and MS were relatively more constrained by seasonal drought stress than the OS throughout the 4-year period, such that interannual variation of climate had a larger effect on the YS and MS and very little effect on GPP at the OS, which was buffered by deeper rooting. At the rapidly developing YS, changes in stand structure, such as increasing leaf area associated with vigorous growth, appear to have larger effects on carbon and water fluxes than variation in climate, although effects of these changes may interact with other biotic effects including shifts in carbon allocation and whole-tree hydraulic conductance. Interannual variation of NEE, based on simulations of GPP and empirical estimates of R_e, was also less variable at the OS than at the other two sites, and whereas interannual variation of NEE at the OS during the 4 years was probably controlled mostly by the variation of R_e, interannual variation in NEE at the YS and MS appeared to be more strongly controlled by the interannual variation of GPP.

[61] Our results suggest that the interannual variation of precipitation is probably the dominant control on carbon and water vapor fluxes in temperate coniferous forests growing in semi-arid regions. Additionally, older forest stands with well-established root systems appear to be better able to buffer the effects of both seasonal drought stress and interannual climatic variation than younger stands. In many forested landscapes, mosaics of different forest development stages are present because of the effects of wildfire and timber harvesting (Figure 1). Carbon uptake and water vapor exchange among stands with different structural characteristics and stages of development can show varying responses to the interannual variation of climate, and the aggregate pattern of carbon and water fluxes at the landscape level will likely depend upon the distribution of different development stages. If there is a higher proportion of younger stands in the landscape because of disturbances like intensive harvesting or wildfire, then GPP across the landscape is likely to undergo large interannual variations in response to climate, whereas a higher proportion of old stands would probably dampen the interannual fluctuation of GPP. In western North America where ponderosa pine forests are common, there are relatively few old stands; thus the interannual variation of GPP in this region is likely to be large. Because interannual variation of NEE in younger pine forests is probably more strongly related to the interannual variation of GPP than R_e, NEE across the region is also likely to vary considerably in response to the interannual variation of climate.

[62] **Acknowledgments.** This study was funded by NASA (grant NAG5-11231), a study on regional carbon dioxide and water vapor exchange over heterogeneous terrain, and the Department of Energy (DOE grant FG0300ER63014) study on carbon dioxide and water vapor exchange in successional stages of Pacific Northwest forest ecosystems. We gratefully acknowledge Adam Pfleeger for invaluable field and laboratory assistance, and tree climbers from the EPA, Corvallis, for their installation of sap flux probes at the old site. The authors are also grateful for the helpful comments and suggestions from two anonymous reviewers. In addition, the first author wishes to thank R. H. Waring for his many ideas and helpful suggestions. We appreciate the Sisters Ranger District of the U.S. Forest Service for allowing us to conduct research at the old growth forest, which is in a Research Natural Area, and the Weyerhaeuser Company, for allowing us to conduct research at the mature and young sites.

References

Anthoni, P. M., B. E. Law, and M. H. Unsworth (1999), Carbon and water vapor exchange of an open-canopied ponderosa pine ecosystem, *Agric. For. Meteorol.*, *95*, 151–168.

Anthoni, P. M., M. H. Unsworth, B. E. Law, J. Irvine, D. D. Baldocchi, S. Van Tuyl, and D. Moore (2002), Seasonal differences in carbon and water vapor exchange in young and old-growth ponderosa pine ecosystems, *Agric. For. Meteorol.*, *111*, 203–222.

Arain, M. A., T. A. Black, A. G. Barr, P. G. Jarvis, J. M. Massheder, D. L. Verseghy, and Z. Nesic (2002), Effects of seasonal and interannual climate variability on net ecosystem productivity of boreal deciduous and conifer forests, *Can. J. For. Res.*, *32*, 878–891.

Aubinet, M., B. Heinesch, and B. Longdoz (2002), Estimation of the carbon sequestration by a heterogeneous forest: Night flux corrections, heterogeneity of the site and inter-annual variability, *Global Change Biol.*, *8*, 1053–1071.

Barford, C. C., S. C. Wofsy, M. L. Goulden, J. W. Munger, E. H. Pyle, S. P. Urbanski, L. Hutyra, S. R. Saleska, D. Fitzjarrald, and K. Moore (2001), Factors controlling long- and short-term sequestration of atmospheric CO_2 in a mid-latitude forest, *Science*, *294*, 1688–1691.

Bowling, D. R., N. G. McDowell, J. M. Welker, B. J. Bond, B. E. Law, and J. R. Ehleringer (2003), Oxygen isotope content of CO_2 in nocturnal ecosystem respiration: 1. Observations in forests along a precipitation transect in Oregon, USA, *Global Biogeochem. Cycles*, *17*(4), 1120, doi:10.1029/2003GB002081.

Caspersen, J. P., S. W. Pacala, J. C. Jenkins, G. C. Hurtt, P. R. Moorcroft, and R. A. Birdsey (2000), Contributions of land-use history to carbon accumulation in U.S. forests, *Science*, *290*, 1148–1151.

Cohen, W. B., M. E. Harmon, D. O. Wallin, and M. Fiorella (1996), Two decades of carbon flux from forests of the Pacific Northwest, *Bioscience*, *46*, 836–844.

Easterling, D. R., G. A. Meehl, C. Parmesan, S. A. Changnon, T. R. Karl, and L. O. Mearns (2000), Climate extremes: Observations, modeling, and impacts, *Science*, *289*, 2068–2074.

Falge, E., et al. (2001), Gap filling strategies for defensible annual sums of net ecosystem exchange, *Agric. For. Meteorol.*, *107*, 43–69.

Farquhar, G. D., and S. von Caemmerer (1982), Modelling of photosynthetic response to the environment, in *Physiological Plant Ecology II: Encyclopedia of Plant Physiology*, edited by O. L. Lange et al., pp. 549–587, Springer-Verlag, New York.

Goldstein, A. H., N. E. Hultman, J. M. Fracheboud, M. R. Bauer, J. A. Panek, M. Xu, Y. Qi, A. B. Guenther, and W. Baugh (2000), Effects of climate variability on the carbon dioxide, water, and sensible heat fluxes above a ponderosa pine plantation in the Sierra Nevada (CA), *Agric. For. Meteorol.*, *101*, 113–129.

Goodale, C. L., et al. (2002), Forest carbon sinks in the Northern Hemisphere, *Ecol. Appls.*, *12*, 891–899.

Goulden, M. L., J. W. Munger, S. M. Fan, B. C. Daube, and S. C. Wofsy (1996), Measurements of carbon sequestration by long-term eddy covariance: Methods and a critical evaluation of accuracy, *Global Change Biol.*, *2*, 169–182.

Granier, A. (1987), Evaluation of transpiration in a Douglas-fir stand by means of sap flow measurements, *Tree Physiol.*, *3*, 309–320.

Griffis, T. J., T. A. Black, K. Morgenstern, A. G. Barr, Z. Nesic, G. B. Drewitt, D. Gaumont-Guay, and J. H. McCaughey (2003), Ecophysiological controls on the carbon balances of three southern boreal forests, *Agric. For. Meteorol.*, *117*, 53–71.

Hargrove, W. H., F. M. Hoffman, and B. E. Law (2003), New analysis reveals representativeness of the AmeriFlux network, *Eos Trans. AGU*, *84*, 529.

Irvine, J., and B. E. Law (2002), Contrasting soil respiration in young and old-growth ponderosa pine forests, *Global Change Biol.*, *8*, 1183–1194.

Irvine, J., B. E. Law, P. M. Anthoni, and F. C. Meinzer (2002), Water limitations to carbon exchange in old-growth and young ponderosa pine stands, *Tree Physiol.*, *22*, 189–196.

Irvine, J., B. E. Law, M. R. Kurpius, P. M. Anthoni, D. Moore, and P. A. Schwarz (2004), Age-related changes in ecosystem structure and function and effects on water and carbon exchange in ponderosa pine, *Tree Physiol.*, *24*, 753–763.

Janssens, I. A., et al. (2001), Productivity overshadows temperature in determining soil and ecosystem respiration across European forests, *Global Change Biol.*, *7*, 269–278.

Kelliher, F. M., D. J. Ross, B. E. Law, D. D. Baldocchi, and N. J. Rodda (2004), Limitations to carbon mineralization in litter and mineral soil of young and old ponderosa pine forests, *For. Ecol. Manage.*, *191*, 201–213.

Kramer, K., et al. (2002), Evaluation of six process-based forest growth models using eddy-covariance measurements of CO_2 and H_2O fluxes at six forest sites in Europe, *Global Change Biol.*, *8*, 213–230.

Landsberg, J. J., and S. T. Gower (1997), *Applications of Physiological Ecology to Forest Management*, Academic, San Diego, Calif.

Law, B. E., D. D. Baldocchi, and P. M. Anthoni (1999a), Below-canopy and soil CO_2 fluxes in a ponderosa pine forest, *Agric. For. Meteorol.*, *94*, 171–188.

Law, B. E., M. G. Ryan, and P. M. Anthoni (1999b), Seasonal and annual respiration of a ponderosa pine ecosystem, *Global Change Biol.*, *5*, 169–182.

Law, B. E., M. Williams, P. M. Anthoni, D. D. Baldocchi, and M. H. Unsworth (2000), Measuring and modelling seasonal variation of carbon dioxide and water vapour exchange of a Pinus ponderosa forest subject to soil water deficit, *Global Change Biol.*, *6*, 613–630.

Law, B. E., A. Cescatti, and D. D. Baldocchi (2001a), Leaf area distribution and radiative transfer in open-canopy forests: Implications for mass and energy exchange, *Tree Physiol.*, *21*, 777–787.

Law, B. E., F. M. Kelliher, D. D. Baldocchi, P. M. Anthoni, J. Irvine, D. Moore, and S. Van Tuyl (2001b), Spatial and temporal variation in respiration in a young ponderosa pine forests during a summer drought, *Agric. For. Meteorol.*, *110*, 27–43.

Law, B. E., P. E. Thornton, J. Irvine, P. M. Anthoni, and S. Van Tuyl (2001c), Carbon storage and fluxes in ponderosa pine forests at different developmental stages, *Global Change Biol.*, *7*, 755–777.

Law, B. E., O. J. Sun, J. Campbell, S. Van Tuyl, and P. E. Thornton (2003), Changes in carbon storage and fluxes in a chronosequence of ponderosa pine, *Global Change Biol.*, *9*, 510–524.

Law, B. E., D. P. Turner, M. A. Lefsky, J. Campbell, M. Guzy, O. Sun, S. Van Tuyl, and W. B. Cohen (2004), Carbon fluxes across regions: Observational constraints at multiple scales, in *Scaling and Uncertainty Analysis in Ecology: Methods and Applications*, edited by J. Wu et al., Columbia Univ. Press, New York, in press.

Meiresonne, L., D. A. Sampson, A. S. Kowalski, I. A. Janssens, N. Nadezhdina, J. Cermak, J. Van Slycken, and R. Ceulemans (2003), Water flux estimates from a Belgian Scots pine stand: A comparison of different approaches, *J. Hydrol.*, *270*, 230–252.

Meyer, W. H. (1938), Yield of even-aged stands of ponderosa pine, *Tech. Bull. 630*, U.S. Dep. of Agric., Washington, D. C.

Moncrieff, J. B., Y. Malhi, and R. Leuning (1996), The propagation of errors in long-term measurements of land-atmosphere fluxes of carbon and water, *Global Change Biol.*, *2*, 231–240.

Myneni, R. B., J. Dong, C. J. Tucker, R. K. Kaufmann, P. E. Kauppi, J. Liski, L. Zhou, V. Alexeyev, and M. K. Hughes (2001), A large carbon sink in the woody biomass of Northern forests, *Proc. Natl. Acad. Sci. U. S. A.*, *98*, 14,784–14,789.

Oliver, W. W., and R. A. Ryker (1990), *Pinus ponderosa* Dougl. ex Laws. Ponderosa pine, in *Silvics of North America*, vol. 1, *Conifers*, *Agric. Handb.*, vol. 654, edited by R. M. Burns and B. H. Honkala, pp. 413–424, U.S. Dep. of Agric., Washington, D. C.

Ryan, M. G. (2002), Canopy processes research, *Tree Physiol*, *22*, 1035–1043.

Ryan, M. G., and B. J. Yoder (1997), Hydraulic limits to tree height and tree growth, *Bioscience*, *47*, 235–242.

Ryan, M. G., D. Binkley, J. H. Fownes, C. P. Giardina, and R. S. Senock (2004), An experimental test of the causes of forest growth decline with stand age, *Ecol. Monogr.*, *74*, 393–414.

Schaefer, K., A. S. Denning, N. Suits, J. Kaduk, I. Baker, S. Los, and L. Prihodko (2002), Effect of climate on interannual variability of terrestrial CO_2 fluxes, *Global Biogeochem. Cycles*, *16*(4), 1102, doi:10.1029/2002GB001928.

Schimel, D., et al. (2000), Contribution of increasing CO_2 and climate to carbon storage by ecosystems in the United States, *Science*, *287*, 2004–2006.

Schimel, D. S., et al. (2001), Recent patterns and mechanisms of carbon exchange by terrestrial ecosystems, *Nature, 414*, 169–172.

Stone, E. L., and P. J. Kalisz (1991), On the maximum extent of tree roots, *For. Ecol. Manage., 46*, 59–102.

Sun, O. J., J. L. Campbell, and B. E. Law (2004), Dynamics of carbon storage in soils and detritus across chronosequences of different forest types in the Pacific Northwest, USA, *Global Change Biol.*, in press.

Suni, T., F. Berninger, T. Markkanen, P. Keronen, U. Rannik, and T. Vesala (2003), Interannual variability and timing of growing-season CO_2 exchange in a boreal forest, *J. Geophys. Res., 108*(D9), 4265, doi:10.1029/2002JD002381.

Turner, D. P., G. J. Koerper, M. E. Harmon, and J. L. Lee (1995), A carbon budget for forests on the conterminous United States, *Ecol. Appl., 5*, 421–436.

Valentini, R., et al. (2000), Respiration as the main determinant of carbon balance in European forests, *Nature, 404*, 861–865.

Valentini, R., G. Matteucci, A. J. Dolman, and E. D. Schulze (2003), Conclusions: The role of canopy flux measurements in global C-cycle research, in *Fluxes of Carbon, Water, and Energy of European Forests*, edited by R. Valentini, pp. 255–266, Springer-Verlag, New York.

Wallach, D., and B. Goffinet (1987), Mean squared error of prediction in models for studying ecological and agronomic system, *Biometrics, 43*, 561–573.

Wallach, D., and B. Goffinet (1989), Mean squared error of prediction as a criterion for evaluating and comparing system models., *Ecol. Modell., 4*, 299–306.

Wang, K. Y., S. Kellomaki, T. S. Zha, and H. Peltola (2004), Component carbon fluxes and their contribution to ecosystem carbon exchange in a pine forest: An assessment based on eddy covariance measurements and an integrated model, *Tree Physiol., 24*, 19–24.

Waring, R. H., and S. W. Running (1978), Sapwood water storage: Its contribution to transpiration and effect upon water conductance through stems of old-growth Douglas-fir, *Plant Cell Environ., 1*, 131–140.

Weltzin, J. F., et al. (2003), Assessing the response of terrestrial ecosystems to potential changes in precipitation, *Bioscience, 53*, 941–952.

Williams, M., E. B. Rastetter, D. N. Fernandes, M. L. Goulden, S. C. Wofsy, G. R. Shaver, J. M. Melillo, J. W. Munger, S. M. Fan, and K. J. Nadelhoffer (1996), Modelling the soil-plant-atmosphere continuum in a Quercus-Acer stand at Harvard forest: The regulation of stomatal conductance by light, nitrogen and soil/plant hydraulic properties, *Plant Cell Environ., 19*, 911–927.

Williams, M., Y. Malhi, A. D. Nobre, E. B. Rastetter, J. Grace, and M. G. P. Pereira (1998), Seasonal variation in net carbon exchange and evapotranspiration in a Brazilian rain forest: A modelling analysis, *Plant Cell Environ., 21*, 953–968.

Williams, M., W. Eugster, E. B. Rastetter, J. P. McFadden, and F. S. Chapin (2000), The controls on net ecosystem productivity along an Arctic transect: A model comparison with flux measurements, *Global Change Biol., 6*, 116–126.

Williams, M., B. J. Bond, and M. G. Ryan (2001a), Evaluating different soil and plant hydraulic constraints on tree function using a model and sap flow data from ponderosa pine, *Plant Cell Environ., 24*, 679–690.

Williams, M., B. E. Law, P. M. Anthoni, and M. H. Unsworth (2001b), Use of a simulation model and ecosystem flux data to examine carbon-water interactions in ponderosa pine, *Tree Physiol., 21*, 287–298.

Wilson, K. B., P. J. Hanson, P. J. Mulholland, D. D. Baldocchi, and S. D. Wullschleger (2001), A comparison of methods for determining forest evapotranspiration and its components: Sap-flow, soil water budget, eddy covariance and catchment water balance, *Agric. For. Meteorol., 106*, 153–168.

Xu, L., and D. D. Baldocchi (2004), Seasonal variation in carbon dioxide exchange over a Mediterranean annual grassland in California, *Agric. For. Meteorol., 123*, 79–96.

Yoder, B. J., M. G. Ryan, R. H. Waring, A. W. Schoettle, and M. R. Kaufmann (1994), Evidence of reduced photosynthetic rates in old trees, *For. Sci., 40*, 513–527.

Zimmermann, M. H. (1983), *Xylem Structure and the Ascent of Sap*, Springer-Verlag, New York.

J. Irvine, B. E. Law, D. Moore, and P. A. Schwarz, College of Forestry, Oregon State University, Corvallis, OR 97331-5752, USA. (paul.schwarz@oregonstate.edu)

M. Kurpius, College of Oceanic and Atmospheric Sciences, Oregon State University, Corvallis, OR 97331-5503, USA.

M. Williams, School of GeoSciences, University of Edinburgh, Darwin Building, Kings Buildings, Mayfield Road, Edinburgh EH9 3JU, UK.

Chapter III

Comparison of heat and moisture fluxes from a modified soil-plant-atmosphere model with observations from BOREAS

JOURNAL OF GEOPHYSICAL RESEARCH, VOL. 109, D08103, doi:10.1029/2003JD003949, 2004

Comparison of heat and moisture fluxes from a modified soil-plant-atmosphere model with observations from BOREAS

Young-Hee Lee[1] and L. Mahrt

College of Oceanic and Atmospheric Sciences, Oregon State University, Corvallis, Oregon, USA

Received 3 July 2003; revised 17 February 2004; accepted 23 February 2004; published 21 April 2004.

[1] This study evaluates the prediction of heat and moisture fluxes from a new land surface scheme with eddy correlation data collected at the old aspen site during the Boreal Ecosystem-Atmosphere Study (BOREAS) in 1994. The model used in this study couples a multilayer vegetation model with a soil model. Inclusion of organic material in the upper soil layer is required to adequately simulate exchange between the soil and subcanopy air. Comparisons between the model and observations are discussed to reveal model misrepresentation of some aspects of the diurnal variation of subcanopy processes. *INDEX TERMS:* 1878 Hydrology: Water/energy interactions; 1818 Hydrology: Evapotranspiration; 3322 Meteorology and Atmospheric Dynamics: Land/atmosphere interactions; *KEYWORDS:* evapotranspiration, canopy model, organic soil layer, BOREAS

Citation: Lee, Y.-H., and L. Mahrt (2004), Comparison of heat and moisture fluxes from a modified soil-plant-atmosphere model with observations from BOREAS, *J. Geophys. Res.*, *109*, D08103, doi:10.1029/2003JD003949.

1. Introduction

[2] Modeling approaches for surface fluxes of heat, moisture and carbon dioxide can be classified into single-source models, two-source models and multilayer models. In the single-source model, evaporation is determined as if the plant canopy were a partly wet plane at the lower boundary of the atmosphere using bulk aerodynamic resistance and stomatal resistance. The bulk stomatal resistance in the single-source model is less well behaved than leaf stomatal resistance in two-source or multilevel models since it is not a purely physiological parameter [*Raupach and Finnigan*, 1988]. Results from single-source models can be particularly sensitive to the roughness lengths for heat and moisture, which can behave erratically over vegetated surfaces.

[3] In two-source models [*Kustas*, 1990; *Sellers et al.*, 1986; *Choudhury and Monteith*, 1988; *Norman et al.*, 1995], an explicit single vegetation layer is considered separately from the ground surface. Although this model is more realistic than the single-source model, vertical structure of the canopy is not resolved. In actual canopies, the stomatal resistance depends significantly on height within the canopy because radiation, turbulence transfer and water supply from the root system vary with height. Consequently, multilayer models have been developed to simulate tall canopies such as forests [*Su et al.*, 1996; *Albertson et al.*, 2001]. These models aim to describe not only the evaporation from the entire canopy, but also the partitioning of the evapotranspiration between various parts of the canopy together with other aspects of the canopy microclimate such as profiles of leaf and air temperature and air humidity. The price of such details is more complexity and parameter input requirements. The choice of model complexity depends on the purpose and availability of computer resources.

[4] Even when multilevel canopy models approximate the actual canopy processes, the coupling between the atmospheric boundary layer and canopy models requires estimation of aerodynamic quantities [*Sun et al.*, 1999] and compliance with Monin-Obukhov similarity theory. In the roughness sublayer immediately above the canopy, the flux-gradient relationship based upon Monin-Obukhov similarity theory can significantly underestimate scalar fluxes [*Simpson et al.*, 1998; *Kaimal and Finnigan*, 1994]. Parameterizations for the roughness sublayer [*Cellier and Brunet*, 1991; *Wenzel et al.*, 1997; *Physick and Garratt*, 1995] are difficult to verify from observations, partly because of the potentially large horizontal gradients on the scale of the roughness elements [e.g., *Katul et al.*, 1999]. Such microscale heterogeneity can contribute to vertical flux divergence due to increasing footprint with height. Two-source models apply Monin-Obukhov similarity theory by assuming that the aerodynamic temperature for Monin-Obukhov similarity is equal to the canopy air temperature. Although this simplification can lead to significant errors [*Sun et al.*, 1999], alternative procedures have not been developed and we employ the same approximation in this study.

[5] The canopy turbulence is driven partly by coherent eddies of canopy scale sometimes leading to locally countergradient fluxes [*Raupach et al.*, 1996]. Existing numerical models of canopy turbulence span a wide range of complexities from K theory to higher order closure modeling and LES modeling [*Katul and Albertson*, 1998; *Shaw and Schumann*, 1992]. Although K theory does not describe countergradient fluxes, for practical purposes, K theory remains an adequate approximation for some applications [*Dolman and Wallace*, 1991] and is still used in many large-scale models [*Bonan*, 1996; *Cotton et al.*, 2003].

[1]Now at Department of Astronomy and Atmospheric Sciences, Kyungpook National University, Daegu, Republic of Korea.

0148-0227/04/2003JD003949$09.00

[6] The coupling between the canopy air and soil through fluxes of heat and moisture can be governed by a shallow soil layer of high organic content above the mineral soil [*Pauwels and Wood*, 1999a; *Van de Wiel et al.*, 2002]. The organic layer is not usually included in soil models. *Blanken et al.* [1997] and others have noted that leaf litter on the forest floor can act as a quasi-insulator and therefore promote large subsurface temperature gradients in addition to greater daytime warming of the subcanopy air in the pre-leaf-out period. More specifically, the soil surface layer with high organic content is normally characterized by smaller thermal conductivity and high porosity compared to mineral soils [*Letts et al.*, 2000]. *Pauwels and Wood* [1999a, 1999b, 2000] also pointed out the importance of an organic surface layer and included an organic surface layer in TOPLATS. The model performed well in simulating surface fluxes above the canopy but slightly overestimated the ground heat flux during the course of the day [*Pauwels and Wood*, 1999b] in BOREAS [*Sellers et al.*, 1995]. Although the modeled ground heat flux is sensitive to parameters such as moss thickness, thermal conductivity and heat capacity [*Pauwels and Wood*, 1999b], subcanopy turbulence also plays an important role in determining ground heat flux. In this study, we focus on evaluation of the subcanopy flux and interaction between the surface organic layer and the subcanopy air.

[7] To examine the interaction between microclimate and physiology, we have coupled the multilevel canopy model of *Williams et al.* [1996] with a soil model and atmospheric boundary layer model for use in regional models. This study evaluates the offline performance of the canopy and soil models in terms of vertical structure within the canopy and interaction with an organic surface layer. The model will be compared with data collected at the old aspen site during BOREAS.

2. Model

[8] The land surface model is based on the canopy model (soil plant atmosphere (SPA) model) of *Williams et al.* [1996, 2001], coupled to a multilayer soil model with snow and frozen soil physics [*Mahrt and Pan*, 1984; *Koren et al.*, 1999; *Peters-Lidard et al.*, 1998] and the surface runoff scheme of *Schaake et al.* [1996]. The canopy model computes the stomatal resistance in each canopy layer to maximize daily carbon gain per unit leaf nitrogen content, within the limitation of canopy water storage and transport of water from soil to the canopy [*Williams et al.*, 1996]. The radiation routines model the incidence, interception, absorption and reflectance of PAR (Photosynthetic Active Radiation), near infrared radiation (NIR) and longwave radiation in each canopy layer [*Amthor*, 1994; *Amthor et al.*, 1994]. A spherical leaf angle distribution is assumed.

[9] Here we apply two vegetation layers with the same thickness. Four soil layers are employed with thicknesses of 0.1, 0.3, 0.6 and 1 m, where the top layer includes organic material. We refer to the above papers for a description of the model components and here describe only parts of the model where changes are made.

2.1. Subcanopy Processes

[10] The total surface fluxes are partitioned into vegetation and ground components. Transport is formulated in terms of the atmospheric eddy diffusivities and leaf boundary layer resistances (Figure 1). The subcanopy air temperatures (T_1 and T_2) and the water vapor mixing ratios (q_1 and q_2) are calculated using the leaf temperature (T_{iv}), the saturation mixing ratio (q_{iv}) evaluated at the leaf temperature, the ground temperature (T_g), the ground saturation mixing ratio (q_g) for the ground temperature and resistances by solving the following equations for water vapor and temperature by iteration:

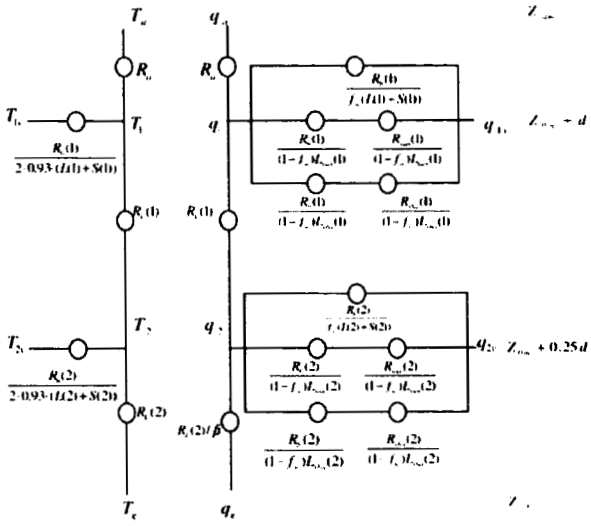

Figure 1. The transfer diagram for the canopy system.

$$\frac{q_a - q_1}{R_a} = \left[\frac{q_1 - q_{1v}}{R_b(1) + R_{sun}(1)} L_{sun}(1) + \frac{q_1 - q_{1v}}{R_b(1) + R_{sha}(1)} L_{sha}(1)\right] \cdot (1 - f_w) + \frac{q_1 - q_{1v}}{R_b(1)} f_w(L(1) + S(1)) + \frac{q_1 - q_2}{R_k(1)} \quad (1)$$

$$\frac{q_1 - q_2}{R_k(1)} = \left[\frac{q_2 - q_{2v}}{R_b(2) + R_{sun}(2)} L_{sun}(2) + \frac{q_2 - q_{2v}}{R_b(2) + R_{sha}(2)} L_{sha}(2)\right] \cdot (1 - f_w) + \frac{q_2 - q_{2v}}{R_b(2)} f_w(L(2) + S(2)) + \frac{q_2 - q_g}{R_k(2)/\beta} \quad (2)$$

$$\frac{T_a - T_1}{R_a} = \frac{2 \cdot 0.93(T_1 - T_{1v})}{R_b(1)} (L(1) + S(1)) + \frac{T_1 - T_2}{R_k(1)} \quad (3)$$

$$\frac{T_1 - T_2}{R_k(1)} = \frac{2 \cdot 0.93(T_2 - T_{2v})}{R_b(2)} (L(2) + S(2)) + \frac{T_2 - T_g}{R_k(2)}, \quad (4)$$

where q_a and T_a are the mixing ratio and the air temperature at the reference height (39 m from the ground) above the canopy, R_a is the aerodynamic resistance in the surface layer, R_k is the subcanopy resistance, R_b is the leaf boundary layer resistance and R_{sun} and R_{sha} are the stomatal resistance for sunlit and shaded leaf areas, respectively, f_w is the wet fraction of leaf and β is the soil wetness function (equation (13)). L_{sun} is the sunlit leaf area index, L_{sha} the

shaded leaf area index and L and S are the leaf area index and stem area index, respectively. While transpiration occurs on one side of the leaf, sensible heat flux occurs from both sides of the leaf due to mechanical mixing. Therefore a factor of 2 is used in equations (3)–(4). The value of 0.93 in equations (3) and (4) accounts for the differences in molecular diffusivities between heat and water vapor. It is assumed that the air adjacent to the shaded leaf surface is the same as that adjacent to the sunlit leaf surface due to sufficient mixing. Therefore no differentiation of leaf boundary layer resistance was made between shaded and sunlit leaf surfaces. The leaf temperature is calculated from the leaf energy balance equation. Neglecting any metabolic and physical storage, the leaf energy balance equation becomes

$$R_n = H_v + \lambda E_v(1 - f_w) + \lambda E_c f_w, \tag{5}$$

where H_v is the leaf sensible heat flux, R_n is the net radiation of the leaf surface, E_v the transpiration and E_c the direct evaporation from wet leaf surfaces. The ground temperature is calculated from the ground surface energy balance.

[11] The aerodynamic resistances for momentum and heat transfer are calculated using the surface layer similarity theory for the eddy diffusivity. The subcanopy resistance for the heat and moisture fluxes between the soil surface and the lowest canopy layer and between canopy layers is estimated as

$$R_k = \int \frac{dz}{K_h}. \tag{6}$$

The eddy diffusivity within the canopy layer for temperature and moisture is assumed to decrease exponentially from the canopy top downward toward the ground surface [*Bonan*, 1996]

$$K_h = K_{sfc} \exp\left(-\alpha\left(1 - \frac{z}{H}\right)\right), \tag{7}$$

where K_{sfc} is the eddy diffusivity at the canopy top calculated from Monin-Obukhov similarity, α is a non-dimensional constant, z is the height above ground and H is the canopy height.

[12] The leaf boundary layer resistance is calculated as in the work of *Jones* [1992]

$$R_b = 100(d/u)^{0.5}, \tag{8}$$

where d is the characteristic dimension of leaf and u is the wind speed in each canopy layer. The default value of 0.08 m from *Williams et al.* [1996] is used for d in this study. The wind profile within the canopy is assumed to decrease exponentially downward as

$$U(z) = U_c \exp\left(-\alpha\left(1 - \frac{z}{H}\right)\right), \tag{9}$$

where U_c is the wind speed at the canopy top.

2.2. Surface Organic Layer

[13] The topsoil layer is generalized to include organic content. The thermal conductivity is computed as

$$K = \Sigma K_i f_i, \tag{10}$$

where K_i is the thermal conductivity of each material component (Table 1) and f_i is the volume fraction of each material. The volumetric heat capacity of the topsoil layer, C (J K^{-1} m^{-3}) is represented as

$$C = \Sigma C_i f_i, \tag{11}$$

where C_i is the volumetric heat capacity of the i_{th} soil component. For the thermal conductivity of the mineral soil, Johansen's parameterization [*Peters-Lidard et al.*, 1998] is used.

[14] For soil evaporation, we adopted the commonly used expression

$$E = \beta E_p, \tag{12}$$

where E_p is potential evaporation, which is calculated by a Penman-based energy balance approach and β is calculated as

$$\beta = \frac{\Theta_1 - \Theta_w}{\Theta_s - \Theta_w}, \tag{13}$$

where Θ_s is saturation soil moisture, Θ_1 is soil moisture at first soil layer and Θ_w is the wilting point.

[15] The organic soil has a small bulk density, typically about 0.13 g cm^{-3}, while mineral soil has a typical value of about 1.3 g cm^{-3} for the BOREAS sites [*Halliwell and Apps*, 1997]. The organic material usually includes highly permeable fibric peat near the surface [*Letts et al.*, 2000], which dries out quickly, corresponding to rapidly decreasing hydraulic conductivity and decreasing surface evaporation. To include this effect into the above formulation, we used the following values as the saturation point and wilting point.

$$\Theta_s = 0.87 \tag{14}$$

$$\Theta_w = 0.22 \tag{15}$$

The saturation point is based on bulk density and wilting point is used as a tuning parameter rather than pure physical quantity. A similar approach was employed by *Pauwels and Wood* [1999a, 1999b] where the soil resistance was calibrated for each tower site to represent the reduction of evaporation from a surface moss layer.

3. Data

[16] We compared the land surface model with eddy correlation data collected at 39 m on the old aspen tower in BOREAS 1994 and at 4 m on a small tower approximately 40 m from the main tower. The study site (56.629°*N* 106.200°*W*) was located in Prince Albert National Park, approximately 50 km NNW of Prince Albert, Saskatchewan, Canada. The site lies near the southern limit of the boreal forest with the transition to parkland occurring approximately 15 km to the southwest. The soil texture is sandy loam covered by about 8 cm of organic material. A natural fire occurred approximately 70 years ago resulting in an even aged stand of

Table 1. Thermal Properties of Soil Constituents From *Farouki* [1986]

Material	Heat Capacity, $\times 10^3 J K^{-1} m^{-3}$	Thermal Conductivity, $W m^{-1} K^{-1}$
Quartz	1942	8.4
Soil minerals	1942	2.9
Soil organics	2503	0.25
Water	4186	0.6
Ice	1883	2.5
Air	1.2	0.026

aspen with a mean canopy height of 21.5 m and mean diameter at the 1.3 m height of 20 cm. Crown space was limited to the upper 5–6 m, beneath which was a branchless trunk space. The understory was dominated by a uniform cover of hazelnut with a mean height of 2 m. The fetch was at least 3 km in all directions.

[17] Two periods were selected for model evaluation and sensitivity tests during which skies were mostly clear except for a few short rain events. The characteristics of the two periods are described in Table 2. The first period is pre-leaf-out and snow free. According to *Blanken et al.* [1997], the leaf-out began in the third week of May. The second period is well after full leaf-out when the leaf area index (LAI) was approximately constant with time. The parameters used in SPA are listed in Table 3. To force the model in an offline mode, we used meteorology data observed at 39 m on the main tower [*Hartog and Neumann*, 2000], precipitation and longwave radiation from the Airborne Fluxes and Meteorology data set [*Osborne et al.*, 1998] and observed soil data from *Black* [2000]. The model time step is 15 min. Meteorological forcing data are available at 30-min intervals, and precipitation and longwave radiation are available at 15-min intervals. We have interpolated meteorological forcing data into 15-min intervals.

[18] While we consider the data to be the "truth" for evaluation of the model, we must recognize a variety of errors. Random flux errors for individual 30-min. records may be greater than 10% and often greater than 20% for nonstationary transition periods and some nocturnal periods [*Mahrt*, 1998]. Subcanopy measurements may be influenced by subcanopy heterogeneity. Measurements of wind and temperature in the subcanopy are not representative of the entire subcanopy layer particularly at night when a strong surface inversion generally forms in the lowest 5 m [*Mahrt et al.*, 2000].

[19] *Nakamura and Mahrt* [2001] found that the above-canopy eddy correlation measurements in BOREAS were generally within the roughness sublayer, below the surface layer where Monin-Obukhov similarity theory applies. Model uses Monin-Obukhov similarity theory, which generally underestimates mixing in the roughness sublayer. As a probable consequence, the observed vertical temperature difference between the two observational levels (13 m, 39 m) is significantly smaller than that predicted using Monin-Obukhov similarity theory (Figure 2), especially in stable conditions, implying greater mixing compared to Monin-Obukhov similarity theory. The influence of the height dependence of the footprint on the observed vertical temperature difference and fluxes cannot be assessed here, which is always a concern in the roughness sublayer.

4. Comparison With Aspen Data

[20] The model was run for two 10-day periods, one in the pre-leaf-out and the other in the post-leaf-out period.

4.1. Pre-Leaf-Out Period

[21] Comparison of the 10-day averaged diurnal cycle between the model and the observations (Figure 3) indicates that the above-canopy and understory fluxes are simulated by the model reasonably well during the pre-leaf-out period, with some exceptions. Table 4 shows the statistical comparisons between model-derived and tower-observed fluxes. Because of the small LAI during this period, the total latent heat flux is dominated by soil evaporation. The relatively low correlation between the model and observed evaporation (Table 4) is due to poor model simulation of the direct evaporation from the soil immediately after rainfall. Although the rainfall amount is small, the observed subcanopy moisture flux, including direct evaporation from the soil and canopy, reaches about 200 Wm^{-2} immediately after rainfall.

[22] The observed sensible heat flux of nearly 150 Wm^{-2} in the subcanopy for the pre-leaf-out period implies significant buoyancy-generation of turbulence energy within the subcanopy. In sparse canopies with low LAI, the use of the usual constant extinction coefficient (equation (7)) can underestimate turbulent mixing within the canopy, resulting in larger vertical temperature gradients in the subcanopy and higher ground surface temperature than observed during daytime. The model shows a warm bias in 4-m subcanopy temperature during daytime (Figure 3), consistent with underestimation of mixing, although advection and errors in the model radiative transfer could also be factors. The apparent cold bias in the nocturnal subcanopy, could be partly due to the location of the observed temperature near the top of a strong surface inversion of about 5-m depth. Since the model does not consider subcanopy stability in the heat transfer in the subcanopy, the model does not capture the strong nocturnal surface inversion, which results in overestimation of the understory sensible heat flux.

4.2. Post-Leaf-Out Period

[23] The post-leaf-out period is characterized by a significantly higher LAI and lower soil moisture content than in the pre-leaf-out period (Table 2). The simulated latent heat flux and soil heat flux are generally close to the observed values (Figure 4), although the understory latent heat flux is overestimated by 30 Wm^{-2} during the late afternoon from 1500 LST to 1800 LST. The transpiration is controlled by the leaf boundary layer resistance and the stomatal resistance. In unstable conditions with significant wind, the leaf boundary layer resistance is usually smaller than the sto-

Table 2. Characteristics of Selected Periods

	Period	PAI(LAI)[a] Hazelnut/Aspen	Initial Topsoil Moisture
Pre-leaf-out	5–14 May	0.3(0.1)/1.2(0.3)	0.23
Post-leaf-out	30 July to 8 Aug.	3.4(3.2)/3.2(2.3)	0.11

[a]PAI is the plant area index (the sum of leaf area index and stem area index) and LAI is the leaf area index.

Table 3. Model Parameters

Parameter	Value	Unit	Source
Stem specific hydraulic Conductivity	20	m, mol, m^{-1}, s^{-1}, MPa^{-1}	estimated
Root resistivity	50	MPa s g $mmol^{-1}$	estimated
Total fine root biomass	657	g m^{-2}	*Steele et al.* [1997]
Canopy layer capacitance	8000	mmol MPa^{-1}	*Williams et al.* [1996]
Minimum leaf water potential	−2.3	MPa	*Kimball et al.* [1997]
RuBP carboxylation catalytic Rate coefficient at 30°C κ_c	37.8	μ mol g^{-1} N s^{-1}	*Williams et al.* [2001]
Electron transport rate Coefficient at 30°C κ_j	49.0	μ mol g^{-1} N s^{-1}	*Williams et al.* [2001]
Soil color	4	no unit	*Kimball et al.* [1997]

matal resistance. Therefore the transpiration is limited by stomatal resistance and is less sensitive to leaf boundary layer resistance. However, when the wind speed is weak, transpiration can be more limited by the leaf-boundary layer resistance. In late afternoon when the subcanopy air becomes stably stratified, the wind speed within the canopy becomes weak due to less downward transport of momentum. The overestimation of subcanopy wind speed causes underestimation of leaf boundary layer resistance, which causes overestimation of transpiration in late afternoon.

[24] Model errors for the sensible heat flux are greater than those for the latent heat flux. The model overestimates the subcanopy sensible heat flux throughout the diurnal period (Figure 4 and Table 4), possibly due to failure to resolve the vertical structure of the understory. The model employs only two layers of vegetation for application in regional models. The two vegetation layers, here each 10 m deep, assume uniform plant distribution within each layer whereas the actual vertical distribution includes a thick overstory of 5–6 m thickness and a 2-m dense understory near ground. The layer-averaged resistance in the lower canopy layer underestimates the leaf boundary layer resistance for the 2-m understory and therefore overestimates the subcanopy sensible heat flux from the understory. Note that transpiration is less sensitive to leaf boundary layer resistance since it is limited by stomatal conductance in unstable conditions, compared to sensible heat flux that depends more on leaf boundary layer resistance.

[25] In the transition periods with low sun angle, the modeled subcanopy is stably stratified while the atmosphere above the canopy is still unstably stratified. The subcanopy mixing in the model depends on the stability above the canopy and therefore does not recognize the difference between the stability above and within the canopy. As a result, the model incorrectly predicts large negative sensible heat flux in the subcanopy during the transition periods whereas the observed subcanopy heat flux is small (Figure 4).

[26] The model overestimates the daytime sensible heat flux above the canopy by 50 W m^{-2}. This overestimation could be due to omission of the heat storage within the canopy and advection of temperature.

[27] The simulated soil heat flux agrees with the observations reasonably well during the day, but is overpredicted at night (Figure 4). The modeled temperature at the 4-m level is in good agreement with the observed temperature during the day but it is too cool at night giving larger temperature gradient than that observed in the upper canopy. The apparent cold bias could be due to location of the observed temperature just above the subcanopy surface inversion (section 4.1) or could be due to model overestimation of the radiative cooling of leaves.

[28] The leaf radiative cooling is coupled to the leaf boundary layer resistance (equation (8)) through its influence on leaf temperature in the leaf energy balance. The leaf boundary layer resistance represents the transfer of heat and moisture between the leaf surface and adjacent air and in the model is only a function of wind speed. In unstable conditions, the mixing in the canopy is significant, such that the canopy wind speed and air temperature are close to those adjacent to the leaf surface. However, in stable conditions, large differences exist between average canopy wind speed and air temperature and wind speed and air temperature adjacent to the leaf surface due to suppression of mixing by the stable stratification. Without consideration of these differences, the heat exchange between the leaf and the atmosphere is overestimated in stable conditions, which reduces the temperature difference between the radiatively cooled leaf surface and the air. The resulting overprediction of leaf temperature causes more emitted longwave radiation and therefore larger net radiative cooling of the canopy. Due to the overcooling in the subcanopy, the subcanopy air temperature decreases to the saturation point causing overestimation of understory condensation (Figure 4).

5. Influence of Organic Material

[29] To examine the effect of the surface organic layer on the subcanopy processes, simulations were performed with and without organic material in the upper soil layer. During

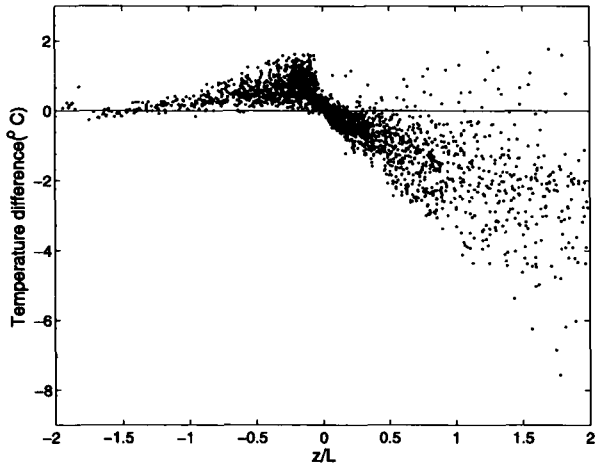

Figure 2. The modeled vertical temperature difference ($T_{13m} - T_{39m}$) minus the observed vertical temperature difference between the displacement height (13 m) and reference height (39 m) as a function of z/L.

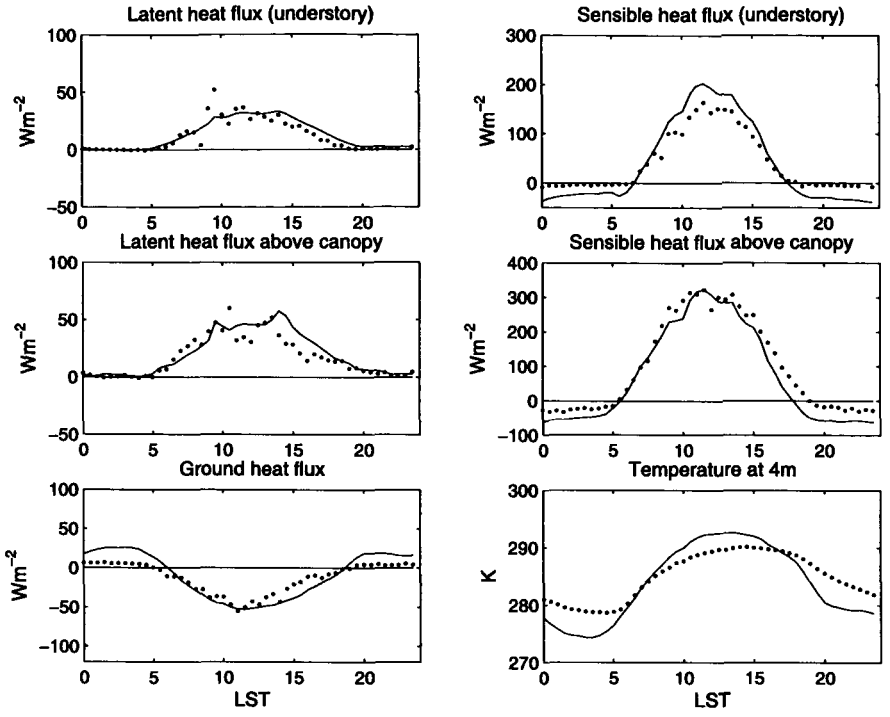

Figure 3. Composite diurnal variation for the observed (circles) and modeled (solid line) variables for the pre-leaf-out period.

the pre-leaf-out period, the simulation with no organic material substantially overestimates soil evaporation and heat flux into the ground and underestimates understory sensible heat flux (Figure 5). The simulation with organic material predicts fluxes much closer to the observed values. The unrealistically large soil evaporation in the simulation with no organic material leads to rapid drying of the soil. The organic material acts as a partial insulator between the soil surface and deep soil. As a result, the surface organic layer makes the subcanopy more unstable during daytime and more stable during night. This improves the comparison with the observations.

[30] The impact of the organic material is smaller after leaf-out because the understory reduces exchange between the ground and the atmosphere (Figure 6). The overestimation of soil evaporation in the simulation without an organic layer leads to underestimation of the vapor pressure deficit in the subcanopy, which in turn leads to underestimation of transpiration. Therefore the sensitivity of latent heat flux to the organic layer is reduced. The simulation with no organic material also overestimates the downward ground heat flux during the daytime, which results in smaller sensible heat flux in the subcanopy.

6. Conclusions

[31] The land surface scheme tested in this study roughly captures the main energy partition between the understory

Table 4. Results of Model Application[a]

Period	Variable	Mean Observation, W m^{-2}	Mean Simulation, W m^{-2}	R, Dimensionless	RMSE, W m^{-2}
Pre-leaf-out					
	H_u	40.62	40.65	0.96	33.62
	H_a	96.51	71.76	0.95	54.71
	LE_u	11.37	12.69	0.62	15.48
	LE_a	17.06	19.76	0.59	21.62
	G	−12.36	−9.00	0.92	14.35
Post-leaf-out					
	H_u	2.39	−0.51	0.69	11.48
	H_a	10.15	4.63	0.88	35.30
	LE_u	21.46	23.76	0.81	23.6
	LE_a	78.02	74.49	0.93	36.42
	G	−5.03	−2.52	0.95	5.29

[a]Subscripts u and a represent understory and above the canopy respectively, R is the correlation coefficient and RMSE is the root mean square error.

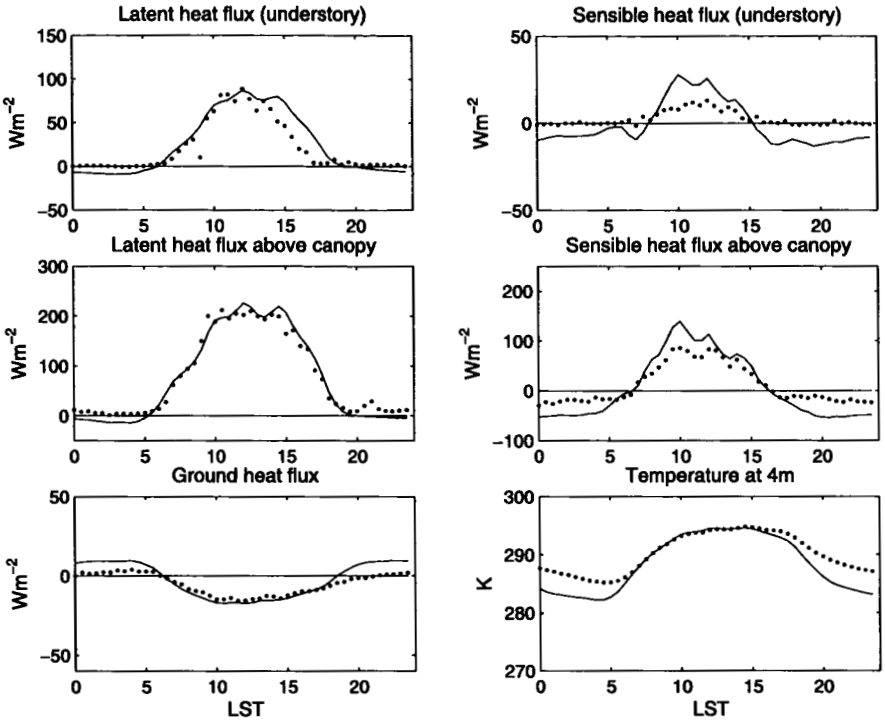

Figure 4. Composite diurnal variation for the observed (circles) and modeled (solid line) variables for the post-leaf-out period.

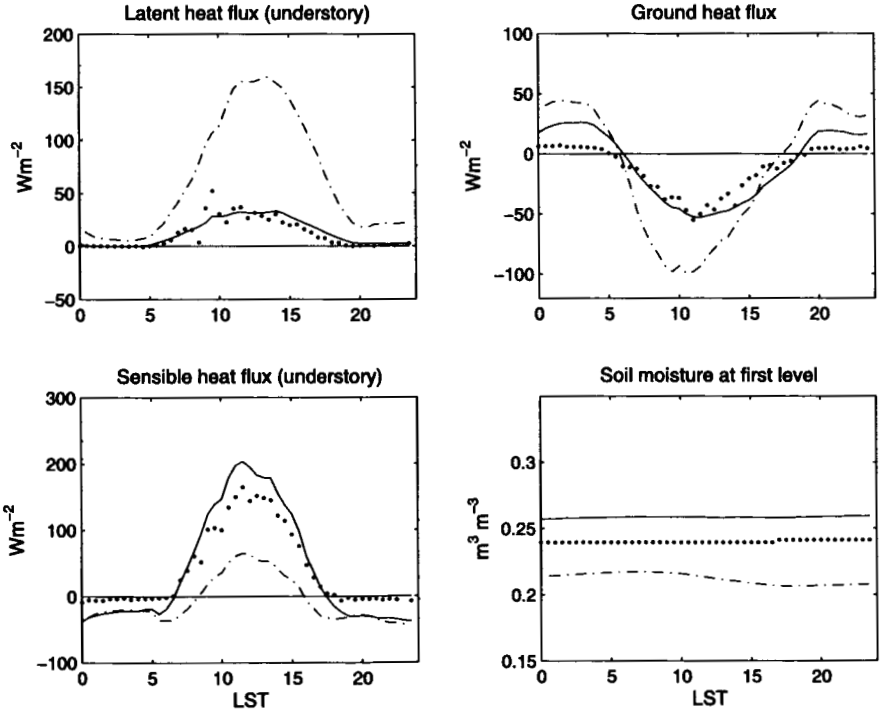

Figure 5. Comparison between the model with (solid line) and without (dash-dot line) the organic layer for the pre-leaf-out period and the observed values (circles).

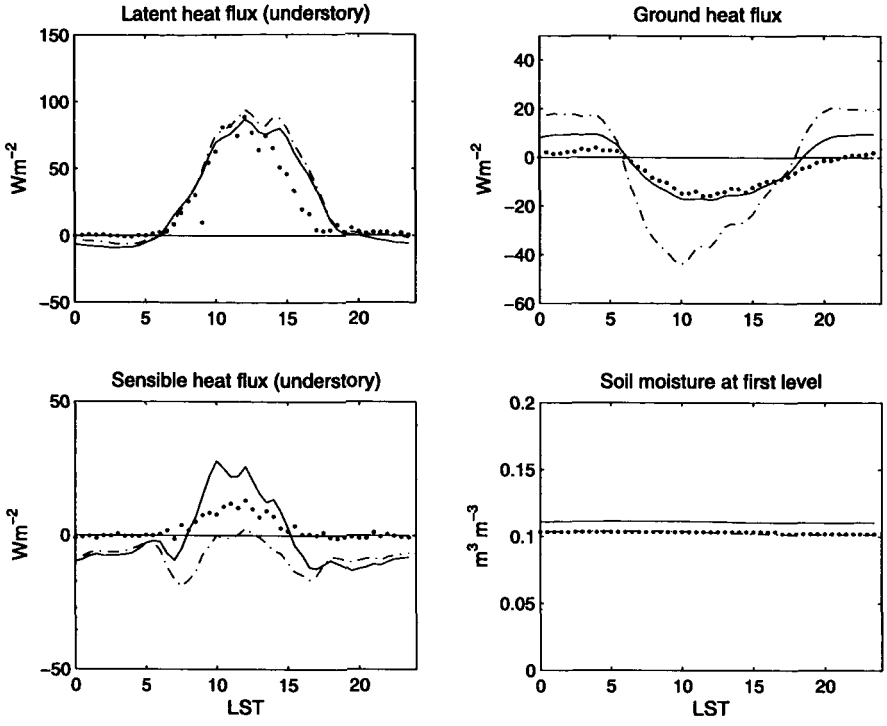

Figure 6. Comparison between the model with (solid) and without (dash-dot line) the organic layer for the post-leaf-out period and the observed values (circles).

and overstory during both pre-leaf-out and post-leaf-out periods. The model also partitions the net energy into latent heat flux and sensible heat flux reasonably well, provided that the modeled upper soil layer includes organic material. Failure to include such material causes substantial overestimation of soil evaporation and subsequent errors in the subcanopy fluxes, particularly prior to leaf-out. The organic material reduces the heat exchange between the ground surface and deeper soil, which makes the subcanopy more stable at night and more unstable during the daytime.

[32] Because of complex interactions between different components of the canopy-ground system, isolating the cause of other errors is difficult without detailed observations of individual processes. For example, underestimation of the leaf boundary layer resistance at night causes overestimation of the transfer of heat from the canopy air to the leaf surface, which leads to overestimation of leaf temperature and overestimation of radiative energy loss from the canopy system. Other errors include overestimation of mixing in the understory due to failure to resolve the vertical structure of the understory.

[33] The model does not directly include the important influence of diurnal variation of subcanopy stability on the mixing. This omission appears to cause overestimation of exchange between the ground and subcanopy air in transition periods and at night when an inversion layer forms in the subcanopy. We are currently examining this influence using data from a variety of open canopies.

[34] **Acknowledgments.** We gratefully acknowledge the collection of data at the aspen site by Andy Black, Xuhui Lee, Ralf Staebler and coworkers. The comments of Jielun Sun, Hank Loesher and two anonymous reviewers are gratefully appreciated. This work was supported by Grant NAG5-11231 from the NASA Terrestrial Ecology Program and Grant 0107617-ATM from the Physical Meteorology Program of the National Sciences Foundation and by the Post-doctoral Fellowship Program of Korea Science and Engineering Foundation (KOSEF).

References

Albertson, J. D., G. G. Katul, and P. Wiberg (2001), Relative importance of local and regional controls on coupled water, carbon, and energy fluxes, *Adv. Water Resour.*, *102*, 1103–1118.

Amthor, J. S. (1994), Scaling CO_2-photosynthesis relationships from the leaf to the canopy, *Photosyn. Res.*, *39*, 321–350.

Amthor, J. S., M. L. Goulden, J. W. Munger, and S. C. Wofsy (1994), Testing a mechanistic model of forest-canopy mass and energy exchange using eddy correlation: Carbon dioxide and ozone uptake by a mixed oak-maple stand, *Aust. J. Plant Physiol.*, *21*, 623–651.

Black, T. A. (2000), BOREAS TF-01 SSA-OA understory flux: Meteorological and soil temperature data, Data set, http://www.daac.ornl.gov, Oak Ridge Natl. Lab., Oak Ridge, Tenn.

Blanken, P. D., T. A. Black, P. C. Yang, H. H. Neumann, Z. Nesic, R. Staebler, G. den Hartog, M. D. Novak, and X. Lee (1997), Energy balance and canopy conductance of a boreal aspen forest: Partitioning overstory and understory components, *J. Geophys. Res.*, *102*, 28,915–28,927.

Bonan, G. B. (1996), A land surface model (LSM version 1.0) for ecological, hydrological and atmospheric studies: Technical description and user's guide, *NCAR Tech. Note NCAR/TN-417+STR*, Natl. Cent. for Clim. Res., Boulder, Colo.

Cellier, P., and Y. Brunet (1991), Flux-gradient relationships above tall plant canopies, *Agric. Forest Meteorol.*, *58*, 93–117.

Choudhury, B. J., and J. L. Monteith (1988), Four layer model for the heat budget of homogeneous land surfaces, *Q. J. R. Meteorol. Soc.*, *114*, 373–398.

Cotton, W. R., et al. (2003), RAMS 2001: Current status and future directions, *Meteorol. Atmos. Phys.*, *82*, 5–29.

Dolman, A. J., and J. S. Wallace (1991), Lagrangian and K-theory approaches in modelling evaporation form sparse canopies, *Q. J. R. Meteorol. Soc.*, *117*, 1325–1340.

Farouki, O. T. (1986), *Thermal Properties of Soils, Ser. on Rock and Soil Mech.*, vol. 11, 136 pp., Trans Tech, Claustal-Zellerfeld, Germany.

Halliwell, D. H., and M. J. Apps (1997), Boreal Ecosystem-Atmosphere Study (BOREAS) biometry and auxiliary sites (soil and detritus data) version 3.02, Can. Forest Serv., Northern Forestry Cent., Edmonton, Alberta.

Hartog, G. D., and H. Neumann (2000), BOREAS TF-02 SSA-OA tower flux: Meteorological and precipitation data, Data set, http://www.daac.ornl.gov, Oak Ridge Natl. Lab., Oak Ridge, Tenn.

Jones, H. G. (1992), *Plants and Microclimate*, Cambridge Univ. Press, New York.

Kaimal, J. C., and J. J. Finnigan (1994), *Atmospheric Boundary Layer Flows*, Oxford Univ. Press, New York.

Katul, G. G., and J. D. Albertson (1998), An investigation of higher-order closure models for a forested canopy, *Boundary Layer Meteorol.*, *89*, 47–74.

Katul, G., et al. (1999), Spatial variability of turbulent fluxes in the roughness sublayer of an even-aged pine forest, *Boundary Layer Meteorol.*, *93*, 1–28.

Kimball, J. S., P. E. Thornton, M. A. White, and S. W. Running (1997), Simulating forest productivity and surface—Atmosphere carbon exchange in the BOREAS study region, *Tree Physiol.*, *17*, 589–599.

Koren, V. I., J. Schaake, K. Mitchell, Q.-Y. Duan, F. Chen, and J. M. Baker (1999), A parameterization of snowpack and frozen ground intended for NCEP weather and climate models, *J. Geophys. Res.*, *104*, 19,569–19,585.

Kustas, W. P. (1990), Estimates of evapotranspiration with a one and two layer model of heat transfer over partial canopy cover, *J. Appl. Meteorol.*, *29*, 704–715.

Letts, M. G., N. T. Roulet, N. T. Comer, M. R. Skarupa, and D. L. Verseghy (2000), Parameterization of peatland hydraulic properties for the Canadian Land Surface Scheme, *Atmos. Ocean*, *38*, 141–160.

Mahrt, L. (1998), Flux sampling errors for aircraft and towers, *J. Atmos. Oceanic Technol.*, *15*, 416–429.

Mahrt, L., and H. L. Pan (1984), A two-layer model of soil hydrology, *Boundary Layer Meteorol.*, *29*, 1–20.

Mahrt, L., X. Lee, A. Black, H. Neumann, and R. M. Staebler (2000), Nocturnal mixing in a forest subcanopy, *Agric. Forest Meteorol.*, *101*, 67–78.

Nakamura, R., and L. Mahrt (2001), Roughness lengths and similarity theory for local and spatially averaged fluxes, *Agric. Forest Meteorol.*, *100*, 47–61.

Norman, J. M., W. P. Kustas, and K. S. Humes (1995), Source approach for estimating soil and vegetation energy fluxes in observations of directional radiometric surface temperature, *Agric. Forest Meteorol.*, *77*, 263–293.

Osborne, H., K. Yound, V. Wittrock, and S. Shewchuck (1998), BOREAS/SRC AMS suite b surface meteorological and radiation data: 1994, Data set, http://www.daac.ornl.gov, Oak Ridge Natl. Lab., Oak Ridge, Tenn.

Pauwels, V. R. N., and E. F. Wood (1999a), A soil-vegetation-atmosphere transfer scheme for the modeling of water and energy balance processes in high latitude: 1. Model improvements, *J. Geophys. Res.*, *104*(D22), 27,811–27,822.

Pauwels, V. R. N., and E. F. Wood (1999b), A soil-vegetation-atmosphere transfer scheme for the modeling of water and energy balance processes in high latitude: 2. Application and validation, *J. Geophys. Res.*, *104*(D22), 27,823–27,839.

Pauwels, V. R. N., and E. F. Wood (2000), The importance of classification differences and spatial resolution of land cover data in the uncertainty in model results over boreal ecosystems, *J. Hydrometeorol.*, *1*, 255–266.

Peters-Lidard, C. D., E. Blackburn, X. Liang, and E. F. Wood (1998), The effect of soil thermal conductivity parameterization on surface energy fluxes and temperatures, *J. Atmos. Sci.*, *55*, 1209–1224.

Physick, W., and J. R. Garratt (1995), Incorporation of a high-roughness lower boundary into a mesoscale model for studies of dry deposition over complex terrain, *Boundary Layer Meteorol.*, *74*, 55–71.

Raupach, M. R., and J. J. Finnigan (1988), Single layer models of evaporation from plant canopies are incorrect but useful, whereas multi-layer models are correct but useless: Discuss, *Aust. J. Plant Physiol.*, *15*, 705–716.

Raupach, M. R., J. J. Finnigan, and Y. Brunet (1996), Coherent eddies and turbulence in vegetation canopies: The mixing-layer analogy, *Boundary Layer Meteorol.*, *78*, 351–382.

Schaake, J. C., V. I. Koren, Q. Y. Duan, K. Mitchell, and F. Chen (1996), A simple water balance model (SWB) for estimating runoff at different spatial and temporal scales, *J. Geophys. Res.*, *101*, 7461–7475.

Sellers, P. J., Y. Mintz, Y. C. Sud, and A. Dalcher (1986), A simple biosphere model (SiB) for use within general circulation models, *J. Atmos. Sci.*, *43*, 505–531.

Sellers, P., et al. (1995), The boreal ecosystem—Atmosphere study (BOREAS): An overview and early results from the 1994 field year, *Bull. Am. Meteorol. Soc.*, *76*, 1549–1577.

Shaw, R. H., and U. Schumann (1992), Large-eddy simulations of turbulent flow above and within a forest, *Boundary Layer Meteorol.*, *61*, 47–64.

Simpson, I. J., G. W. Thurtell, H. H. Neumann, G. Den Hartog, and G. C. Edwards (1998), The validity of similarity theory in the roughness sublayer above forests, *Boundary Layer Meteorol.*, *87*, 69–99.

Steele, S. J., S. T. Gower, J. G. Vogel, and J. M. Norman (1997), Root mass, net primary production and turnover in aspen, jack pine and black spruce forests in Saskatchewan and Manitoba, Canada, *Tree Physiol.*, *17*, 577–587.

Su, H. B., K. T. Paw, and R. H. Shaw (1996), Development of a coupled leaf and canopy model for the simulation of plant-atmosphere interaction, *J. Appl. Meteorol.*, *35*, 733–748.

Sun, J., W. Massman, and D. Grantz (1999), Aerodynamic variables in the bulk formulation of turbulent fluxes, *Boundary Layer Meteorol.*, *91*, 109–125.

Van de Wiel, B. J. H., R. J. Ronda, A. F. Moene, H. A. R. De Bruin, and A. A. M. Holtslag (2002), Intermittent turbulence and oscillations in the stable boundary layer over land. Part I: A bulk model, *J. Atmos. Sci.*, *59*, 942–958.

Wenzel, A., N. Kalthoff, and V. Horlacher (1997), On the profiles of wind velocity in the roughness sublayer above a coniferous forest, *Boundary Layer Meteorol.*, *84*, 219–230.

Williams, M., E. B. Rastetter, D. N. Fernades, M. L. Goulden, S. C. Wofsy, G. R. Shaver, J. M. Melillo, J. W. Munger, S. M. Fan, and K. J. Nadelhoffer (1996), Modelling the soil-plant-atmosphere continuum in a Quercus-Acerstand at Harvard forest: The regulation of stomatal conductance by a light, nitrogen and soil/plant hydraulic properties, *Plant Cell Environ.*, *19*, 911–927.

Williams, M., B. E. Law, P. M. Anthoni, and M. Unsworth (2001), Use of a simulation model and ecosystem flux data to examine carbon-water interactions in ponderosa pine, *Tree Physiol.*, *21*, 287–298.

Y.-H. Lee, Department of Astronomy and Atmospheric Sciences, Kyungpook National University, Daegu 702-701, Republic of Korea. (young@knu.ac.kr)

L. Mahrt, College of Oceanic and Atmospheric Sciences, Oregon State University, Corvallis, OR 97331, USA. (mahrt@coas.oregonstate.edu)

Chapter IV

Effect of stability on mixing in open canopies

Effect of stability on mixing in open canopies

Young-Hee Lee

Department of Astronomy and Atmospheric Sciences
Kyungpook National University
Daegu,702-701, Korea

L. Mahrt*

College of Oceanic and Atmospheric Sciences
Oregon State University
Corvallis, OR 97331 USA

1 June 2005

*corresponding author: Tel:1 541 737 5691; fax: 1 541 737 2540; email: mahrt@coas.oregonstate.edu

Abstract

In open canopies, the within-canopy flux from the ground surface and understory can account for a significant fraction of the total flux above the canopy. This study incorporates the important influence of within-canopy stability on turbulent mixing and subcanopy fluxes into a first-order closure scheme. Toward this goal, we analyze within-canopy eddy-correlation data from the old aspen site in the Boreal Ecosystem - Atmosphere Study (BOREAS) and a mature ponderosa pine site in Central Oregon, USA. A formulation of within-canopy transport is framed in terms of a stability-dependent mixing length, which approaches Monin-Obukhov similarity theory above the canopy roughness sublayer.

The new simple formulation is an improvement upon the usual neglect of the influence of within-canopy stability in simple models. However, frequent well-defined cold air drainage within the pine subcanopy inversion reduces the utility of simple models for nocturnal transport. Other shortcomings of the formulation are discussed.

Key words: Canopy mixing, Cold air drainage, Similarity theory, Subcanopy turbulence

1 Introduction

The need to understand and quantify biosphere-atmosphere exchange has led to substantial interest in within-canopy turbulence. Coherent eddies encompassing the entire canopy often dominate the vertical transport and can lead to fluxes counter to the local vertical gradient within the canopy (Raupach

et al., 1996, Blanken et al., 1998, Finnigan, 2000). The primary source of canopy turbulence is often thought to be downward transport of turbulence from above the canopy.

Modelling within canopy transport normally assumes a Lagrangian or Eulerian approach. This study follows the Eulerian approach. A common modelling approach extrapolates the mixing coefficient from the surface layer above the canopy downward through the canopy using a specified functional dependence on height (e.g., Shuttleworth and Wallace, 1985; Bonan, 1996). Modelling the flux at a given level includes first-order closure (e.g., Wilson et al., 1998), K-epsilon (Katul et al., 2004), second-order closure (e.g., Poggi et al., 2004) and large-eddy models (e.g., Shaw and Shumann, 1992, Albertson et al., 2001). These models generally require a flux-gradient approximation at some level of parameterization, often expressed in terms of a mixing length (e.g., Raupach et al., 1996; Wilson et al., 1998; Katul et al., 2004; Poggi et al., 2004).

Using a mixing-layer analogy, Raupach et al. (1996) introduced the shear-length for describing turbulence above the canopy top. This length scale has been incorporated into several mixing-length formulations. For example, Wilson et al. (1998) proposed a height-dependent mixing length that approaches the shear length scale near canopy top. Poggi et al. (2004) employed a length scale related to element diameter and the distance from the ground in addition to the shear-length scale in the mixing length formulation. On the other hand, Massman and Weil (1999) focused on the influence of local leaf area index on the mixing length and related the mixing length inversely to the local drag coefficient such that the mixing length was smaller at levels with more local leaf area index.

Less attention has been given to the mixing length for momentum and

heat within open canopies and the potential role of surface heating and cooling at the ground/understory surface. Buoyancy effects in the subcanopy have been included in a few LES models (e.g. Dwyer et al., 1997; Albertson et al., 2001). Brunet and Irvine (2000) investigated the influence of stability on the shear-length scale for an open canopy and suggested that the primary effect of atmospheric stability is to modify the shear-length scale through change of wind speed and wind shear at the canopy top. However, they did not examine the influence of local stability on mixing within the canopy. Based on eddy-correlation data, Mahrt et al. (2000) found that the drag coefficient in the subcanopy at the old aspen site in BOREAS decreased with increasing subcanopy stability but did not increase from near-neutral to unstable conditions. However, they did not provide a formulation for such transport.

Much of the work above is influenced by observations of the important contribution of coherent structures to the within-canopy flux, appearing to originate above the canopy, often conceptualized in terms of within-canopy sweeps and ejection (e.g. Paw U et al. 1992). Such structures do not penetrate the strongly stratified subcanopy associated with a open overstrory and clear nocturnal conditions (Mahrt, et al . 2000). In open canopies, daytime subcanopy turbulence may be generated more by local buoyancy than downward transport of turbulence from above the canopy. Resulting underestimation of subcanopy turbulence can significantly influence estimates of land-surface exchange in open canopies.

In this study, we analyze eddy-correlation data from two open canopies and construct a simple subcanopy formulation of the mixing length, which includes the influence of subcanopy stability.

2 Data

This study analyses eddy-correlation data collected from a mature ponderosa pine site in central Oregon, USA (Schwartz et al., 2004). Turbulent fluxes were measured above the canopy and at two levels within the canopy, one in the crown space (10 m) and one in the trunk space (3 m). The flux at 3m was measured at a subcanopy tower separated from main tower by 40 m to avoid disturbance of the flow at the tower base. Wind speed and air temperature were measured at 5 levels (3 m, 6 m, 10 m, 20 m, 30 m) on the main tower. Air temperature was also measured on the subcanopy tower at 1 m, 2 m and 3 m.

This study also analyzes tower data collected at five levels on the main tower in the old aspen site in BOREAS (Sellers et al., 1995; Blanken et al., 1997). Momentum fluxes were computed from 30-min records. The instrumentation at the old aspen site is detailed in Blanken et al. (1997). Here we include only the post leafout period when the data were the most complete.

Both canopies are characterized by a LAI of about 3 (Table 1), which we refer to as open canopies. While such values are not low compared to sparser canopies with a LAI of unity or less. Here, "open" refers to large diurnal variation of atmospheric stability within the canopy layer due to radiative heating and cooling of the ground/understory surface. The nocturnal temperature profiles at the old aspen site correspond to a strong surface inversion in the lowest 5 m and weaker stratification above (Mahrt et al., 2000). The stratification of the daytime aspen canopy layer is near neutral. The diurnal variation of the stratification at the pine site is much greater than that at the aspen site in spite of similar LAI values for the overstory. The strong diurnal variation of stability at the pine site is due partly to more clumping,

dryer surface conditions, less understory, higher sun angles, much less cloud cover and minimal integrable atmospheric water vapour content, all acting to increase the radiative heating and cooling of the ground surface/understory.

Fluxes are computed using deviations from 10-minute averages and then are averaged over one hour to reduce random flux errors. Fluxes in the subcanopy are subject to some uncertainty from possible flux loss due to pathlength averaging and expected horizontal heterogeneity above the nonuniform understory. Based on our assessment of momentum flux loss due to pathlength averaging, by comparing with three-dimensional hotfilm anemometry (unpublished), we have determined that pathlength average can lead to significant momentum flux loss in the lowest meter above short grass and that existing correction formulas are not suitable. However, we have not carried out suitable measurements in the subcanopy.

Table 1 Site description.

Sites	Average canopy height (m)	LAI	displacement height (m)	roughness length (m)
Old aspen	20.1	3.0	13.4	2.0
Pine	15.5	3.3	11	1.2

The displacement height for the aspen site (Table 1) is taken from Nakamura and Mahrt (2001) while the displacement height for the pine site was estimated by trial and error to produce the best fit to Monin-Obukhov similarity theory at the top of the tower for near-neutral conditions.

3 Transport in the canopy layer

3.1 Mixing length

We express the within-canopy flux in terms of an eddy diffusivity

$$\overline{u'w'} = -K_m \frac{\partial \overline{u}}{\partial z}, \tag{1}$$

In the data analysis below, the momentum flux will be computed as the magnitude of the vector momentum flux and the mean shear will be computed as the magnitude of the vector shear without concern for alignment of the wind and shear vectors.

The eddy diffusivity is formulated as

$$K_m = l_m u_* \tag{2}$$

where l_m is the mixing length for momentum and u_* is the height dependent friction velocity in the canopy defined as the square root of the magnitude of the momentum flux. The mixing length for momentum

$$l_m \equiv \frac{u_*}{\partial u / \partial z} \tag{3}$$

is evaluated directly from eddy-correlation and wind profile measurements at the pine and aspen sites.

The mixing length for momentum at the aspen site was computed from the observed fluxes and vertical gradients for three different stability classes, based on the stability at the top of the tower (39-m level): the unstable case ($-1 < (z-d)/L \leq -0.1$), the near neutral case ($-0.1 < (z-d)/L \leq 0.1$) and the stable case ($0.1 < (z-d)/L \leq 1$). For this study, transition periods are eliminated and we analyze only daytime data between 1000 and 1600 local time and nocturnal data between 2100 and 0500 local time. Vertical gradients are computed from simple finite differencing.

The resulting mixing length for momentum, averaged over all of the qualifying records, increases slowly with height in the subcanopy and more rapidly with height above the canopy (Figure 1). The mixing length is much smaller in the subcanopy in stable conditions compared to neutral and unstable conditions, probably due to weaker downward transport of turbulence energy into the canopy layer. The profile of the mixing length for the pine site is based on only three levels and is not shown.

To formulate the height dependence of the mixing length, we recognize that height above the ground surface influences the within-canopy mixing while the mixing length must approach Monin-Obukhov similarity theory in the surface layer above the canopy roughness sublayer. For neutral conditions within the canopy, we propose the simple height dependence

$$l_{mn} = \beta z \tag{4}$$

where l_{mn} is the neutral value of the mixing length for momentum, z is the height above the ground surface. β is an empirical coefficient to-be-determined and not necessarily equal to the von Karman constant. The nondimensional coefficient β is estimated from the observed profiles, yielding 0.18 at the aspen site and 0.30 at the pine site. Either β depends on canopy architecture, or, it cannot be estimated from our observations within a factor of two.

In order that the mixing length satisfy Monin-Obukhov similarity theory in surface layer above the canopy, β at the top of the roughness sublayer, z_r, should approach

$$\beta = 0.4(z_r - d)/z_r \tag{5}$$

where d is the displacement height and z_r can be estimated following Raupach

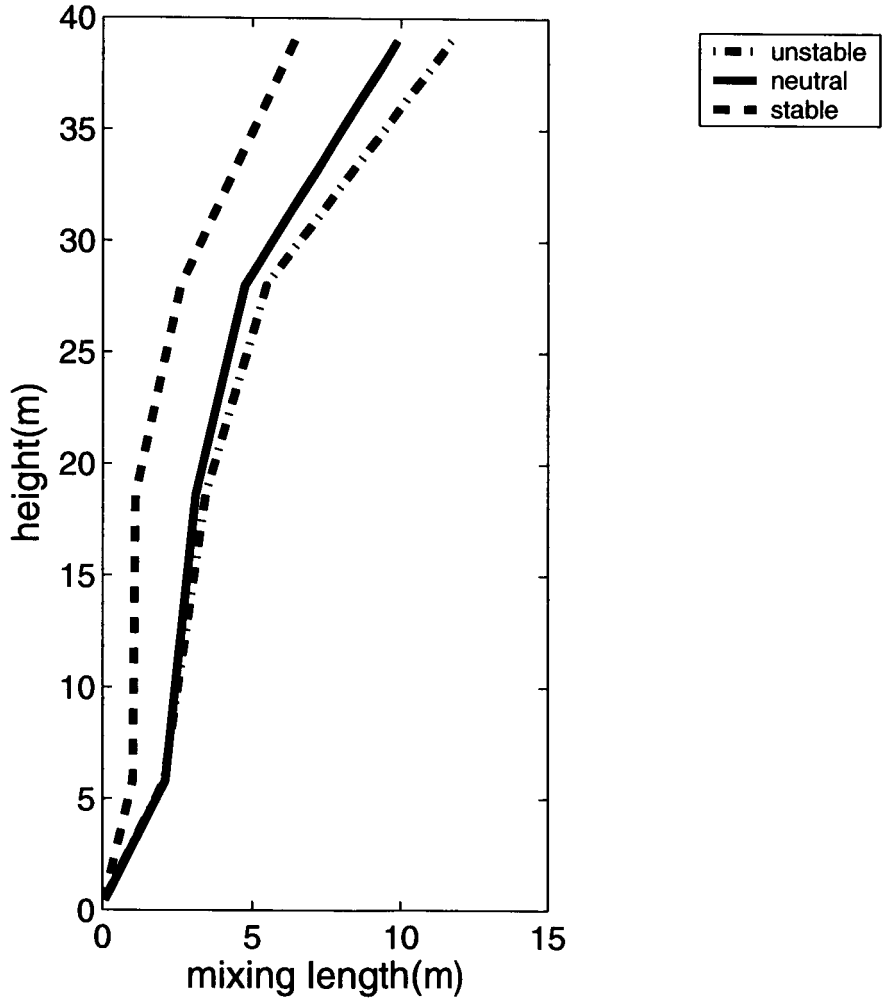

Figure 1: Height dependence of the mixing length for momentum estimated from vertical profiles at the old aspen site for the post leafout period.

(1994) as $z_r = d+2(h-d)$ where h is the canopy height. Assigning $d = C\,h$,

$$\beta = 0.4[1 - \frac{C}{2-C}] \tag{6}$$

As an exercise, we specify the displacement height to be 2/3h (C=2/3), in which case β becomes 0.2, which is closer to value at the aspen site. For the open canopies of this study, the value of C may be smaller leading to a somewhat larger value of β. Although there is no reason to expect the profile fit to Eq. 4 to agree with Eq. 6, we note that they both predict comparable magnitudes. Below, we use values of β from the profile fit since it avoids estimating the height of the roughness sublayer and displacement height.

3.2 Stability influence on momentum transfer

In analogy to Monin-Obukhov similarity theory, the stability-dependent mixing length can be expressed as

$$l_m = \frac{\beta z}{\phi_m}. \tag{7}$$

Here, the nondimensional wind shear is defined as

$$\phi_m \equiv \frac{\beta z \partial \overline{u}/\partial z}{u_*}. \tag{8}$$

We do not expect ϕ_m to closely follow Monin-Obukhov similarity theory within the canopy because the stress varies rapidly with height. The flux-gradient relationship in the subcanopy will be limited in different ways by the distance from the ground surface/understory, the spacing between the trunks and the distance from the overstory. However, both the heat flux and the friction velocity are important influences so that the local Obukhov length, Λ, is one of the governing length scales. So that the stability approaches

Monin-Obukhov similarity theory at the top of the roughness sublayer, we formulate the subcanopy stability parameter as

$$\frac{z}{\Lambda}(\frac{z_r - d}{z_r}) \tag{9}$$

where the ratio in parentheses allows continuity of the local canopy stability functions to that above the roughness sublayer.

The nondimensional wind shear (Figures 2-3) varies more slowly with stability than predicted by the normal stability functions for Monin-Obukhov similarity theory at both the aspen and pine sites. The relationship between the nondimensional shear and stability exhibits substantial scatter, which could be due partly to the difficulty of measuring fluxes in the subcanopy (Section 2) and the omission of additional physical influences. In spite of the large scatter, inclusion of the influence of subcanopy stability is needed, although more data is required to determine the optimum stability function. The disagreement between the observations and the usual Monin-Obukhov stability functions is greatest at the lowest level of the aspen site, just above the understory, where the stability dependence is almost undetectable. Inclusion of a displacement height for the thick understory of 2-m height increases the rate at which the nondimensional shear changes with stability and thus increases the stability influence. However, this increase is not nearly large enough to allow reasonable approximation with the usual Monin-Obukhov stability functions. However, the agreement with the Monin-Obukhov stability functions improves with height (Figure 2).

The smaller observed nondimensional shear (greater mixing) for stable conditions, compared to the prediction by the usual stability functions, is presumably due to mechanical generation of mixing by the vegetation elements, not included in Monin-Obukhov similarity. However, the nondimensional shear above the canopy is also observed to be smaller than predicted

by linear dependence on stability for strong stability (e.g. Beljaars and Holtslag, 1991; Cheng and Brutsaert, 2005). The larger nondimensional shear for unstable conditions, most evident at the pine site, could be due to the partial constraint of the convective eddies by the height of the overstory, which enters as an additional length scale not included in Monin-Obukhov similarity.

3.3 Stability influence on heat transfer

The pine canopy is characterized by unstable stratification (Figure 4) and significant upward heat flux in the daytime and strong stable stratification at night. The diurnal variation of the within-canopy stability is less at the aspen site as discussed in Section 2.

The heat transport is expressed in terms of the eddy diffusivity for heat

$$\overline{\theta' w'} = -K_h \frac{\overline{\partial \theta}}{\partial z} \tag{10}$$

The eddy diffusivity for heat can be related to the mixing length for heat. The mixing length for heat for near neutral conditions is difficult to estimate from data because of large scatter. We equate the neutral values of the mixing lengths for heat and momentum but allow them to have different stability functions.

The nondimensional temperature gradient is defined as

$$\phi_h \equiv \frac{\beta z \partial \overline{\theta} / \partial z}{\theta_*} \tag{11}$$

where

$$\theta_* \equiv -\frac{\overline{w'\theta'}}{u_*} \tag{12}$$

was evaluated at the two eddy-correlation levels at mature pine site, one in the crown space (10m) and the other in the trunk space (3m). This

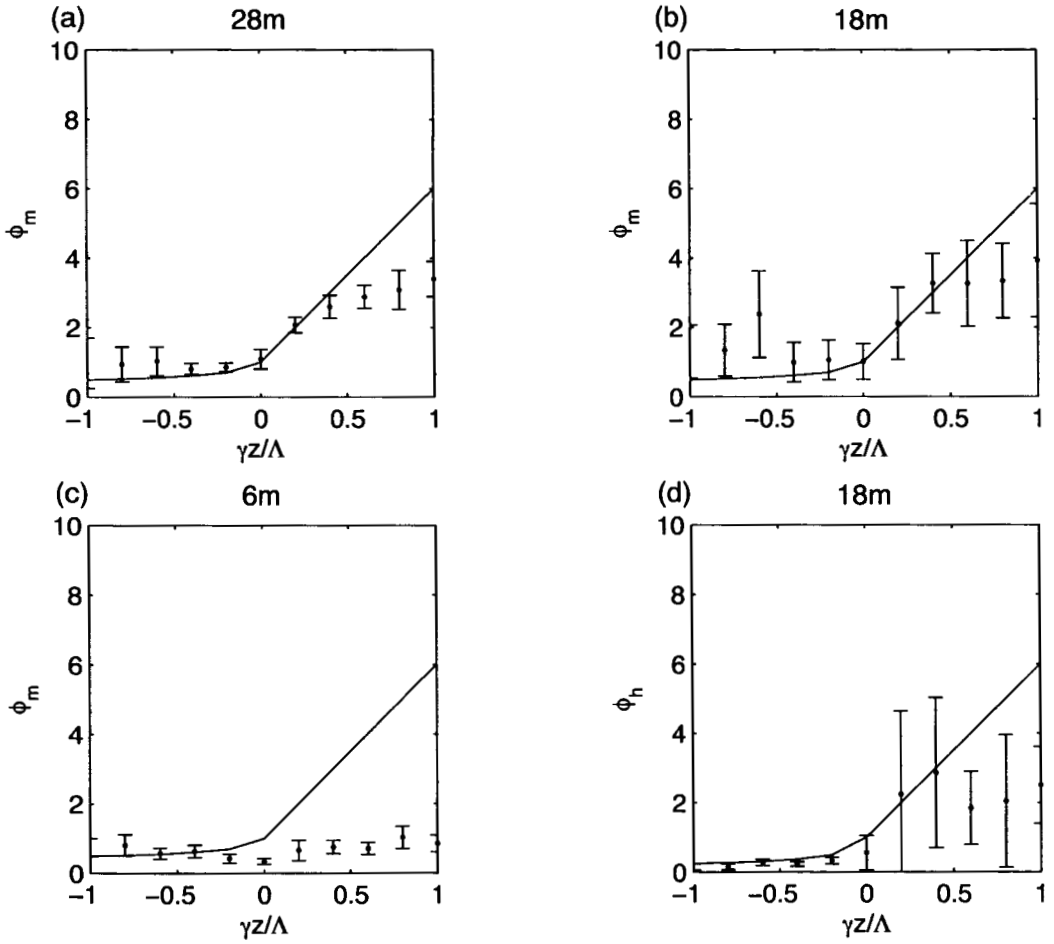

Figure 2: The nondimensional shear as a function of stability for 3 different levels at the Aspen site and the nondimensional temperature gradient at the 18-m level. The top of the canopy is approximately 20 m. The solid line corresponds to the stability function from Dyer (1974) applied to γ z/L, where z is the height above the ground surface. $\gamma \equiv \frac{z_r - d}{z_r}$.

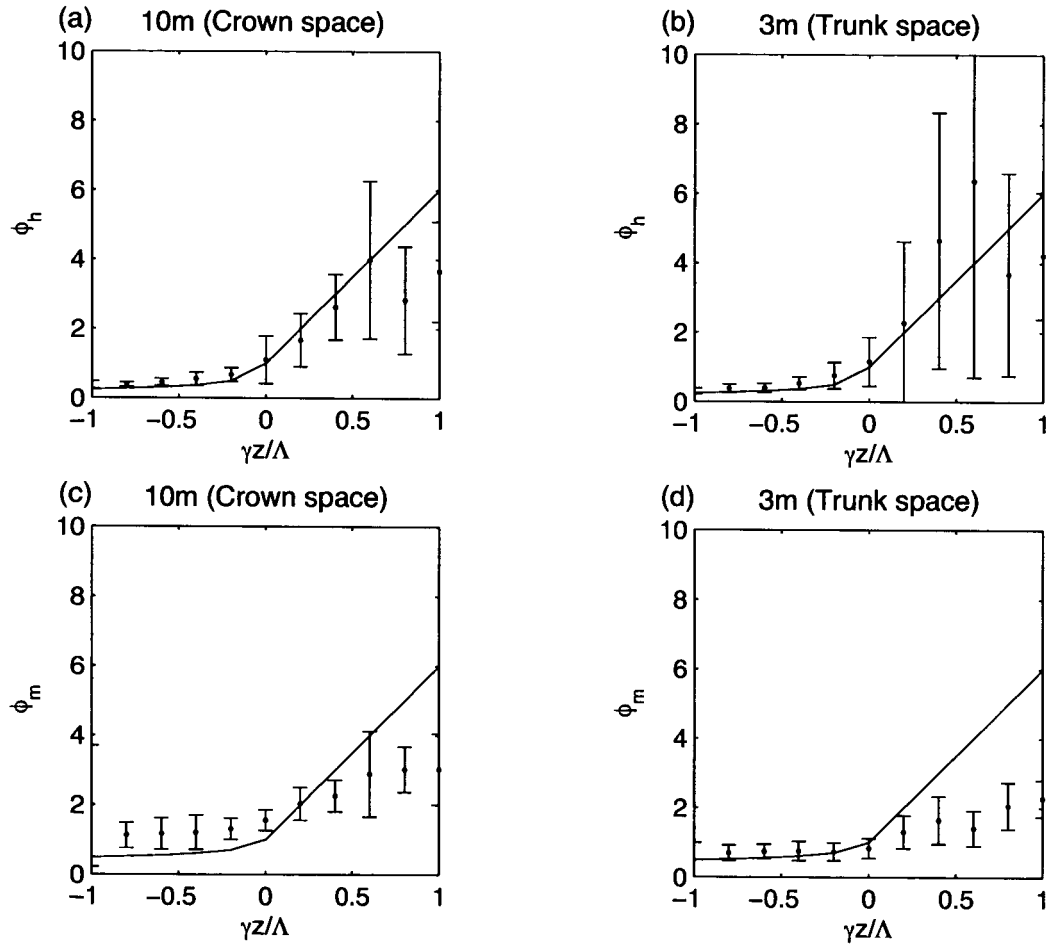

Figure 3: The nondimensional shear and nondimensional temperature gradient for two levels at the pine site. The top of the canopy is approximately 15 m. The solid line corresponds to the stability function from Dyer (1974) applied to γ z/L. $\gamma \equiv \frac{z_r - d}{z_r}$.

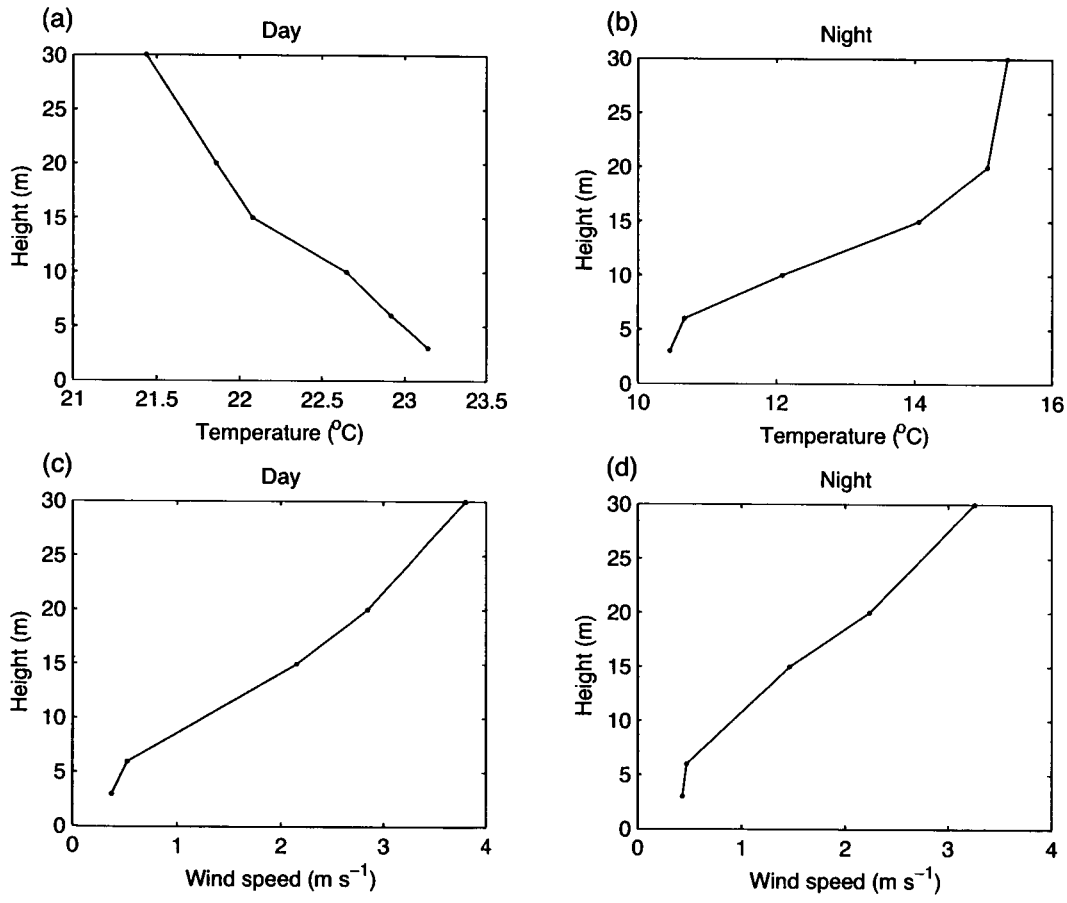

Figure 4: Averaged profiles of wind speed and temperature at the Pine site.

relationship was also evaluated at the 18-m level at the aspen site where the heat flux and vertical temperature gradients are best defined for evaluation of the relationship. Evaluation of vertical gradients must recognize that the time-averaged temperature can vary horizontally in the subcanopy on the microscale, especially close to the ground surface at the pine site. We use only data where the horizontal temperature difference at 3m between two subcanopy towers and the main tower is less than 0.5 K, which eliminates some of the most stable cases.

At the pine site, the nondimensional temperature gradient more closely follows the Monin-Obukhov stability function compared to that for momentum (Figure 3). Apparently, the influence of diabatic heating in the canopy layer and associated height-dependence of the heat flux does not strongly modify the dependence of the flux-gradient relationship on stability. However, the influence of stability on the nondimensional temperature gradient is not as well defined for the aspen site (Figure 2). At both sites, the scatter is large for stable conditions, indicating large errors in the flux calculations and/or additional influences on the nondimensional temperature gradient, not included in z/Λ.

Although the nondimensional temperature gradient for heat exhibits a stronger dependence on within-canopy stability compared to the nondimensional shear, the present data do not allow confident assessment of the vertical structure of the differences between the mixing lengths for heat and momentum.

With the above findings and uncertainties, we formulate the eddy diffusivity for heat as

$$K_h = \frac{l_{mn} u_*}{\phi_h} \tag{13}$$

where l_{mn} is the mixing length for momentum for neutral conditions (Eq. ??),

u_* is the height-dependent friction velocity and ϕ_h is the nondimensional temperature gradient with the usual Monin-Obuhkov stability functions, which formally enter here as the stability dependence of the mixing length. Since the dependence of the nondimensional shear on stability is less certain than that for temperature, we choose to follow the traditional top down approach of extrapolating the stress downward from the surface layer using a profile model. Ultimately, a separate equation for the momentum budget is needed for the canopy layer.

4 Influence of LAI on canopy momentum flux

Estimation of the diffusivity for heat from the stability-dependent mixing length in the previous section requires information on the mean profile of the local friction velocity in the canopy, which we now parameterize based on the observed behavior. The ratio of the subcanopy friction velocity to that above the canopy increases with increasing instability (Figure 5), presumably due to greater mixing in the daytime as suggested by larger within-canopy mixing lengths in the daytime (Figure 1). We will include the influence of the vertical structure of the LAI on the height dependence of the friction velocity. For the aspen site, the downward accumulated Leaf Area Index (LAI_{acc}) is estimated based on the canopy structure of the aspen (Blanken et al. 1997). We then relate the momentum flux in the mean wind direction to stability and canopy architecture as

$$u_*^2 = u_{*o}^2 exp[-2\alpha(LAI_{acc})^{0.5}] \tag{14}$$

where α is a stability-dependent coefficient evaluated below and u_{*o} is the friction velocity in the surface layer above the canopy. The exponential form allows the momentum flux to approach the surface layer value above the

canopy. The square root dependence on the accumulated LAI was determined as a reasonable fit to near-neutral conditions. Although Eq. 14 adequately simulates the vertical profile of local friction velocity at the aspen site, the significantly deviations of the observed from the predicted values at the pine site (Table 2) either indicate inadequate vertical resolution of the flux profiles at the pine site or imply that the local friction velocity for near-neutral conditions are affected by factors other than accumulated LAI. The pine site is characterized by greater foliar clumping and clumping of trees, allowing easier vertical exchange and greater within-canopy momentum flux compared to Eq. 14.

Table 2. Vertical profile of the height-dependent friction velocity normalized to the value above the canopy for neutral conditions. The ratio is defined as the local u_* divided by friction velocity above the canopy, u_{*o}.

Aspen site				Pine site			
z(m)	LAI_{acc}	Ratio		z(m)	LAI_{acc}	Ratio	
		observed	estimated			observed	estimated
28	0	1	1	30	0	1	1
18.6	1.	0.49	0.37	10	1.5	0.62	0.29
5.8	3.	0.19	0.18	3	3	0.13	0.18
0.45	6.5	0.05	0.08				

Using the observed fluxes, we have computed α from Eq. 14. We have visually fit the stability dependence of α for unstable conditions as (Figure 5)

$$\alpha = \frac{1.0}{(1 - 4z/L)^{0.25}}. \tag{15}$$

Application of this stability dependence in Eq. 14 leads to reasonable prediction of the ratio of the subcanopy stress to the stress above the canopy for

unstable conditions at both the aspen and pine sites. For stable conditions, α appears to be independent of stability (Figure 5). While the above inclusion of differences between stable and unstable conditions is rather crude, it is expected to be an improvement upon the usual practice of neglecting the influence of stability on the subcanopy transport. However, with the frequent occurrence of drainage flow and capping inversion at the pine site (Section 5), the vertical communication is too weak to apply Eq. 14 and a separate time-dependent momentum equation is needed near the surface.

5 Nocturnal structure of the pine subcanopy

Part of the large scatter for the nocturnal flux-gradient relationship at the pine site is due to cold air drainage and wind directional shear. While some cold air drainage also occurred at the aspen site (Lee, 1998), it seemed to be less common and have less impact on the vertical structure of the flow within the canopy compared to the pine site. With cold air drainage at the pine site (westerly flow near the surface), the nocturnal stratification is much stronger and concentrated at the top of the cold air drainage, between 10 and 20 m (Figure 4). For individual hours, the stratification is often confined to a single 5-m observational layer but is vertically spread in the composited profile of Figure 4. As a result, the nocturnal vertical temperature gradients at the 10 m level are probably often seriously underestimated. A network of wind and temperature measurements indicates cold air drainage down the eastward descending slope, just west of the tower site. In the absence of cold air drainage, the subcanopy flow is generally from the south and the stratification above the understory is weaker.

The joint frequency distribution between the wind speed at 30 m and the temperature difference in canopy between 3m and 20m (Figure 6) indicates

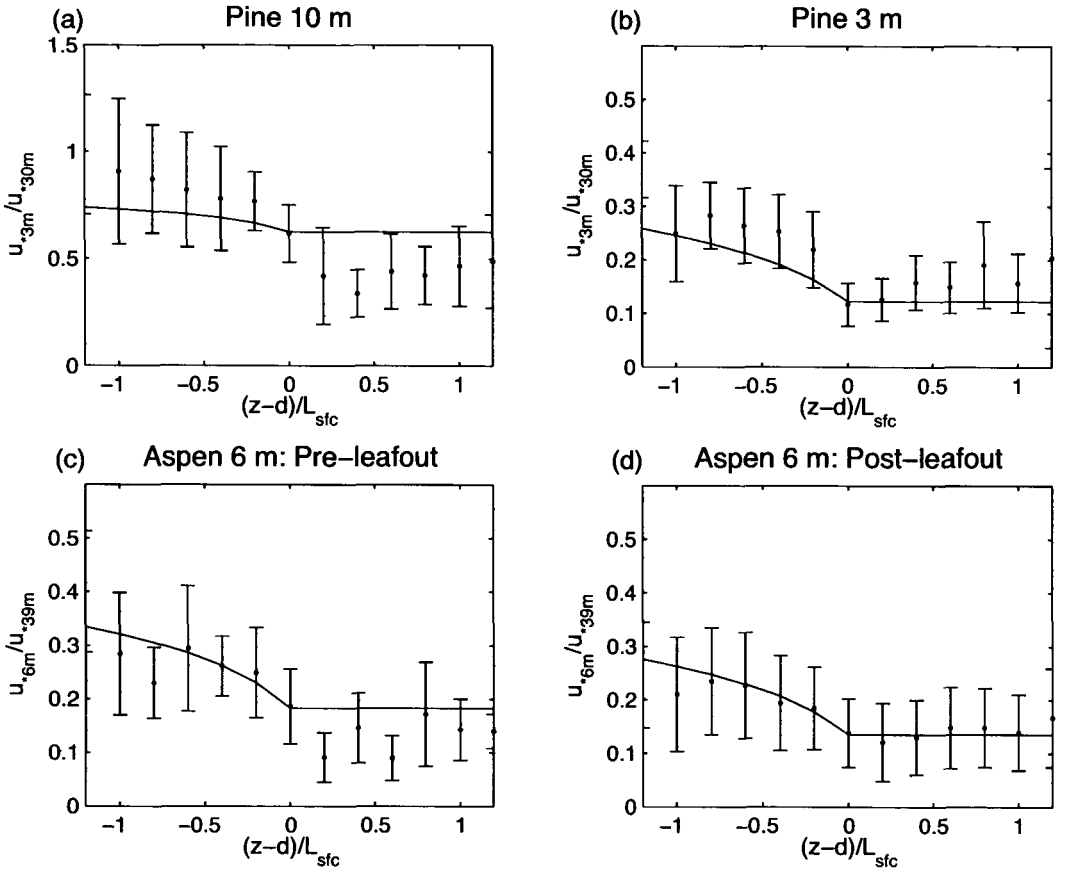

Figure 5: The ratio of friction velocities as a function of stability where L_{sfc} is the Obukhov length based on fluxes at the 39-m level, assumed to be in the surface layer. The solid line represents the prediction of the ratio based on the fit to Eq. 15 for unstable conditions and independent of the stability for stable conditions.

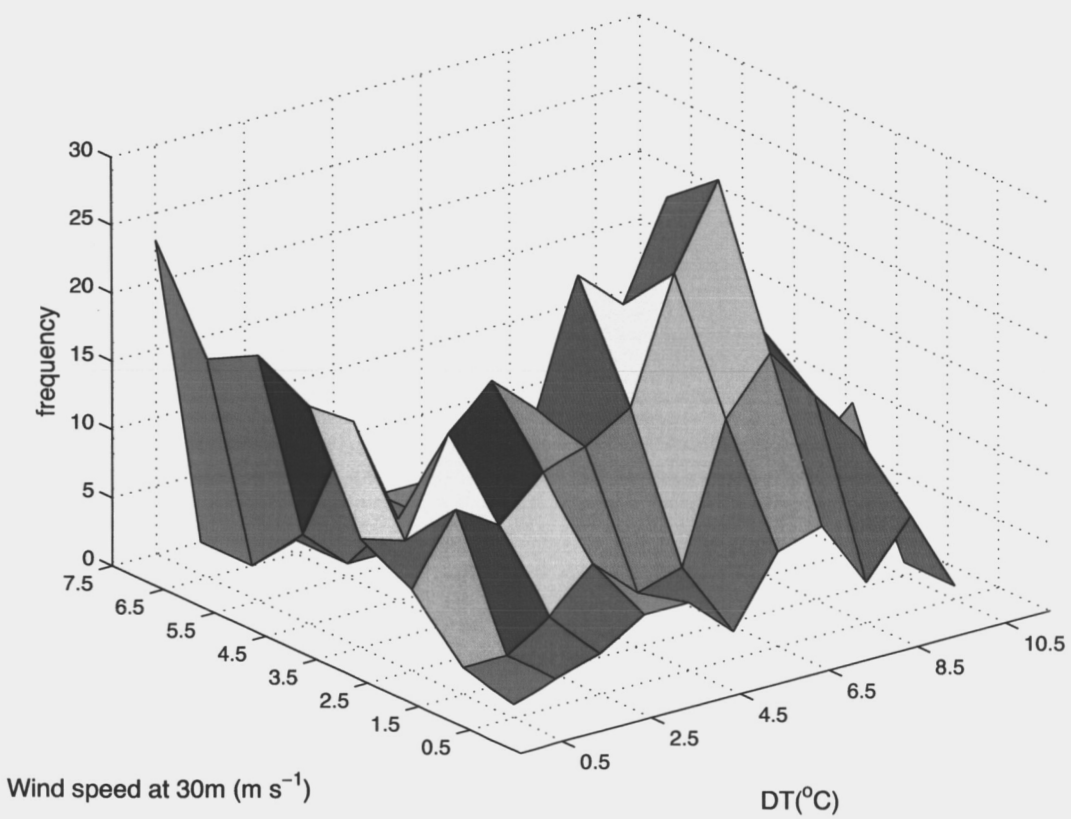

Figure 6: Joint frequency distribution of the 30 m wind speed and the canopy inversion strength between 3 and 20 m (DT) at the pine site. Color pattern is only for visualization.

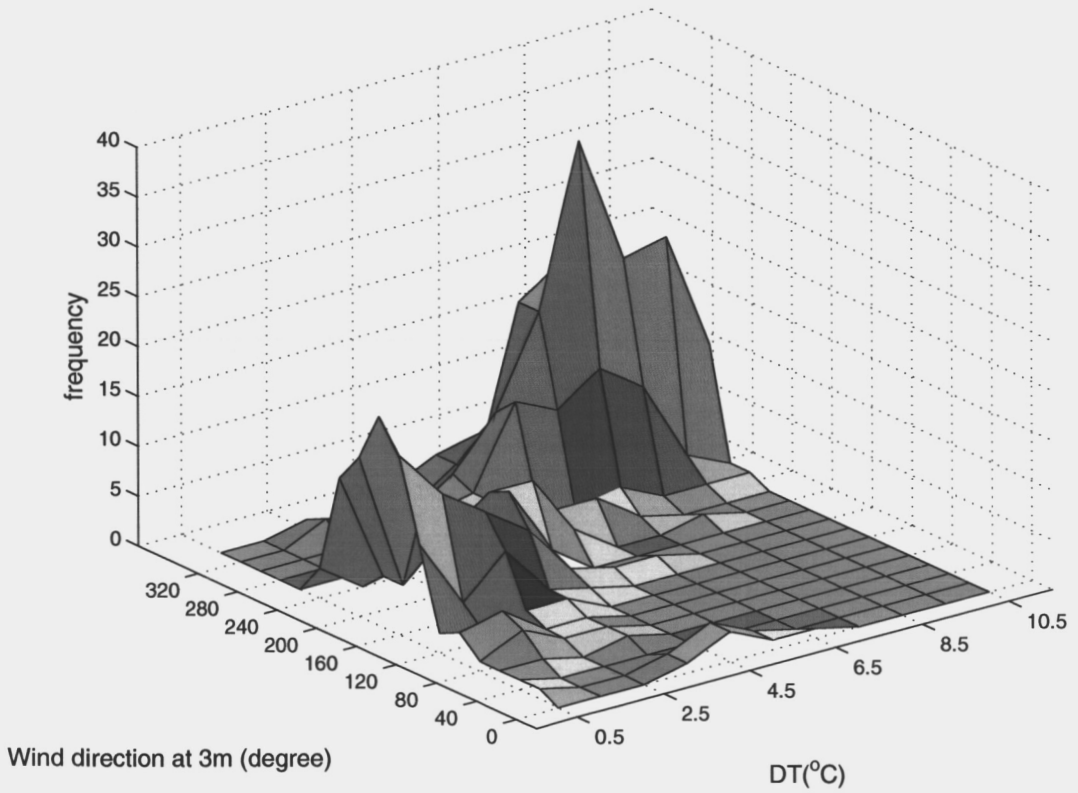

Figure 7: Joint frequency distribution of subcanopy 3-m wind direction and the canopy inversion strength between 3 and 20 m (DT) at the pine site.

that most of the nights with inversions greater than a few degrees occur with weak winds above the canopy and that strong winds generally correspond to weaker inversions of less than a few degrees. Almost all of the strong inversions occur with westerly subcanopy drainage flow. Weak canopy inversions correspond to southerly subcanopy flow more aligned with the flow above the canopy (Figure 7). The systematic development of subcanopy drainage flows and associated directional shear and strong inversions at the pine site probably account for much of the large scatter in the flux-gradient relationship. Inclusion of the directional shear associated with the drainage flow requires a separate momentum equation for the subcanopy.

6 Summary

The structure of turbulent transport within the canopy has been examined with eddy-correlation measurements from a relatively open ponderosa pine site and from an aspen site. The dependence of the nondimensional temperature gradient and mixing length for heat on stability approximately follow MO similarity theory even though the assumptions required for such similarity theory are not met. The nondimensional shear and mixing length for momentum deviate more from MO similarity. Deviations are most significant close to the top of the understory where the mixing coefficient depends much less on stability than would be estimated from the MO stability functions. Inclusion of the influence of subcanopy stability on subcanopy transfer is expected to improve formulation of transport of heat, momentum and presumably trace gases such as carbon dioxide.

Subcanopy drainage flows with strong capping inversions are common at the pine site and contribute to deviations from simple similarity theory. Accurate formulation of the within-canopy transport for these situations would

require a separate subcanopy momentum equation. We are collecting data with better vertical resolution to determine the influence of this inversion on decoupling between surface fluxes and fluxes above the canopy.

In spite of these difficulties and uncertainties with the above analyses, it is possible to improve upon existing simple formulations of within-canopy mixing, which completely neglect the dependence of within-canopy mixing on the stability. For example, an eddy diffusivity for heat has been constructed (Eq. 13) from the mixing length for neutral conditions (Eqs. 4, 5), the usual Monin-Obukhov stability functions and the formulation of the profile of the within-canopy friction velocity scale (Eqs. 14, 15), which depends on downward accumulated LAI and within-canopy stability.

More complete subcanopy flux profiles and their microscale variability are needed to provide more dependable profiles of the mixing length for heat and the dependence of the nondimensional shear on canopy architecture and within-canopy stability.

ACKNOWLEDGMENTS

We gratefully thank Michael Unsworth, Reina Nakamura and Gaby Katul for their useful comments on the manuscript and Andy Black, Xuihui Lee and the rest of the BOREAS aspen team for the data from the aspen site. We also acknowledge Meredith Kurpius and John Wong for data collection at the pine site and Dean Vickers for data processing and flux calculations. This work was supported by Grant NAG5-11231 from the NASA Terrestrial Ecology Program, Grant FG0203ER63653 from the Department of Energy Terrestrial Carbon Program and Grant 0107617-ATM from the Physical Meteorology Program of the National Sciences Foundation

References

Albertson, J. D., Katul, G. G., Wiberg, P., 2001. Relative importance of local and regional controls on coupled water, carbon, and energy fluxes. *Adv. Water Res.* , 24, 1103-1118.

Beljaars, A. C. M., and Holtslag, A. A. M., 1991. Flux parameterization over land surfaces for atmospheric models. *J. Appl. Meteorol.*, 30, 327-341.

Blanken, P.D., Black, T. A., Yang, P. C., Neumann, H. H., Nesic, Z., Staebler, R., den Hartog, G., Novak, M. D., Lee X., 1997. Energy balance and canopy conductance of a boreal aspen forest: partitioning overstory and understory components. J. Geophys. Res. 102, 28915-28927.

Blanken, P.D., Black, T. A., Neumann, H. H., den Hartog, G., Yang, P. C., Nesic, Z., Staebler, R., Chen, W. and Novak, M. D., 1998. Turbulent flux measurements above and below the overstory of a Boreal aspen forest. *Boundary-Layer Meteorol.* 89, 109-140.

Bonan, G. B., 1996. A land surface model (LSM version 1.0) for ecological, hydrological and atmospheric studies: Technical description and user's guide. NCAR/TN-417+STR, NCAR Technical note.

Brunet, Y. and Irvine, R., 2000. The control of coherent eddies in vegetation canopies: Streamwise structure spacing, canopy shear scale and atmospheric stability. *Boundary-Layer Meteorol.* 94, 139-163.

Cheng, Y. and Brutsaert, W., 2005. Flux-profile relationships for wind speed and temperature in the stable atmospheric boundary layer. *Boundary-Layer Meteorol.*, 114, 519-538.

Dyer, A.J., 1974. A review of flux-profile relationships, *Boundary-Layer Meteorol.*, 7, 363-372.

Dwyer, M. J., Patton, E. G., Shaw, R. H., 1997. Turbulent kinetic energy budgets from a large eddy simulation of airflow above and within a forest canopy. *Boundary-Layer Meteorol.*, 84, 23-43.

Finnigan, J., 2000. Turbulence in plant canopies. Annu. Rev. Fluid. Mech. 32, 519-571.

Katul, G. G., Mahrt, L., Poggi, D. and Sanz, C., 2004. One- and two-equation models for canopy turbulence. *Boundary-Layer Meteorol.*, 113, 81-109.

Lee, X., 1998. On micrometeorological observations of surface-air exchange over tall vegetation. *Agric. For. Meteorol.* , 91, 39-49.

Mahrt, L., Lee, X., Black, A., Neumann, H. and Staebler, R. M., 2000. Vertical mixing in a partially open canopy. *Agric. For. Meteorol.* , 101, 67-78.

Massman, W. J. and Weil, J. C., 1999. An analytical one-dimensional second-order closure model of turbulence statistics and the lagrangian time scale within and above plant canopies of arbitrary structure. *Boundary-Layer Meteorol.*, 91, 81-107.

Nakamura, R. and Mahrt, L., 2001. Roughness lengths and similarity theory for local and spatially averaged fluxes. *Agric. For. Meteorol.* , 100, 47-61.

Paw U, K. and Brunet, T., Y. Collinearu, Y. S., Shaw, R., Maitani, T., Qiu J. and Hipps, L., 1992. On coherent structure in turbulence above and within agricultural plant canopies. *Agric. For. Meteorol.* , 61, 55-68.

Poggi, D., Katul, G. G. and Albertson, J. D., 2004. Momentum transfer and turbulent kinetic energy budgets within a dense model canopy. *Boundary-Layer Meteorol.* 111, 589-614.

Raupach, M. R., 1994. Simplified expressions for vegetation roughness length and zero-plane displacement as function of canopy height and area index. *Boundary-Layer Meteorol.*, 71, 211-216

Raupach, M. R., Finnigan, J. J., Brunet, Y., 1996,. Coherent eddies and turbulence in vegetation canopies: Mixing-layer analogy. *Boundary-Layer Meteorol.*, 78, 351-382.

Shaw, R. H. and Schumann, U., 1992. Large-eddy simulation of turbulent flow above and within a forest. *Boundary-Layer Meteorol.* 61, 47-64.

Schwarz, P., Law, B., Williams, M., Irvine, J., Kurpius, M., and Moore, D., 2004. Climatic versus biotic constraints on carbon and water fluxes in seasonally drought-affected ponderosa pine ecosystems. *Global Biochem. Cycles* 18, GB4007, doi:10.1029/2004GB002234.

Sellers, P., Hall, F., Margolis, H., Kelly, B., Baldocchi, D., den Hartog, G., Cihlar, F., Ryan, M. G., Goodison, B., Crill, P., Ranson, K. J., Lettenmaier, D.,

and Wickland, D. E., 1995. The Boreal Ecosystem - Atmosphere study (BOREAS): An overview and early results from the 1994 field Year. *Bull. Amer. Meteorol. Soc.*, 76, 1549-1577.

Shuttleworth, W. J., and Wallace, J. S., 1985. Evaporation from sparse crops - An energy combination theory. *Quart. J. Roy. Meteorol. Soc.*, 111, 839-855.

Wilson, J. D., Finnigan, J. J., and Raupach, M. R., 1998. First-order closure for plant canopy flows. *Quart. J. Roy. Meteorol. Soc.*, 124, 705-732

Chapter V

Metolius Ameriflux Working Document

Metolius Ameriflux Working Document

Boundary Layer Group
College of Oceanic and Atmospheric Sciences
Oregon State University
Corvallis, OR 97331 USA

February 2005

1 Introduction

This document describes the methods used to arrive at annual NEE, GEP and respiration estimates. General procedures common to all sites and all years are discussed in Sections 1-6. Site and year specific processing details follow the general discussion.

This is a working document to describe the measurements and data processing that lead to the standard Ameriflux data set for the Metolius OR sites. It is not intended to be a manuscript for publication, nor does it include ongoing research efforts, although features of special interest along with some interpretation is presented in the discussion subsection of each site-year section. The biological measurements are not directly discussed in this document.

The goal is construct quantitative and representative estimates for net ecosystem exchange of carbon (NEE) and to partition NEE into GEP (photosynthesis) and respiration components. However, there are numerous potential problems. Long periods of missing data that coincide with a particular stage of biological activity could contribute a bias in the estimates. The flux instruments have quality problems in wet weather, which includes most of the winter season in the study area. The open-path LICOR is subject to calibration drift as the condition of the surface of the windows changes.

The flux measurement height may be in the roughness sublayer, especially in convective conditions, and there is no information on the horizontal or vertical variation of the flux. The single storage measurement site could be unrepresentative due to preferred locations of nocturnal carbon dioxide accumulation. There could be a significant mismatch between the flux footprint and the storage footprint, especially in stable conditions. The fetch changes with wind direction and stability, and the wind direction and stability vary systematically with season and time of day. Advection may be significant, but is not known.

2 Data collection

Fast response wind and temperature data from a sonic anemometer (Campbell CSAT3) and fast response number density data from a colocated open-path CO2/H2O analyser (LICOR-7500) positioned above the canopy are logged and saved at 10 or 20 hz for subsequent analysis. The mean CO2 concentration profile is measured at multiple levels using a single closed-path gas analyser (LICOR-6262) with multiple switching ports. Ancillary data can include mean temperature and wind profiles, radiation terms, soil properties, precipitation and a micronetwork of meterological measurements in some cases.

3 Quality control

A complete description of this program is at

`http://blg.oce.orst.edu/Software/QC_v3/guide/guide.html`.

The qc program is applied to raw time series of fast response variables used in eddy correlation flux calculations. This variable set includes $(u, v, w, T_v, q, co2)$. The program performs the following steps:

- Fast response specific humidity q (gg^{-1}) and $co2$ concentration (ppm) are computed from fast response number density (millimole m^{-3}) measurements and fast response ambient air density (temperature and pressure fluctuations). This is sometimes called a point-by-point WPL "correction".

- Small segments of missing data in time series are replaced using linear interpolation. Small is defined as small enough such that the flux is not significantly effected, based on previous experience with other data sets.

- The times series are despiked. The spike threshold is 3.25 times the local standard deviation. Continious spikes for periods longer than 5

seconds are considered real events and not spikes. Spikes are replaced using linear interpolation. Some data that is flagged by the qc testing is subjected to a "heavy-despiking" algorithm that removes longer sequences of spikes.

- A series of tests are imposed that check the variable set for an unphysical range of values, unusally small or large variance, skewness and kurtosis, and for discontinuites in the mean. When suspect data is found it is masked out (set to missing data value).

- A fast response "clean" data set is written for subsequent analysis.

The LICOR-7500 has data quality problems when moisture (rain,snow,dew) or particulates accumulate on the windows. The CSAT generally has less problems than the LICOR-7500.

Any quality control process is not 100% reliable. It is sometimes difficult to distinguish between instrument problems and rare but plausible physical behaviour.

4 Second generation

A complete description of this program is at

`http://blg.oce.orst.edu/Software/2nd_and_3rdgen/`.

This program computes means, variances, fluxes and spectra. Fluxes are computed for 3 different local averaging time scales; 100 seconds, 300 seconds and 600 seconds. For Ameriflux we use the 600-second fluxes. There is no detrending and fluxes are calculated using unweighted, non-overlapping, box-car averages. Fluctuations (e.g. w') for all points in the first 600-second window are computed by subtracting the 600-second mean. The same is done for $co2$. The product (e.g. $w'co2'$) is then computed for all points in the window and then averaged over the window. This is repeated for the next 600-second window, etc.

No corrections are made for potential high frequency flux loss due to path-length averaging by the sonic or the LICOR, or for potential high frequency flux loss due to physical seperation between the sonic and the LICOR.

Multiresolution cospectra and spectra are computed and saved for analysis of the scale-dependence of the fluxes.

We note that use of a 600-second local averaging time scale for computing fluxes in strongly stratified conditions may include poorly sampled mesoscale motions. As a result, the flux is characterized by large random sampling error. The contribution to the calculated flux at these large time scales (low frequencies) may be larger than the contribution from turbulent scales in very weak turbulence.

4.1 Tilt correction

A tilt correction is applied to the wind components prior to computing fluxes. The tilt correction can be time-dependent to accomodate changes in the sonic orientation due to any physical realignments that may take place during the year. In this case, the entire procedure (see below) is repeated seperately for each period. Individual hours with weak horizontal winds (less than 2 ms^{-1}) are excluded from the tilt correction development procedures since the tilt angle can be erratic in weak winds.

A practice constant offset is removed from the vertical motion making $\overline{w}$ zero for the entire period. The removal of the offset does not directly affect the computed flux, since only a constant is removed for each record. However, we note that applying a subsequent tilt rotation to the data with no prior removal of the offset, converts the vertical motion offset into horizontal flow.

After removing the practice offset, a practice tilt angle is computed for each 1-hour record which eliminates the record mean vertical motion. These tilt angles are averaged over the entire period for a sequence of wind direction categories, giving wind direction-dependent average tilt angles. When the practice tilt angles appear to be consistant with a tilted anemometer, the actual tilt correction is applied. For each 1-hour data record, a lookup table

is used to determine the offset and tilt angle to use depending on the time and the wind direction, and the rotation is done on the fast response wind components. The process includes a horizontal rotation to along-wind (u) and cross-wind (v) components such that $\overline{u} > 0$ and $\overline{v} = 0$ to distinguish between along- and cross-wind components of the wind stress. This method does not force the record-mean vertical motion to zero. The correction is applied to all records regardless of wind speed.

5 Third generation

A complete description of this program is at

`http://blg.oce.orst.edu/Software/2nd_and_3rdgen/.`

This program calculates quantities related to evaluating Monin Obukov similarity theory. Several estimates for different types of flux sampling errors are computed including random sampling error, systematic error, a flux intermittency parameter and flux non-stationarity.

Half-hour mean quantities are computed from the 2nd generation 600-second data. Three 10-minute average values are averaged to make one 30-minute average. The sensible heat flux is calculated from the sonic heat flux (which is close to the virtual temperature flux) and the moisture flux.

6 Ameriflux processing

6.1 Flow distortion

The fluxes for half-hourly periods where the flow is potentially disturbed due to sonic support structures, other instruments or the tower itself are masked out (set to missing data value). The width of the wind sector deemed to have potential flow distortion is specific to each site and depends on the type of tower, boom length and configuration.

6.2 Outliers

Flux outliers are removed to avoid their influence on gap-filling. Values of the eddy correlation (EC) flux outside a user specified range are masked out. The range is selected after consulting a time series plot of all the fluxes, and should include only a very small fraction of the data. It is likely that some of these outliers are associated with instrument problems that were not detected by the quality control testing.

6.3 Gap-filling

The steps in the gap-filling procedure are outlined below.

- 1. Temporal fill wide gaps using linear interpolation. A wide gap is a sequence of consecutive days with a very high percentage of missing data (90% or more). Typically, the percent of missing data in these cases is 100%. When equivalent width data segments just prior to and subsequent to the wide gap segment have a lower percent missing data (60% or less), then linear interpolation is used to fill across the wide gap. Means are computed for the prior and subsequent segments for each of 48 half-hour periods. The half-hourly values are then interpolated across the wide gap. This procedure is implemented using a sequence of block windows of width 35,30,..10,5 days.

- 2. Vertical fill 1-pt and 2-pt gaps using linear interpolation for $co2(z)$ and $T(z)$. A 1-pt gap is one vertical level with missing data with good data both above and below, for the same time period.

- 3. Temporal fill 1-pt and 2-pt gaps using linear interpolation for all variables. A 1-pt gap here is one half-hour with missing data with good data for the prior and subsequent half-hour periods.

- 4. The mean diurnal averages are calculated for all variables using all non-missing data within a 15 day window width. The mean diurnal average consists of the averages over the window for each of 48 half-hour

periods during the day. Missing data within the window is replaced with the correpsonding average over the window if at least 50% of the data for that period were included in the average. For example, if a particular half-hour period is missing for 8 or more of the 15 days in the window, the missing data for that half-hour period will not be replaced by the average.

This entire process is then repeated partitioning the data into 8 three-hour periods instead of 48 half-hour periods. The probability of finding enough data to meet the 50% criteria is greatly increased because the time-of-day criteria is relaxed from a half-hour to three-hours. In general, this will depend on the character of the missing data and could be site-specific. When replacing missing data with the average, the six half-hour averages in the three-hour period are all assigned the same value.

- 5. Repeat step 4 for increasing window sizes of 30, 45, etc. days until all data is gap-filled for all variables.

6.4 Storage term

The storage of $co2$ and heat in the air between the ground and the flux measurement height is computed by vertically integrating the local time tendancy. The time change is computed using centered ($2\ \delta t$) differences and half-hour means. The vertical integration is done assuming a piecewise linear fit to the $co2(z)$ and $T(z)$ profile data. The profiles are extrapolated from the first measurement level down to the surface using the slope between the first and second levels.

6.5 u_*-filtering

Nocturnal measurements of the $co2$ EC flux plus storage sometimes increase with increasing friction velocity (u_*). Since respiration is not thought to be function of u_*, this indicates that other processes may be acting. The

generally accepted interpretation is that horizontal or vertical advection of $co2$ must be important. Another possible interpretation is that the storage measurement is unrepresentative, possibly due to horizontal heterogentiy of the storage. Another is that the flux footprint region could be quite different than the footprint of the storage measurement in stable flows.

One approach to this problem is to apply u_* filtering, where a model of respiration is developed using the nocturnal $F_c + S_c$ measurements in only strong mixing (high u_*) conditions. In such conditions, advection and horizontal heterogentiy are probably less important. The critical u_* value is site dependent. The friction velocity is calculated as the square root of the magnitude of the 30-minute averaged wind stress components

$$u_* = (\overline{w'u'}^2 + \overline{w'v'}^2)^{1/4}. \quad (1)$$

The critical u_* value is estimated in off-line mode by exmaining the u_*-dependence of F_c+S_c. The year is broken up into a sequence of 60-day periods to accomodate seasonal differences. Plots of nocturnal $F_c + S_c$ bin-averaged by u_* category are examined to see if and where a levelling off occurs with increasing u_*. Such plots are included for each site in the latter part of this document. Ideally, $F_c + S_c$ should not be sensitive to u_* for u_* larger than the critical value. We define "nocturnal" as the half-hour periods where the solar zenith angle exceeds ninety degrees.

Sensitivity tests indicate that the $F_c + S_c$ vs (u_*) relationship is heavily influenced by outliers. A more robust relationship is found after discarding points in the upper 2% and lower 2% of the frequency distribution of both $F_c + S_c$ and u_*. Negative nocturnal values of $F_c + S_c$ are discarded. Such values are suspect probably due to large random flux sampling errors which are more severe in stable conditions.

Once the critical u_* is determined, nocturnal F_c+S_c for high u_* conditions is related to predictors of respiration, such as subcanopy air temperature, soil temperature and soil moisture, to develop a model of respiration. The precise form of the model depends on the special characteristics of the site and the availablity of measurements. When available, soil chamber measurements of

respiration are consulted in the model development. Specific details of the respiration model are discussed below in the individual site-year sections.

A potential problem with the "u_*-filter respiration modelling" approach is that the warmest soil temperatures occur in summer during the day with weak mixing (low u_*) conditions. The respiration during such conditions can not be estimated using $F_c + S_c$, and thus these conditions can not be included in developing the model coefficients. To estimate respiration for such conditions, the model must be used to extrapolate to higher temperatures, although the reliability of such an extrapolation is not known.

Respiration is estimated by applying the model to all daytime and nocturnal periods regardless of mixing strength. Recall that the model coefficients were derived using the $F_c + S_c$ measurements for only the high u_* nocturnal periods, and can be specified seperately for each 60-day period.

GEP is calculated as $F_c + S_c$ minus the modelled respiration during the day, and is set to zero at night. NEE is then given by GEP + respiration. Respiration, GEP and NEE are defined as negative for carbon uptake by the ecosystem and positive for release of carbon to the atmosphere.

Annual NEE (gCm^{-2}) is computed as

$$NEE = N_d \ 86400 \ 10^{-3} \ (12/44) \ A \tag{2}$$

where A is the annual average NEE (mg co2 $m^{-2}s^{-1}$) and N_d is the number of days per year. The same approach is used for computing annual sums of respiration and GEP.

7 IP03

The first application of the OSU-BLG processing was for the 2003 data from the intermediate pine site near Sisters, OR, USA. The above canopy flux measurements were made 31 m above ground using a CSAT3 sonic anemometer and open-path LICOR-7500. The average height of the canopy was 17 m, so the flux instruments were approximately 14 m above canopy, or at 1.8 canopy

heights. Significant solar radiation reaches the forest floor underneath the canopy in summer indicating a fairly sparse canopy. During summer nights, the subcanopy layer remains significantly stratified even with the highest above canopy u_* conditions.

Mean $co2(z)$ (closed path LICOR-6262) was measured at 1, 4 and 30 m. Mean temperature (HOBOs) was measured at 3, 6, 10, 20 and 30 m. Mean horizontal winds (Handars) were measured at 3, 6, 10, 20 and 30 m. The soil heat flux was measured at 5 locations and averaged. Soil temperature was measured at 6 depths between 2 and 64 cm at one location. Soil moisture content was measured at one location. Automated daily mean chamber measurements of soil respiration were made during April through Spetember.

7.1 Data coverage

A total of 6790 hours of data were logged (78% annual coverage). Approximately 10% of these hours contained enough missing data that they could not be saved and were discarded. Approximately 10% of the surviving hours were discarded by quality control tests. Problems with either the $co2$ or $h2o$ measurement (usually both) from the LICOR-7500 were 25 times more likely to occur than problems with the CSAT.

Subsequent to quality control, a problem with the 31-m fluxes was discovered for the period 11-Sep to 29-Sep (DOY 255-272), and these data were discarded. An additional problem with the 31-m fluxes was discovered during the tilt correction phase of the processing for the period from 4-Nov to the end of the year, and these data were discarded. Apparently, the mount holding the sonic anemometer to the boom came loose.

The gap-filling did not work very well for the sensible and latent heat fluxes and the $co2$ flux during November and December, where there was almost no good quality flux data. The large amount of missing data (Table 1) severly tested the gap-filling procedures.

Table 1. IP03 percent of available EC $co2$ flux (F_c) and storage (S_c) data.

Month	J	F	M	A	M	J	J	A	S	O	N	D
F_c	38	68	40	46	21	74	91	81	31	76	5	0
S_c	88	100	98	99	90	33	72	0	83	56	54	42

7.2 Respiration modelling

Nocturnal $F_c + S_c$ increases with increasing u_* at this site during some periods of the year (Figure 1). Based on these data, we select a critical u_* value of 0.5 ms^{-1} for the purpose of applying the u_*-filtering, and apply this constant value for the entire year. The respiration from nocturnal EC flux plus storeage measurements during high u_* periods agrees reasonably well with the automated chamber measurements (horizontal lines in Figure 1). The eddy correlation estimates of respiration are slightly higher than the chamber values presumably due to respiration from the foilage, which would not be captured by the chamber measurements.

The subcanopy air temperature, 2-cm soil temperature and 4-cm soil temperature were all reasonably good predictors of respiration (measured nocturnal $F_c + S_c$ in high u_* conditions). We choose the 4-cm soil temperature. The temperature-dependence was fit to the form

$$R_{es} = \alpha \ T^{\beta} \tag{3}$$

using least squares regression. The respiration was first bin-averaged by temperature category (circles in Figure 2) and then the regression was done on the bin-averaged data to obtain the coefficients, $\alpha = 0.037$ and $\beta = 0.563$ and the model (solid line Figure 2). The model coefficients change slightly to 0.033 and 0.595, respectively, using a critical u_* of 0.7 ms^{-1} instead of 0.5.

Theoretically, the respiration from the soil should increase exponentially with soil temperature and decrease with decreasing soil moisture content.

The reason that soil temperature alone describes the observed respiration so well at the Metolius sites is that soil moisture content is negatively correlated with soil temperature, at least for the first half of the year. During July the soil moisture content reaches a minimum, and then does not decrease any further through the late summer and fall. The implicit inclusion of soil moisture content in the soil temperature leads to the relatively weak soil temperature dependence of the respiration found here.

The daily average, temperature-dependent respiration model agrees quite well with the daily average, corrected, automated soil chamber measurements through the end of June, but then is significantly larger than the chamber measurements during July through September. Adding soil moisture content to the respiration model does not significantly change this result. This could be due to the soil moisture measurement "pegging" at a low value during July and remaining relatively unchanged until the late fall rains begin. The soil moisture is measured using the CS615, which when installed vertically, gives a measure of the soil moisture content in the upper 30 cm of soil. Another possibility is that the fractional respiration coming from the foilage is higher in late summer than in early summer. The chamber measurements miss foilage respiration.

As a sensitivity test, the respiration model coefficients were calculated seperately for each of six 60-day window time periods during the year. This approach allows a different temperature dependence for different seasons of the year. The motivation is that while soil temperatures are similar in early and late summer, the soil moisture content is significantly less in late summer. The comparison with the automated chamber data is very similar to that described above for the simpler respiration model with constant coefficients for the whole year. That is, the model respiration is in good agreement with the automated chamber measurements through June, but then is larger than the chamber measurements for July through September. The respiration during late summer and fall is slightly reduced for the seasonal model compared to the constant coefficient model, and is therefore slightly closer to the chamber measurements. Since the approach using constant year-long

coefficients appears to be just as reasonable as the more complex model with seasonal-dependent coefficients, we choose to apply the simpler one.

Research is ongoing on the respiration.

7.3 Annual estimates

The estimate of annual NEE at this site is perhaps high compared to expectations for a semi-arid ponderosa pine site (Table 2). As a sensitivity test, increasing the u_* threshold from 0.5 to 0.7 ms^{-1} slightly decreases the respiration, and thus increases the annual carbon uptake, contrary to expectations. The fact that increasing the critical u_* from 0.5 to 0.7 does not increase the respiration is not conclusive since: 1) the amount of high u_* data is limited and 2) the footprint increases with wind speed.

As another sensitivity test, discarding the u_*-filter approach and using the automated chamber measurements for respiration, decreases the annual respiration and increases the annual carbon uptake. In this calculation, the respiration model with critical $u_* = 0.5\ ms^{-1}$ is used when the chamber data is missing. The chamber measurements are not extrapolated into the winter season.

The July mean diurnal cycle of the terms in Table 2 is shown in Figure 3, while the annual cycle of weekly-averages is in Figure 4. These fields are based on the standard calculation with u_*-filtering and a threshold value of 0.5 ms^{-1}.

Table 2. IP03 annual estimates (gCm^{-2}).

F_c	S_c	GEP	R_{es}	NEE
-513	0	-1302	936	-366

7.4 Discussion

An under-estimate of respiration would contribute to the large negative NEE indicating relatively large carbon uptake compared to expectations for this site. Comparisons with the automated chamber measurements are inconclusive. In June and July with the warmest soil temperatures, the chamber measurements of respiration exceed our modelled estimate, however, the chamber estimates are significantly lower than the model estimates in the early and late summer. It is not clear why the chamber measurements drop off so sharply in late July and early August, while the soil temperature and soil moisture are not changing rapidly. Spatial heterogenity is an issue with the chamber measurements.

A possible reason for the relatively large NEE estimate is that even with strong mixing above the canopy (high u_* conditions), the mixing underneath the canopy is still suppressed due to a suprisingly strong subcanopy temperature stratification. The subcanopy stratification decreases with increasing u_* above the canopy as expected, but does not go to zero. In summer, the stratified layer results from strong radiative cooling at the surface due to clear skies, dry soil and a sparse canopy. Because of the suppressed mixing in the subcanopy layer, the nocturnal flux measurements made above the canopy may under-estimate the respiration even under the strongest mixing conditions observed.

Another potential complication is that when the wind is from the south or southwest, it comes from a region with smaller LAI. The tower site is in an area of local maximum LAI. At night, the surface footprint is larger (enormous with subcanopy stratification) and is expected to be smaller with daytime heating. Therefore, the daytime carbon uptake is dominated by the high LAI area in the vicinity of the tower, while the nighttime respiration is more strongly influenced by areas with lower LAI.

8 IP04

The second application of the OSU-BLG processing was for the 2004 data from the intermediate pine site near Sisters, OR, USA. See the IP03 section for details. Differences between the two years are discussed here.

More levels of mean $co2$ and temperature were deployed on the flux tower in 2004. Mean $co2(z)$ (closed path LICOR-6262) was measured at 1, 3, 6, 15 and 31 m, and mean temperature (HOBOs) was measured at 3, 6, 10, 15, 20 and 30 m.

8.1 Data coverage

2004 has less missing data compared to 2003 (Table 3). For the entire year, a valid $co2$ EC flux measurement was logged and passed the quality control testing for 82% of the 30-minute periods. The correpsonding number for the $co2$ storeage measurements is 88%, with nearly all the missing storeage data being in January. There is no flux data prior to 18-January.

Table 3. IP04 percent of available EC $co2$ flux (F_c) and storage (S_c) data.

Month	J	F	M	A	M	J	J	A	S	O	N	D
F_c	25	74	79	76	84	83	90	83	86	83	76	67
S_c	3	92	99	95	98	72	99	100	100	99	99	100

8.2 Respiration modelling

Based on the u_*-dependence of $F_c + S_c$, we choose a critical u_* threshold of 0.55 ms^{-1} and apply this constant value for the entire year (Figure 5). The u_*-dependence is similar to what was found at this site in the previous year.

The temperature-dependence of the respiration (measured nocturnal $F_c + S_c$ in high u_* conditions) was fit to

$$R_{es} = \alpha \ T^{\beta} \tag{4}$$

using least squares regression where T is the 4-cm soil temperature.

The model coefficients ($\alpha = 0.054$ and $\beta = 0.489$) tend to over-estimate respiration for cooler soil temperatures, and under-estimate respiration for warmer temperatures (Figure 6). The model fit is sensitive to the warmest soil temperatures included in the regression, here about 25 C. The data suggest that the respiration actually decreases or levels off with increasing soil temperature for soil temperatures above 20 C. This decrease is unexpected based on our understanding of soil respiration, and could be due to random sampling problems caused by an insufficient data sample size. The general problem discussed in Section 7.2 also applys here.

8.3 Annual estimates

Table 4. IP04 annual estimates (gCm^{-2}).

F_c	S_c	GEP	R_{es}	NEE
-604	0	-1479	1142	-337

The July mean diurnal cycle is shown in Figure 7, while the annual cycle of weekly-averages is in Figure 8.

8.4 Discussion

The annual NEE for 2004 (337 gCm^{-2}) is about 8% less than that found for 2003 (366 gCm^{-2}). Both GEP and respiration increased in 2004 compared to the previous year.

9 YP04

This is the new young pine site near Sisters, OR, USA. The above canopy flux measurements were made 12 m above ground using a CSAT3 sonic anemometer and open-path LICOR-7500. The average height of the canopy was 3 m, so the flux instruments were at 4 canopy heights. The short pines are uniformly and sparsely distributed and the canopy is not closed.

Mean $co2(z)$ (closed path LICOR-6262) was measured at 1, 5, 12 and 18 m. The 18 m mean $co2$ measurements did not begin until June. Mean temperature (HOBOs) was measured at 1, 2.5 and 5 m. The soil heat flux data is bad until the very end of the year, when two new heat flux plates were installed. Soil temperature was measured at 3 depths between 2 and 32 cm at one location. Soil moisture content was measured at one location. There is no pyranometer at this site.

9.1 Data coverage

The missing EC flux data is fairly evenly distributed through the year, and there are no months with more that 50% missing data (Table 5). This type of missing data is better suited to the gap-filling methods. There is very little missing $co2$ profile data.

Table 5. YP04 percent of available EC $co2$ flux (F_c) and storage (S_c) data.

Month	J	F	M	A	M	J	J	A	S	O	N	D
F_c	51	66	77	80	80	89	66	77	78	74	77	59
S_c	97	100	100	98	91	89	99	100	99	99	99	100

9.2 Respiration modelling

There is no clear u_*-dependence of $F_c + S_c$ at this site, presumably due to the low LAI and sparsely distributed short pines (Figure 9). The shortness of the trees also helps eddies communicate with the surface. That is, there appears to be strong coupling between the 12-m measurement level and the surface, even on weak mixing nights.

The temperature-dependence of the respiration (measured nocturnal $F_c + S_c$) was fit to

$$R_{es} = \alpha \; T^{\beta} \tag{5}$$

using least squares regression where T is the 2-cm soil temperature. (Figure 10). The coefficients are $\alpha = 0.044$ and $\beta = 0.410$ based on the 2-cm soil temperature (there are no 4-cm soil temperature measurements). Because there is no critical u_* value, all the nocturnal data were used to develop the respiration model coefficients, not just the high u_* nocturnal data.

9.3 Annual estimates

Table 4. YP04 annual estimates (gCm^{-2}).

F_c	S_c	GEP	R_{es}	NEE
-233	0	-981	878	-103

Annual NEE at the young site is about one-third of that found for the intermediate site. The July mean diurnal cycle is shown in Figure 11, while the annual cycle of weekly-averages is in Figure 12.

9.4 Discussion

In contrast to the intermediate site, there is no indication that respiration is "missed" by the EC flux measurement at 12 m for low u_* nocturnal conditions at the young site.

There is evidence of early morning vertical flushing of $co2$ associated with upward EC $co2$ flux shortly after sunrise. This is accompanied by a sharp decrease in mean $co2$ concentration. This also coincides with a shift in wind direction from southwesterly to northeasterly, which could be associated with a thermally induced upslope flow. The terrain slopes down to the east and northeast.

10 Intercomparisons

The annual course of the cummulative NEE (gCm^{-2}) for each site-year is shown in Figure 13. The cummulative NEE is computed as

$$Cummulative\ NEE = 1800\ 10^{-3}\ (12/44)\ NEE_{ac} \qquad (6)$$

where NEE_{ac} is the cummulative sum of variable NEE in the data file, where NEE in the data file has units of (mg co2 $m^{-2}s^{-1}$) and represents a 30-minute time average.

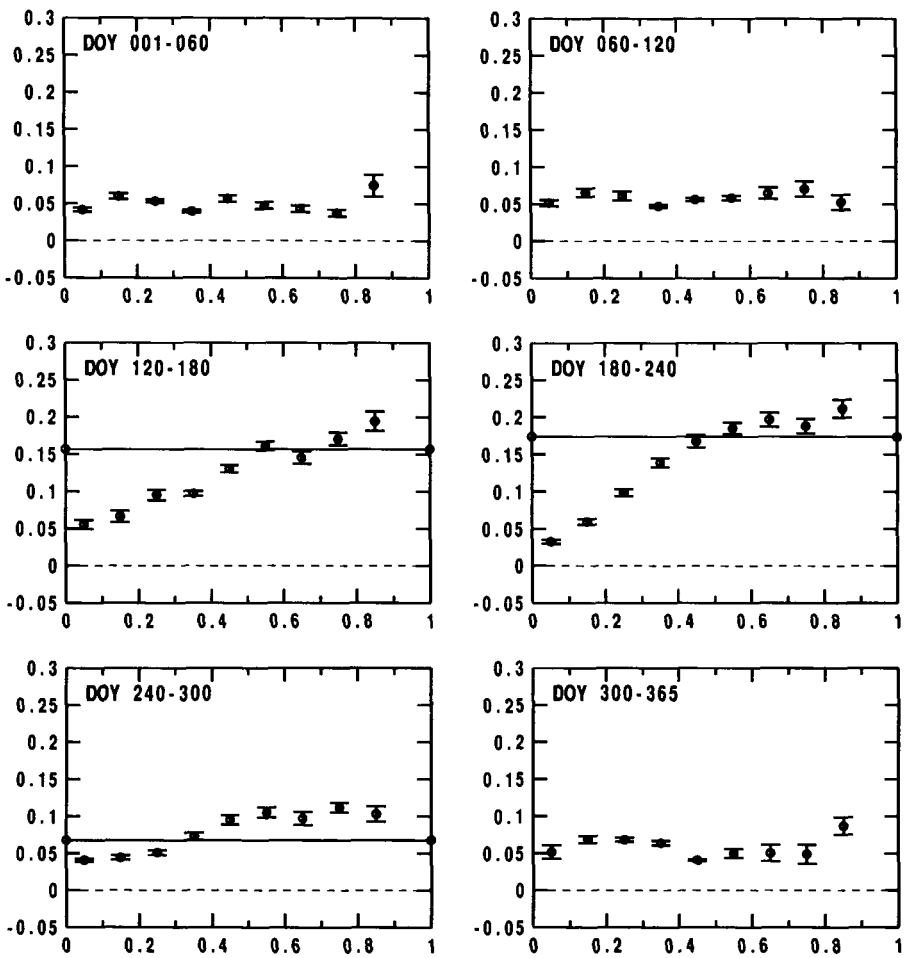

Figure 1: IP03 seasonal pattern of bin-averaged nocturnal $F_c + S_c$ (mg co2 $m^{-2}s^{-1}$) versus friction velocity (ms^{-1}). Solid horizontal lines are estimates of daily mean soil $co2$ efflux (respiration) from automated chamber measurements, corrected using a relationship between manual and automated chamber data.

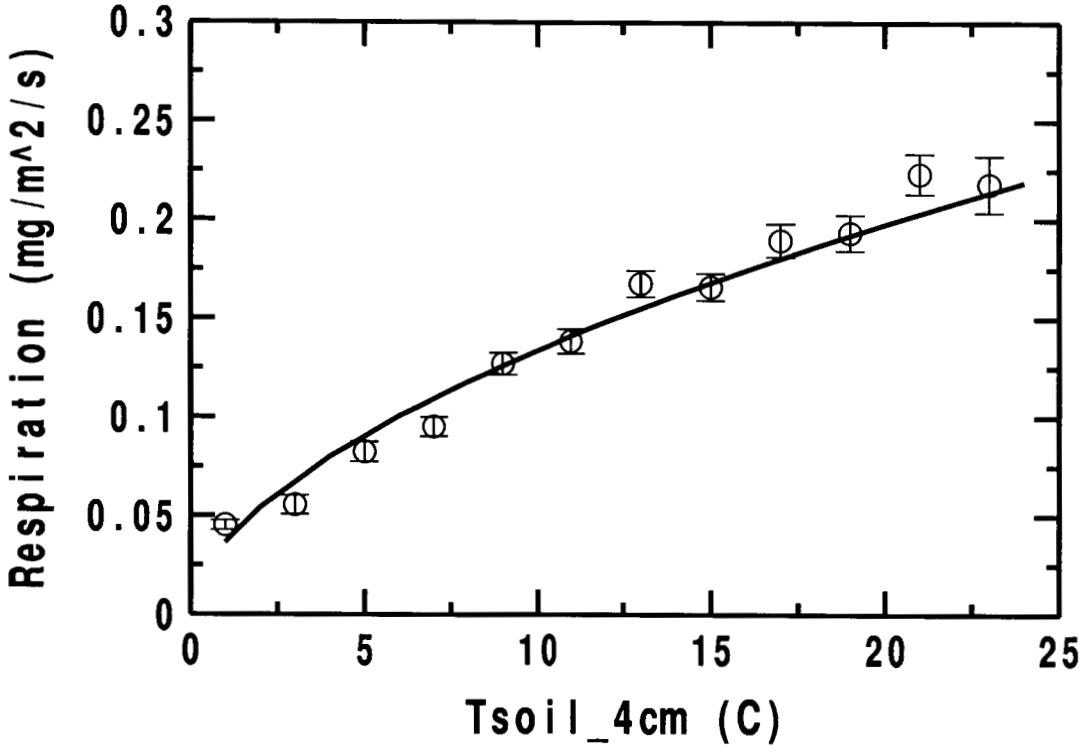

Figure 2: IP03 soil temperature-dependent respiration model.

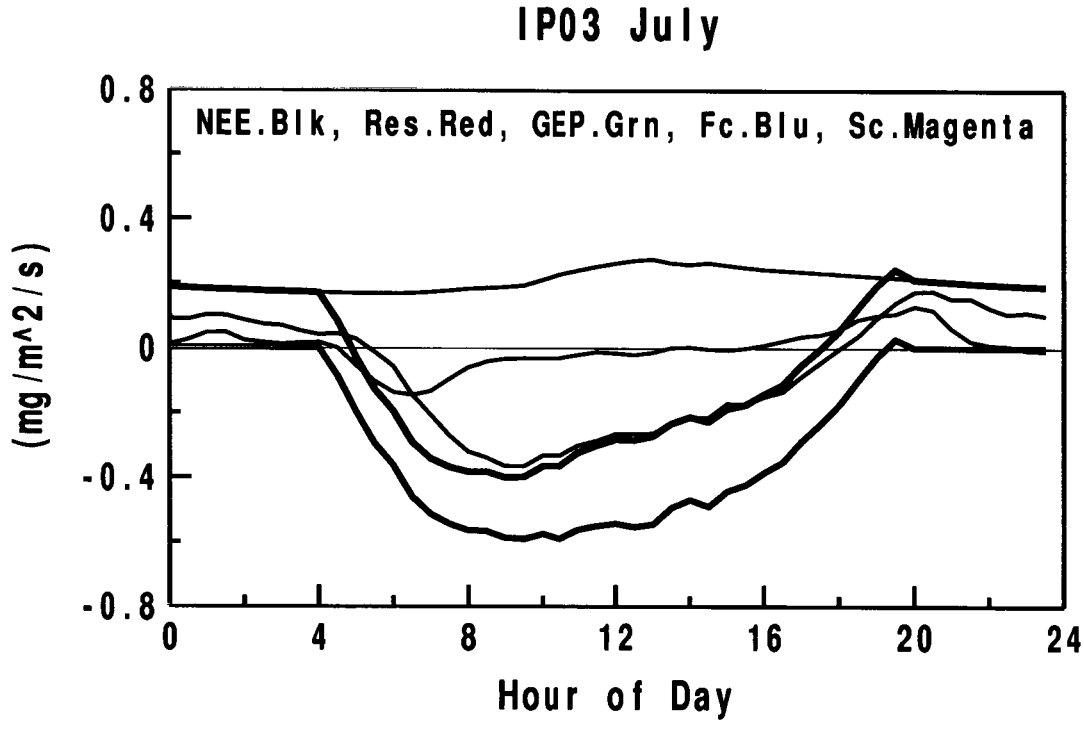

Figure 3: IP03 average July diurnal cycle of selected quantities.

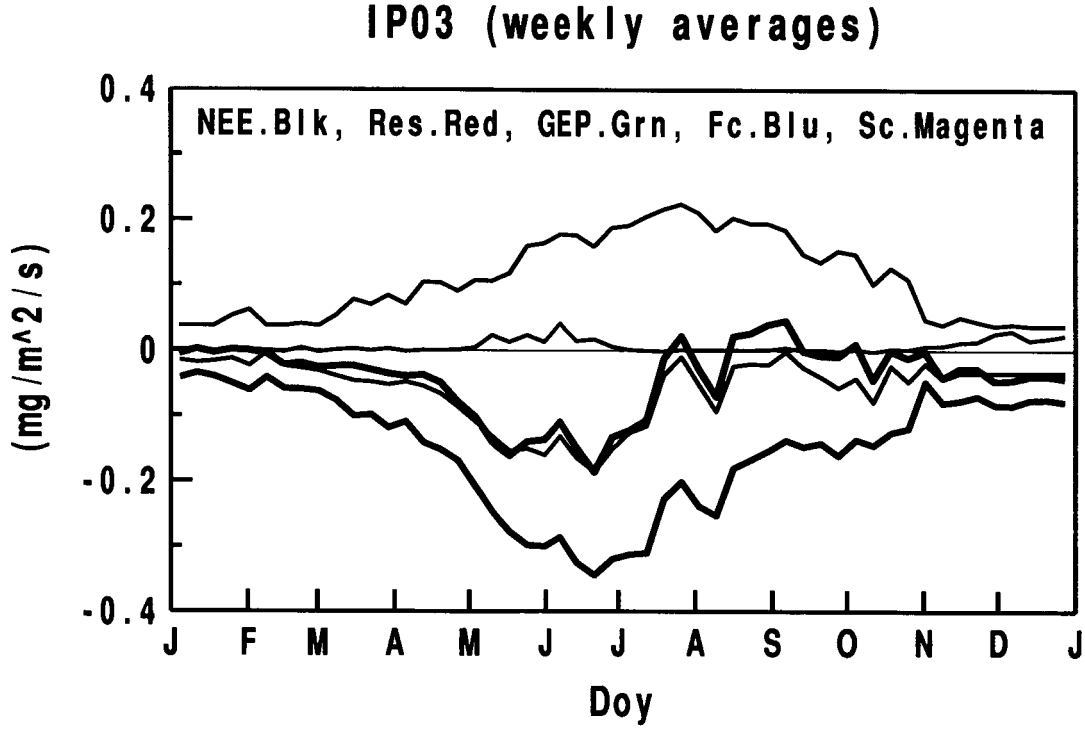

Figure 4: IP03 annual cycle of weekly-averaged selected quantities.

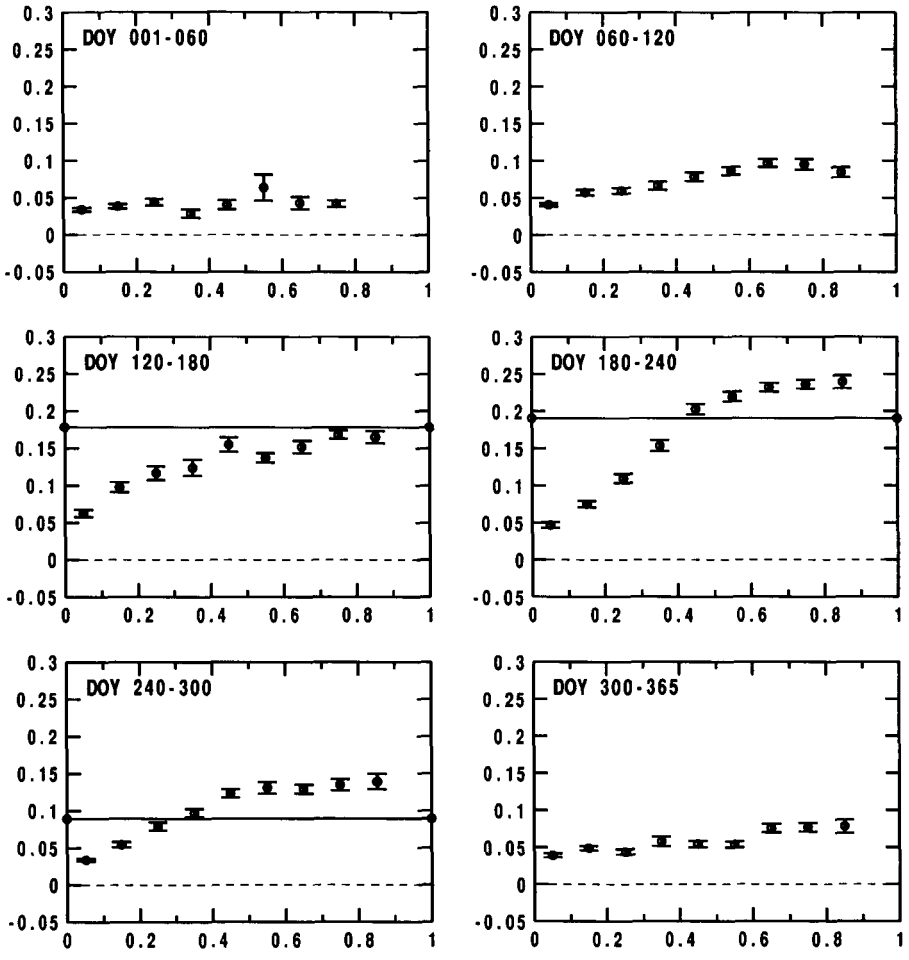

Figure 5: IP04 seasonal pattern of bin-averaged nocturnal $F_c + S_c$ (mg co2 $m^{-2}s^{-1}$) versus friction velocity (ms^{-1}). Solid horizontal lines are estimates of daily mean soil $co2$ efflux (respiration) from automated chamber measurements, corrected using a relationship between manual and automated chamber data.

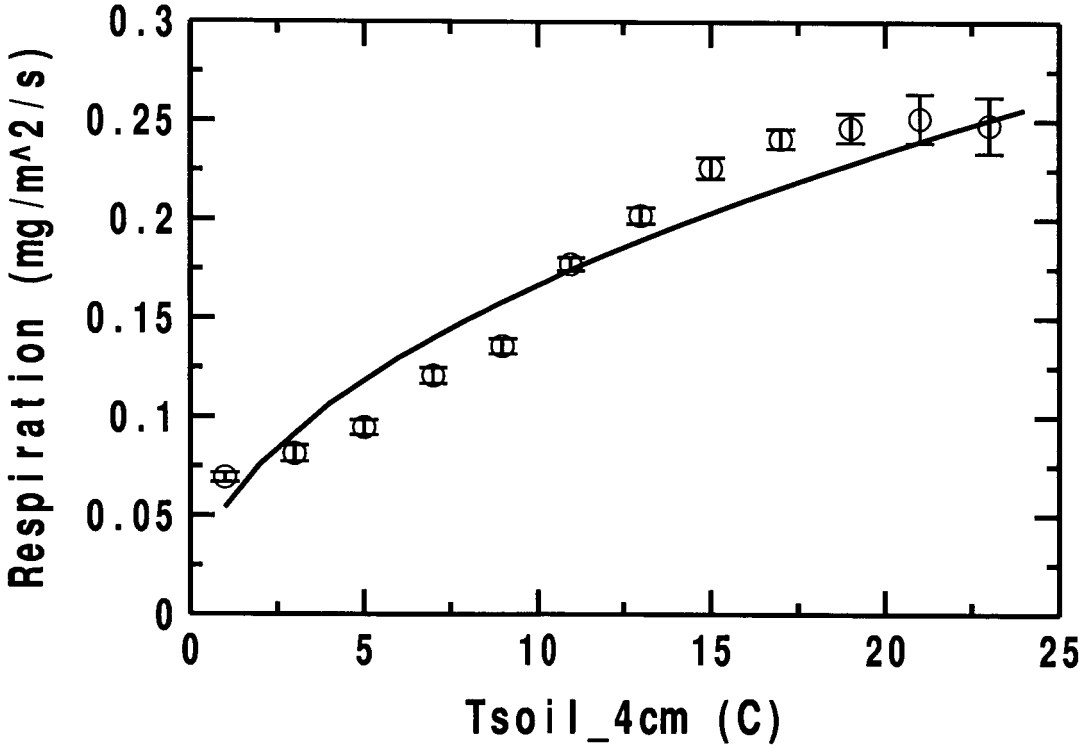

Figure 6: IP04 soil temperature-dependent respiration model.

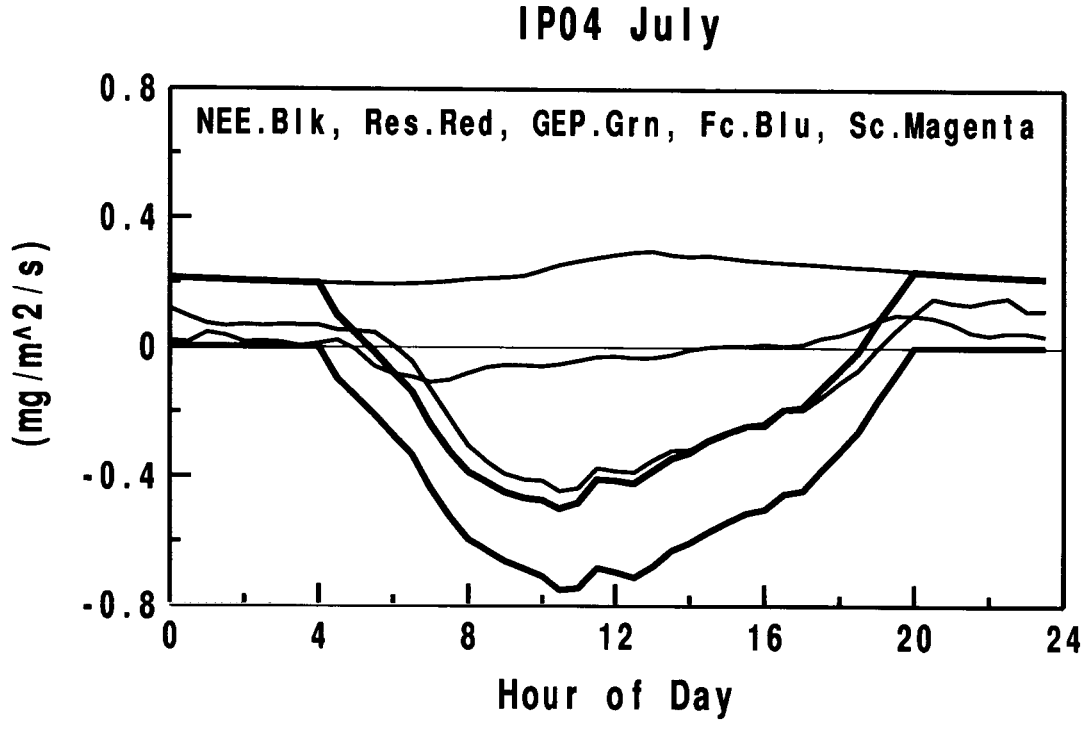

Figure 7: IP04 average July diurnal cycle of selected quantities.

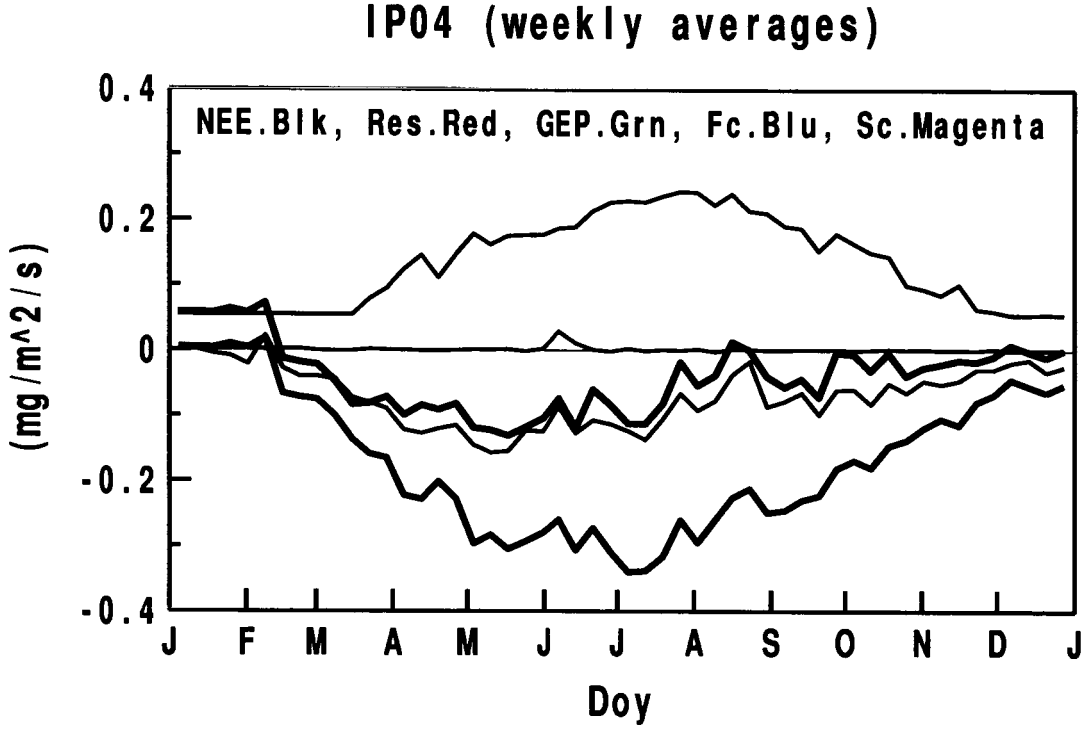

Figure 8: IP04 annual cycle of weekly-averaged selected quantities.

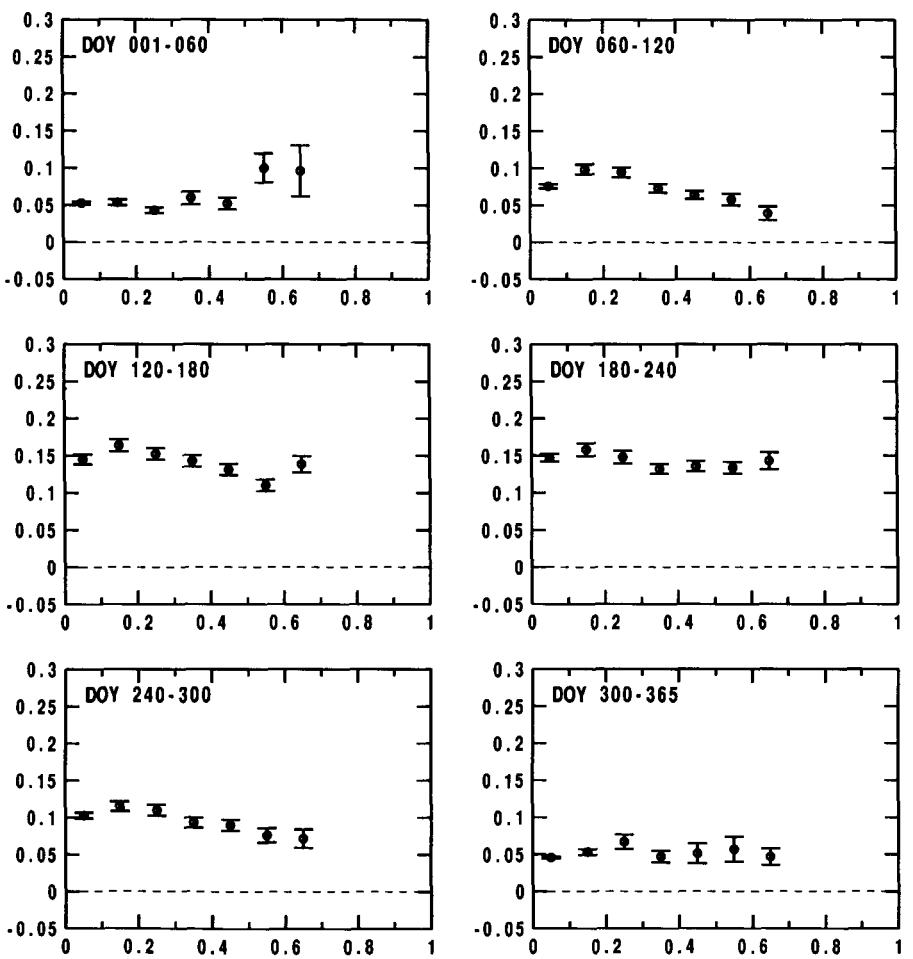

Figure 9: YP04 seasonal pattern of bin-averaged nocturnal $F_c + S_c$ (mg co2 $m^{-2}s^{-1}$) versus friction velocity (ms^{-1}).

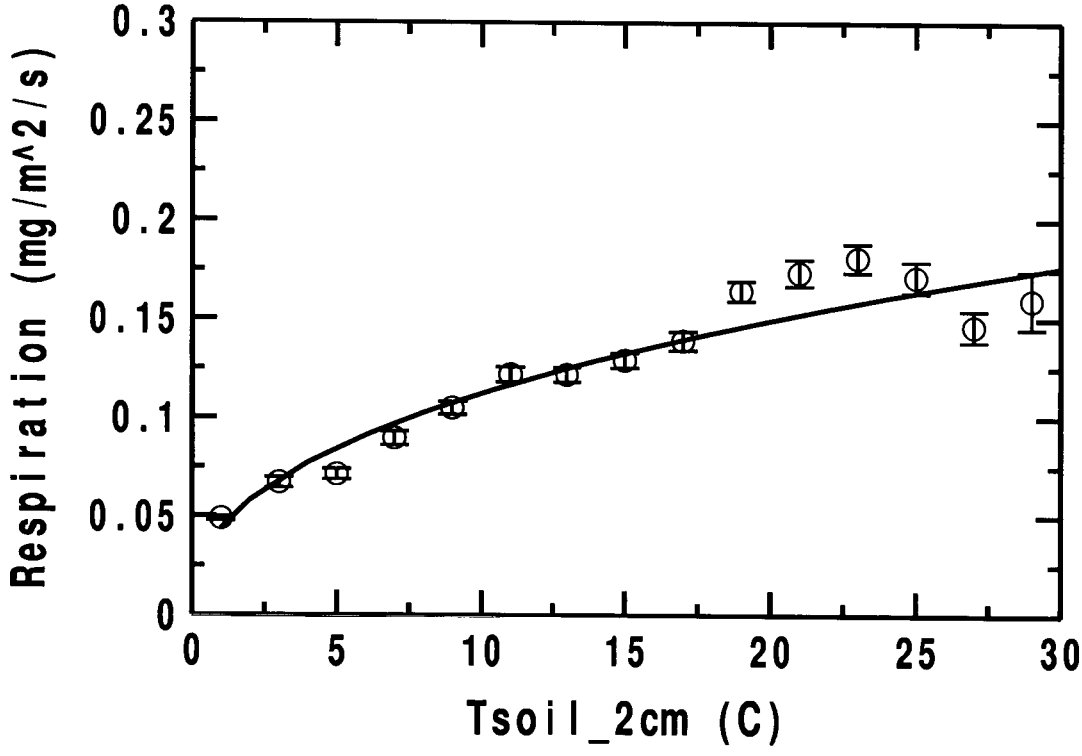

Figure 10: YP04 soil temperature-dependent respiration model.

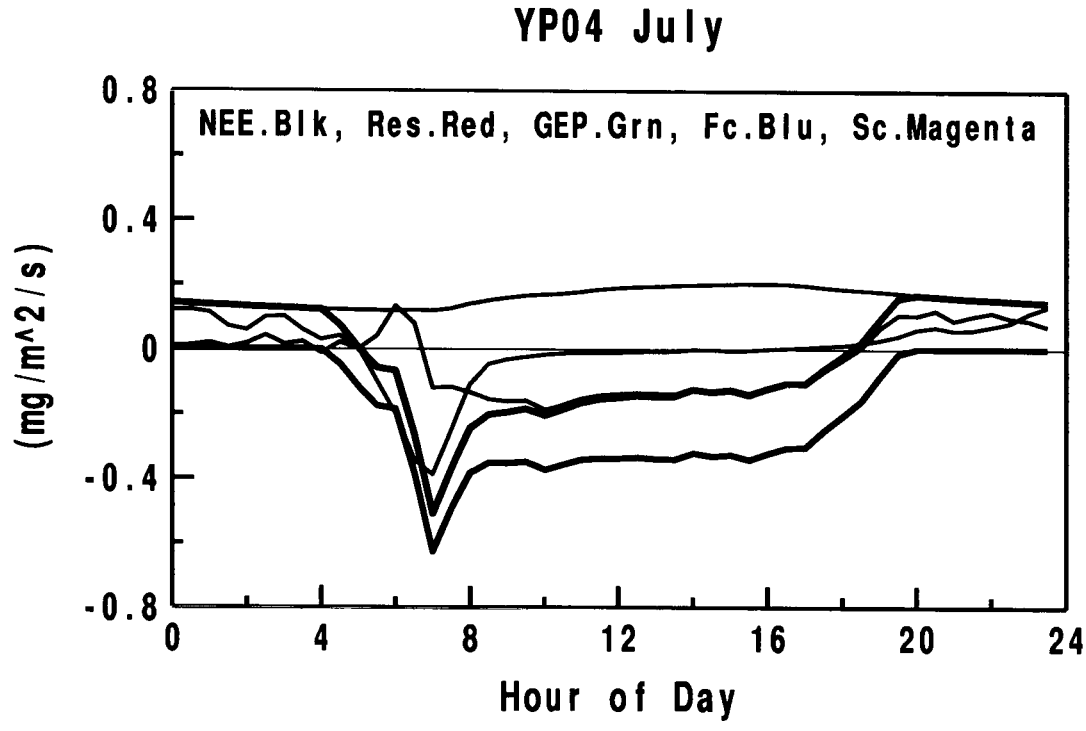

Figure 11: YP04 average July diurnal cycle of selected quantities.

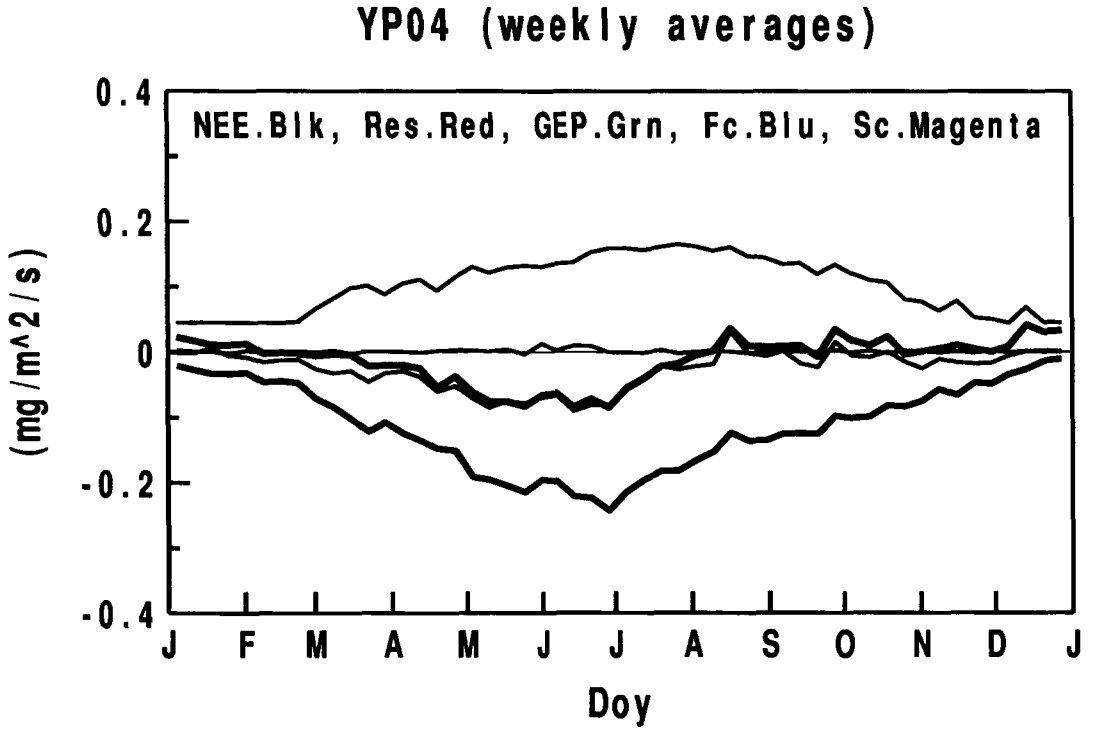

Figure 12: YP04 annual cycle of weekly-averaged selected quantities.

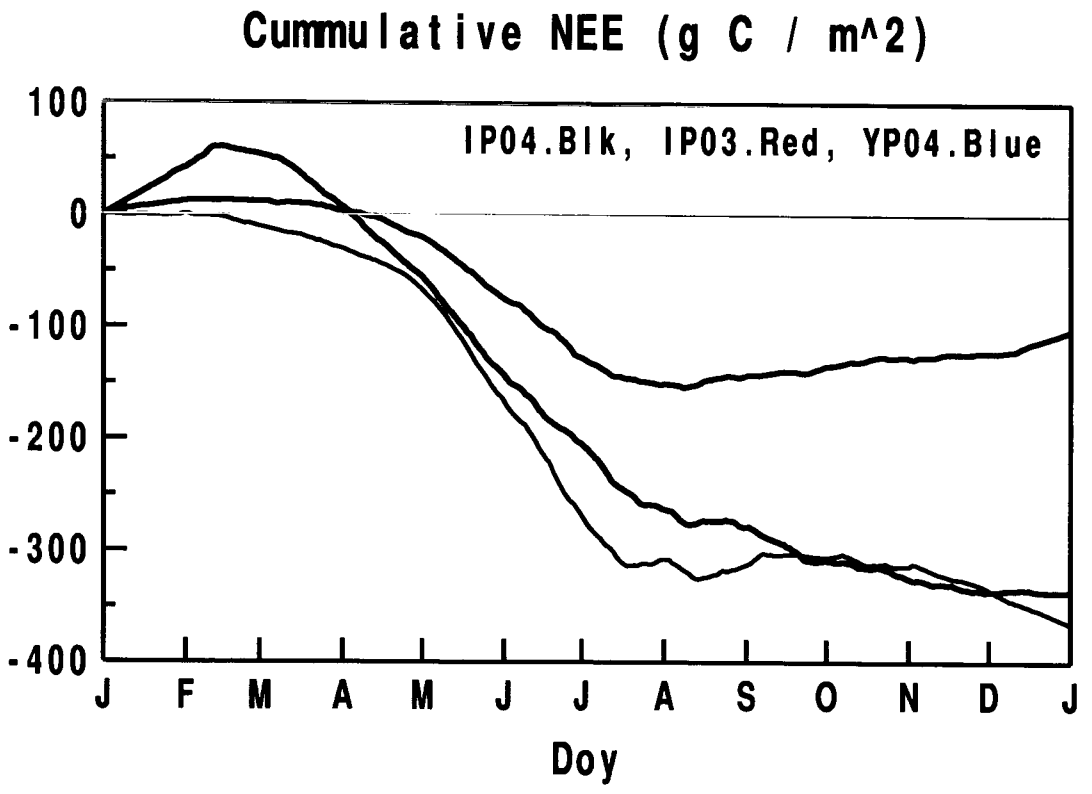

Figure 13: Cummulative NEE for all site-years.

Chapter VI

Feasibility of measuring mean vertical motion for estimating advection

Feasibility of measuring mean vertical motion for estimating advection

Dean Vickers and L. Mahrt

College of Oceanic and Atmospheric Sciences, Oregon State University,

Corvallis, OR, USA

29 July 2005

Corresponding author address: Dean Vickers, College of Oceanic and Atmospheric Sciences, Oceanography Admin Bldg 104, Oregon State University, Corvallis OR 97331-5503, USA.

E-mail: vickers@coas.oregonstate.edu

Abstract

Numerous recent studies calculate horizontal and vertical advection terms for budget studies of net ecosystem exchange of carbon. One potential uncertainty in such studies is the estimate of mean vertical motion. This work addresses the reliability of vertical advection estimates by contrasting the vertical motion obtained from the standard practise of measuring the vertical velocity and applying a tilt correction, to the vertical motion calculated from measurements of the horizontal divergence of the flow using a network of towers. Results are compared for three different tilt correction methods.

Estimates of mean vertical motion are sensitive to the choice of tilt correction method. The short-term mean (10 to 60 minutes) vertical motion based on the horizontal divergence is more realistic compared to the estimates derived from the standard practise. The divergence shows long-term mean (days to months) sinking motion at the site, apparently due to the surface roughness change. Because all the tilt correction methods rely on the assumption that the long-term mean vertical motion is zero for a given wind direction, they fail to reproduce the vertical motion based on the divergence.

Keywords

Vertical Advection, Mean Vertical Motion, Tilt Correction, Horizontal Divergence

1 Introduction

Early studies estimating net ecosystem exchange of carbon (NEE) typically included only the storeage and eddy flux components. It is now generally accepted that this method leads to what appears to be an underestimate of nocturnal respiration of carbon dioxide on nights with weak mixing. One possible interpretation of the missing carbon dioxide is that horizontal or vertical advection is important (Lee, 1998; Baldocchi et al., 2000; Aubinet et al., 2003; Staebler and Fitzjarrald, 2004). An empirical patch for this problem is the so called u_* filter approach, where the measured eddy flux during weak turbulence nocturnal periods, where advection is most likely to be important, is replaced with a model of the respiration based on the eddy flux during strong mixing nocturnal periods (Pattey et al., 2002).

The method of calculating NEE proposed by Lee (1998) added a vertical advection term to the storeage and eddy flux terms in the NEE budget. This approach was applied by Baldocchi et al. (2000) who reported that including vertical advection improved their budget closure, however, they inferred that horizontal advection may also be important. Aubinet et al. (2003) concluded that horizontal advection of carbon dioxide was mostly cancelled by vertical advection. Their hypothesis was that horizontal and vertical advection are linked by an entrainment mechanism where the air above the canopy is brought downward into the subcanopy in drainage flows. This suggests that it is inappropriate to include only the vertical component of advection in the budget. Staebler and Fitzjarrald (2004) found that vertical advection of carbon dioxide was small while horizontal advection was significant. Including horizontal advection improved their NEE budget closure, especially in the summer. Feigenwinter et al. (2004) found that horizontal and vertical

advection of carbon dioxide tended to cancel at night, yet pointed out that the large scatter in the advective fluxes needs further investigation.

All of the above studies estimate mean vertical motion by applying a tilt correction (Section 3) to the vertical velocity measured by a 3-dimensional sonic anemometer, however, it has not been demonstrated that such an approach is capable of resolving a small time-averaged vertical motion. Can the true vertical motion be extracted from the measurements which are contaminated by flow distortion, tilt of the sensor and sloping terrain? In this study, we investiagate the feasibility of quantifying mean vertical motion, and thus vertical advection, using sonic anemometer measurements.

A network of towers were deployed to provide two independent estimates of mean vertical motion; 1) from measurement of vertical velocity at a central tower, and 2) from the horizontal divergence using a network of towers surrounding the central tower. From incompressible mass continuity, the time-averaged vertical velocity based on the divergence is given by

$$\overline{w}(h) = -\int_{z=0}^{z=h} (\frac{\partial \overline{u}}{\partial x} + \frac{\partial \overline{v}}{\partial y}) dz \qquad (1)$$

using the usual notation where overbars denote a time-average and $\overline{w}(0)$ =0. Multiple measurement levels of the horizontal flow on the surrounding towers provide some details on the vertical structure of the horizontal gradients of the mean wind. Two levels of vertical velocity measurements above the canopy on the central tower provide a consistancy check and allow identification of complex flow situations where the magnitude of the vertical velocity may not increase with height.

A strong relationship between the mean vertical motion from the two independent methods would provide confidence for estimates of vertical mo-

tion, and subsequent estimates of vertical advection. However, when the two estimates substantially disagree, such confidence can not be established. This approach is not definitive due to potential errors in both estimates of $\overline{w}$. The comparison is complicated by the fact that $\overline{w}$ at a point responds to divgerence on a large range of spatial scales while our network for calculating the divergence resolves only one spatial scale. We attempt to address this problem by examining the relationships between the $\overline{w}$ estimates for a wide range of averaging times.

2 Field experiment

The measurements are from a semi-arid young ponderosa pine site in central OR, USA, during August, September and October of 2004. The young 3-m tall pine trees were uniformly and sparsely distributed across the site. Beneath the pines was bare sandy soil with sparse clumps of grass. A stand of much taller pines surround the site. The site was chosen in part due to the large roughness change and the expected acceleration of the mean flow (divergence) over the shorter trees. The boundary between the young and taller pines is roughly denoted by the edge of the area in Figure 1. Within the boundaries of the site, the vegetation could be classified as very homogeneous. The terrain slopes steadily upward to the southwest and west with 100 m elevation gain over the first 5 km, or a slope of 2%, and slopes weakly downward ($< 1\%$) or is flat in other directions. More than one-half the time the wind direction was in the sector 230 to 300 deg (westerly winds).

The central tower was equipped with 3-dimensional CSAT3 sonic anemometers (Campbell Scientific) at 5 and 12 m above ground recording the three wind components and the sonic temperature at 10 hz. The orientation of

the anemometers was carefully measured with a SmartTool (MD Buliding Products), a digital instrument with a precision of 0.1 deg. The pitch, roll and azimuth of the 12-m anemometer were measured as 0.9, 0.0 and 272 deg, respectively. Two-dimensional sonic anemometers (Vaisala Inc, formerly Handar) were deployed at 1, 5 and 12 m above ground on towers A and C and at 1 and 5 m on towers D, E and B for measuring the mean horizontal wind. All periods with flow from 60 through 150 deg were discarded due to possible flow distortion due to flow through the tower and support structures prior to reaching the instruments.

The site is characterized by sustained synoptic high pressure and weak mean flow in summer and fall. For the 3 month experiment, the average wind speed was 0.7, 1.4 and 1.9 ms^{-1} at the 1, 5 and 12-m levels on tower B, respectively. The weak mean flow, clear skies and sparse canopy lead to strong radiational cooling of the ground at night, resulting in strong stratitifcation and very weak turbulence near the surface.

Direct comparison between the mean wind speed measured by a CSAT3 and a Handar is afforded by the dual deployment at 5 m on the central tower. The 10-minute vector average wind speed from the CSAT3 (Handar) was 1.36 (1.34) ms^{-1} for the entire experiment, and the two wind speeds were correlated at $r = 0.98$.

3 Tilt correction

3.1 Background

A tilt correction is applied to 3-dimensional sonic anemometer measurements to remove; 1) apparent vertical motion due to tilt of the sensor from true

(gravitational) vertical, and 2) apparent vertical motion due to sloping topography. Both of these influences lead to an artifical wind direction dependence of the vertical velocity as measured by the anemometer. As noted by Paw U et al. (2000) and others, it is not possible to distinguish between these two effects from the vertical velocity measurements alone. A tilted sensor over flat terrain measures an apparent upward vertical motion for horizontal flow in one direction and apparent downward motion for flow in the opposite direction. The apparent vertical motion signature is identical for a perfectly levelled sensor over idealized sloping terrain with terrain following flow. Directionally dependent flow distortion effects are typically assumed to be accounted for by the internal software in the anemometer, although Högström and Smedman (2004) recently pointed out that the manufacturer's corrections, which are based on low turbulence level wind tunnel studies, may not be optimum for the higher turbulence conditions found in the field.

In earlier days of micrometeorological measurements, standard procedure was to rotate the three wind components into streamline coordinates for each 30-minute or 1-h time period individually (e.g., Kaimal and Finnigan, 1994). This approach defines the short-term mean vertical motion to be zero. The main motivation for this approach was that the mean vertical motion measurements could not be trusted due to contamination by sensor tilt and elevation slope, limited sample size and possibly flow distortion.

More recently, Lee (1998) and others identified the importance of non-zero $\overline{w}$ for calculating vertical advection of carbon dioxide. Even very small values of $\overline{w}$ can lead to significant advection in the presence of large vertical gradients, such as typically found near the surface for carbon dioxide on nights with weak mixing. Since the streamline coordinates approach exactly removes all short-term mean vertical motion, other methods were adopted

which allow non-zero short-term $\overline{w}$.

In the new standard approach, the long-term $\overline{w}_m(\phi)$ averaged over weeks to months is removed from the short-term averages of $\overline{w}_m$, where ϕ is wind direction and $\overline{w}_m$ is the measured time-averaged vertical velocity (Lee, 1998; Baldocchi et al., 2000; Paw U et al., 2000; Wilzcak et al., 2000; Finnigan et al., 2003). The procedure is similar in concept to applying a high-pass filter to the mean vertical motion seperately for each wind direction. The approach assumes that the long-term mean vertical motion for a given wind direction is zero. The short-term deviations in $\overline{w}$ that remain after removing the long-term $\overline{w}_m(\phi)$ are presumed to correspond to short-term events of either horizontal convergence or divergence. Long-term measurements are required to implement this approach in order to obtain robust estimates of the long-term $\overline{w}_m(\phi)$.

While the philosophy of removing the directionally dependent, long-term mean vertical motion is present in all current tilt correction methods, the details of applying it vary between studies. Lee (1998) proposed linear regression of $\overline{w}_m$ on the mean horizontal wind speed seperately for each wind direction category, which accounts for the fact that the apparent vertical motion due to sensor tilt is proportional to the horizontal wind speed. In the planar fit technique (Wilczak et al. ,2001), multiple linear regression of $\overline{w}_m$ on the two horizontal wind components results in a tilted plane. This method applies to the idealized case where the surface is uniformly tilted (planar) with respect to the sensor, or equivalently, where the sensor is tilted over perfectly flat terrain. A third approach examines the wind direction dependence of the tilt angle (Paw U et al., 2000; Vickers and Mahrt, 2003; Feigenwinter et al., 2004). The ϕ-dependence of the long-term average tilt angle can be represented either by the bin-averaged estimate or using a regression fit to

azimuthal angle. When the ϕ-dependence can be approximated by a simple sinusoidal function of azimuth angle, this method is identical conceptually to the planar fit technique (Paw U et al., 2000). In this sense, the planar fit approach is a special case of the tilt angle method. For non-idealized terrain, a planar fit may not be appropriate, and the bin-average ϕ-dependence can be used.

The regression used by Lee's approach and the planar fit method exactly remove the mean vertical motion averaged over the entire experiment, while the tilt angle method does not. Lee's approach removes the long-term $\overline{w}$ for each wind direction category individually, while the planar fit and tilt angle methods do not.

3.2 Problems

As pointed out by Lee (1998), a potential problem is that the tilt correction may remove real vertical motion associated with local circulations driven by surface heterogenity. Examples include a change in surface roughness, differential daytime heating and systematic diverging nocturnal drainage flows. The site here is influenced by a surface roughness change, however, it is not known if systematic circulations induced by daytime differential heating are important. It is also not known if the drainage flow is divergent (accelerating) or convergent (decelerating) at the site. For westerly flow, the site is approximately at the bottom of a slope in that the elevation increases faster to the west than it decreases to the east. A complication with identifying the drainage flow at this site is that the predominant flow is from the same direction as the drainage flow.

Given the rough-to-smooth surface roughness change for all wind direc-

tions, and the persistant synoptic high pressure pattern, we would expect overall mean sinking motion at the site. Such long-term mean vertical motion would be at least partially removed by any of the tilt correction methods described above.

We note that drainage flow is not a sufficient condition for horizontal divergence and mean sinking motion. Drainage flows need to converge somewhere. This is an important point because nearly every NEE study in the literature reports mean sinking motion at night and attributes it to drainage flows. If this were indeed the case, it indicates that the site selection criteria were biased in that all sites are in a similar nocturnal flow regime. Mean sinking motion coupled with decreasing carbon dioxide concentration with height results in a vertical advection term that is the correct sign to explain the missing carbon dioxide found at most sites. However, because other terms in the NEE budget, such as horizontal advection and horizontal flux divergence, are typically not known, it is impossible to make definitive conclusions. The typical reported finding of rising motion during the day and sinking motion at night could be an artifact of the tilt correction method.

3.3 Methodologies

We apply three different tilt correction methods to the data. The same procedures are applied independently to the 5 and 12-m measurements although we focus on the 12-m estimates of $\overline{w}$. All time mean quantities in this section, denoted with an overbar, represent 100-s time averages. The choice of 100-s averaging includes wind direction variability on scales down to 100 s. Longer averaging times would miss additional meandering of the mean wind which could contaminate the wind direction dependence of $\overline{w}$. It is difficult

to say, because many studies do not include the details, but it appears that studies in the NEE literature often employ a 30-minute averaging time to define the mean wind direction for the purpose of developing the tilt correction. Berger et al. (2001) use the 1-h average wind direction. Wilczak et al. (2001) propose using 5-minute average wind components to derive the regression coefficients in the planar fit approach. We note that the tilt correction parameters could be developed using the high rate (e.g. 10 hz) data, although at some point it becomes impractical for the planar fit method where a matrix must be inverted to perform the multiple regression.

The Lee (1998) approach uses regression of the vertical velocity on the horizontal wind speed for each wind direction category, generating a sequence of wind direction dependent coefficients $\alpha(\phi)$ and $\beta(\phi)$. The corrected mean vertical velocity ($\overline{w}$) is then given by

$$\overline{w} = \overline{w}_m - (\alpha(\phi) + \beta(\phi)\ U) \tag{2}$$

where we use 36 wind direction categories of width 10 deg each and the mean horizontal wind speed is given by

$$U = (\overline{u}^2 + \overline{v}^2)^{1/2}. \tag{3}$$

The planar fit approach uses multiple regression of the vertical velocity on the two components of the horizontal wind, and the corrected vertical motion is given by

$$\overline{w} = \overline{w}_m - (a + b\ \overline{u} + c\ \overline{v}) \tag{4}$$

where the coeffcients a, b and c are calculated using all the data. The tilt angle approach calculates a tilt angle as

$$T_a = \arctan(\frac{\overline{w}_{mn}}{U}) \tag{5}$$

where $\overline{w}_{mn}$ is the measured vertical velocity that has the experiment wide mean (potential instrument offset) removed. The procedure temporarily removes periods with the weakest mean flow ($U < 0.5\ ms^{-1}$), where calculation of the tilt angle is not well posed and the tilt angle becomes erratic (e.g., Paw U et al., 2000). The corrected mean vertical velocity is then estimated for all the data, including the weakest wind periods, as

$$\overline{w} = \overline{w}_{mn} - U\ \tan(T_a(\phi)). \tag{6}$$

where $T_a(\phi)$ is the bin-averaged wind direction dependent tilt angle using 36 wind direction categories of width 10 deg.

3.4 Results

The three different tilt correction methods yield different $\overline{w}$ estimates (Figure 2). Although the correlations between 30-minute average $\overline{w}$ estimates are high, the root-mean-square differences of a few $cm\ s^{-1}$ are significant, and the maximum differences are as large as 10 $cm\ s^{-1}$. These large differences are discouraging for prospects of estimating mean vertical motion using a tilt correction method.

The magnitude of the tilt angles found here (Figure 3) are comparable to or smaller than what we have typically found for other sites on relatively flat terrain with carefully levelled sensors. A sinusoidal dependence is a reasonable approximation to $T_a(\phi)$, implying that the planar fit method could be appropriate for this site. Differences between the bin-averaged $T_a(\phi)$ values and a pure sinusodial dependence, as implied by the planar fit method,

may be due to an insufficient number of samples (random sampling error) for the less frequent wind directions. On the other hand, some sites may be characterized by directionally dependent slopes that can not be reasonably represented by a planar fit, in which case the bin-averages of $T_a(\phi)$ may be the better representation. In addition, higher order flow distortion effects may contribute to more complex azimuthal dependencies of the tilt angle, such as a double peak. For example, Högström and Smedman (2004) highlight the calibration problems and flow distortion characteristics of Gill Solent sonic anemometers. Such problems may be less severe for the unobstructed design of the CSAT3.

One cause of significant differences between the Lee and the tilt angle methods is demonstrated in Figure 4. For Lee's method, the regression of $\overline{w}_m$ on horizontal wind speed gives negative slope (negative β) despite the fact that for 75% of the data, where the wind speed is less than 2 ms^{-1}, the measured average vertical velocity is positive and increases with increasing wind speed. The tilt angle method indicates very weak long-term mean positive vertical motion ($T_a(\phi) = 0.06$ deg). For this wind direction category, the two diffferent approaches for correcting the vertical velocity generally have the opposite sign. Because Lee's regression method includes a constant term α, the correction $(\overline{w} - \overline{w}_m)$ can be of either sign depending on wind speed, while the tilt angle method correction, which is near zero for this case, is always the same sign for a given wind direction.

Lee's method appears to fail for this example due to the combination of a nonlinear dependence of $\overline{w}_m$ on wind speed and a strongly skewed wind speed distribution due to the high frequency of occurence of weak winds. The magnitude of the slope β in Lee's method decreases with increasing averaging time by removal of some of the stronger wind speed cases. Recall that the

vector average wind speed decreases with increasing averaging time due to wind direction variability. The tilt angle approach is more robust for this example in that the mean tilt angle is less sensitive to the choice of averaging time than are the coefficients from the regression approach.

4 Divergence

The horizontal coordinate system was rotated for each 100-s period such that horizontal $\overline{u}$ gradients are proportional to $\overline{u}$ at tower A minus $\overline{u}$ at tower C, and v gradients by tower E minus tower D. Horizontal gradients were evaluated over a fixed distance of approximately 200 m (Figure 1). No significant wind speed bias problems were found by an intercomparison study of the Handar anemometers. The horizontal gradients of $\overline{u}$ and $\overline{v}$ were calculated at the 3 measurement levels (1, 5 and 12 m) using finite differencing. Vertical integration of the horizontal gradients from the surface to 12 m was performed using a piecewise linear fit to the four levels, where the gradients are zero at $z = 0$.

For the shorter towers D and E, where the measurements are limited to 1 and 5 m, we assume the horizontal gradient of the mean wind is constant with height between 5 and 12 m. The measured gradients on the taller towers support this assumption. The fact that the horizontal gradient of the mean wind does not significantly increase above 5 m suggests that the primary mechanism generating divergence at this site is the surface roughness change.

One issue with the divergence method of estimating $\overline{w}$ is the length scale over which the horizontal gradients are calculated. Ideally, the gradients would be calculated over a short distance in the immediate vicinity of the

vertical velocity measurements, however, the limited resolution of the horizontal wind speed measurements requires a sufficient seperation distance such that wind speed differences can be resolved. In some special circumstances, such as with propogating divergence, the combination of seperation distance and averaging time could strongly influence the calculated divergence. However, if the divergence is primarily stationary and the horizontal wind components vary approximately linearily with distance, then the seperation distance and averaging time become less important. We did not find a strong averaging time dependence in the vertically integrated divergence.

The divergence calculations indicate that this is a site of mean sinking motion for all wind directions and all times of day and night. We would expect to see weaker divergence due to the surface roughness change for those wind directions with longer fetch over the clearing prior to reaching the tower network. Theoretically, the divergence is a maximum at the upwind edge of the clearing and decreases with increasing distance (e.g., Garratt, 1990). The observations do indeed show that the minimum divergence occurs with northwest flow, where the tower network is located in the south-east corner of the clearing.

5 Comparisons

In this section we compare the $\overline{w}$ estimates calculated from $\overline{w}_m$ and the different tilt correction methods (the direct methods) with the $\overline{w}$ estimate based on the horizontal divergence. There is large scatter for individual 30-minute average estimates and small correlation (Figure 5). A 30-minute mean vertical motion of 10 $cm\ s^{-1}$, which implies an increase in the mean wind speed across the network of about 1.7 ms^{-1}, is probably too large to

be realistic and is not supported by the divergence measurements. Such magnitude vertical motions are found for all the direct methods, but not for the divergence method. This might indicate that the divergence approach is more robust. More spatial information is incorporated into the divergence calculation. If a 10 $cm\ s^{-1}$ $\overline{w}$ was due to an error in specification of the tilt angle, the error in the ϕ-dependence of T_a would need to be about 3 deg for a mean wind speed of 2 ms^{-1}. It appears unlikely than an error of this magnitude occurs.

The correlation between $\overline{w}$ from the tilt angle and planar fit methods and $\overline{w}$ from the divergence method increases with increasing averaging time, however, this is not the case for Lee's method (Figure 6). The RMS $\overline{w}$ differences for all the direct methods decrease with increasing averaging time. This implies that a portion of the scatter is random. The standard deviation of the direct method $\overline{w}$ estimates is typically a factor of 2 greater than the standard deviation of $\overline{w}$ based on the divergence.

All of the direct methods result in large scatter and large short-term fluctuations in $\overline{w}$ compared to the divergence method. Despite the apparent noise in the direct estimates, short-term fluctuations in $\overline{w}$ from the direct and divergence methods can be highly correlated (Figure 7). In this example, both the direct and divergence estimates clearly show enhanced sinking motion associated with stronger wind speeds, and enhanced rising motion with weaker winds. The direct method $\overline{w}$ fluctuations are too large to be due to errors in the tilt correction, despite being strongly wind speed dependent. The stronger amplitude response of the direct method $\overline{w}$ compared to the divergence estimate for this example remains unexplained.

The agreement between the direct and divergence methods is worse when the magnitude of $\overline{w}$ from the direct methods does not increase monotonically

with height between the surface and 12 m (not shown). Such periods may represent complex flow situations that are impossible to resolve without a much finer grid of measurements. This situation occurred about one-half the time independent of the tilt correction method. Removing such periods improved the correlation between the 30-minute mean $\overline{w}$ estimates from the tilt angle and divergence methods from 0.39 to 0.47. These periods also include cases where $\overline{w}$ at both the 5 and 12-m levels is very small, in which case small random errors possibly due to flow distortion probably dominate the estimates.

For very shallow nocturnal boundary layers, the vertical velocity measurement at 12 m may be partially decoupled from the horizontal flow field beneath it. To test this, we compared the estimates of vertical motion at 5 m instead of 12 m above the surface. No significant improvement in the relationships was found at 5 m compared to 12 m (not shown). Interpretation is complicated by the fact that theoretically the relationship would be expected to degrade at 5 m compared to 12 m because the magnitude of $\overline{w}$ normally decreases with height (smaller signal to noise ratio) and any problems associated with surface heterogenity increase near the surface.

As a further sensitivity study, the direct method $\overline{w}$ estimates were recalculated at 12 m using the same procedures described above but only using nocturnal data. Despite this attempt to "tune" the tilt correction for nocturnal conditions, the relationship between the direct vertical motion estimates and the divergence based estimates did not significantly improve (not shown).

5.1 Composites

In the three month composite diurnal cycle, the $\overline{w}$ estimates from the planar fit and tilt angle methods have some similarities to each other, and some similarity to the divergence based estimate of $\overline{w}$ (Figure 8). The similar composite diurnal behaviour is encouraging, although agreement on individual short time scales (30-minutes to 1-h) is the critical test for the ultimate goal of estimating vertical advection for process orientated studies. Contrary to the other methods tested, the Lee approach leads to significant mean rising motion in the afternoon.

The direct and divergence methods disagree on the sign of the composite $\overline{w}$ during most of the night. Direct methods generally show rising motion of about 1 $cm\ s^{-1}$ in contrast to weak sinking motion of 0.5 $cm\ s^{-1}$ based on the divergence (Figure 8). The nocturnal sign difference could be due to the removal of the long-term mean $\overline{w}$ by the tilt correction methods. As discussed above (section 3), the tilt correction methods fail at sites with non-zero long-term mean vertical motion. Assuming that the divergence estimate is correct, and that long-term mean sinking motion due to the surface roughnesss change is realistic for this site, then the vertical advection of carbon dioxide that would be calculated using the direct method nocturnal $\overline{w}$ would be of the wrong sign for most of the night regardless of the choice of tilt correction method.

The wind direction, wind speed and time of day dependencies of the composite $\overline{w}$ residuals for the tilt angle method and the uncorrected $\overline{w}_m$ estimates are shown in Figure 9. The residual is defined as $\overline{w}$ for the direct method minus $\overline{w}$ from the divergence. The uncorrected estimate has the experiment wide mean (offset) of 0.9 $cm\ s^{-1}$ removed, and not removing the offset would

make the uncorrected residuals in Figure 9 even larger positive. For the most common conditions of a 255 deg wind at 1.9 ms^{-1}, the composite residual is near zero for the tilt angle method. Assuming that the estimate based on the divergence is close to the true mean vertical motion, and comparing with the uncorrected estimate of vertical motion, it appears that the tilt angle method used here over-corrects in stronger winds and under-corrects in weaker winds. This is also seen in the diurnal pattern of the residual which is negative during the day, when the mean wind speed is significantly higher than at night.

The positive residual for south-southwest flow (Figure 9) may be due in part to an exponential rather than linear fetch dependence of the divergence. An exponential dependence would be most pronounced near the upwind edge of the clearing, which is where the network is located for south-southwest flow. If the divergence decreased exponentially with fetch, the mean $\overline{w}$ corresponding to the divergence would be found in the upwind part of the network, not in the center of the network. As such, our direct measurement at the central tower site may underestimate the mean sinking motion. A larger negative $\overline{w}$ from the divergence than from the direct method leads to a positive residual in Figure 9.

6 Conclusions

A three month field experiment was performed to contrast the mean vertical motion measured at a point on a central tower with the mean vertical motion calculated from the horizontal divergence measured using a network of towers surrounding the central tower. Three different tilt correction methods were applied. The RMS difference in the 30-minute average $\overline{w}$ estimates due to the

choice of tilt correction method was 2 to 3 $cm\ s^{-1}$. The 3-month composite diurnal pattern of $\overline{w}$ was sensitive to the choice of tilt correction method.

The hour to hour variations in $\overline{w}$ from the direct methods are probably too large to be representative of a large spatial area. In such cases, the direct $\overline{w}$ estimates could be responding to divergence on horizontal scales smaller or larger than the divergence network. The RMS differences between the 30-minute average direct estimates of $\overline{w}$ and the estimates based on the divergence are 4 to 5 $cm\ s^{-1}$, and as a result, little confidence can be placed in the hour-to-hour variations in the $\overline{w}$ estimates, or in subsequent estimates of vertical advection. Of the three direct methods tested at this site, the tilt angle method best matched the divergence.

The direct methods and the divergence method agree on some features of the composite diurnal cycle of $\overline{w}$, however, the divergence indicates long-term mean sinking motion for all times of day and night, apparently due to the surface roughness change. Because the direct methods all remove the long-term mean, they fail to reproduce this result. As a consequence, the direct methods give the wrong sign of $\overline{w}$ at night, and thus would give the wrong sign of the nocturnal vertical advection of carbon dioxide.

Our conclusion is that more confidence can be attached to vertical advection estimates when the mean vertical motion is calculated from the horizontal divergence. A densor network of vertical velocity and divergence measurements would enable more definitive conclusions. Unfortuneatly, the measurements required to calculate the divergence are more costly and not normally available.

Acknowledgements

This research was supported by the NASA Terrestrial Ecology Program

under Grant NAG5-11231 and by the U.S. Department of Energy Terrestrial Carbon Program (DOE grant FG0203ER63653), for the project on the effects of disturbance and climate on carbon dioxide and energy exchange of ponderosa pine forests. The site is part of the AmeriFlux network.

References

Aubinet,M., Heinesch,B., and Yernaux,M., 2003. Horizontal and vertical CO2 advection in a sloping forest. *Boundary-Layer Meteor.* **108**, 397-417.

Baldocchi,D., Finnigan,J., Wilson,K., Paw U,K.T., and Falge,E., 2000. On measuring net ecosystem carbon exchange over tall vegetation on complex terrain. *Boundary-Layer Meteor.* **96**, 257-291.

Berger,B.W., Davis,K.J., Yi,C., Bakwin,P.S., and Zhao,C.L., 2001. Long-term carbon dioxide fluxes from a very tall tower in a northern forest: Flux measurement methodology. *J. Atmos. Oceanic Technol.* **18**, 529-542.

Feigenwinter,C., Bernhofer,C., and Vogt,R., 2004. The influence of advection on the short term CO2 budget in and above a forest canopy. *Boundary-Layer Meteor.* **113**, 201-224.

Finnigan,J., Clement,P., Malhi,Y., Leuning, R., and Cleugh, H.A., 2003. A re-evaluation of long-term flux measurement techniques, Part I: Averaging and coordinate rotation. *Boundary-Layer Meteor.*, **107**, 1-48.

Garratt,J.R., 1990. The internal boundary layer - a review. *Boundary-Layer Meteor.*, **50**, 171-203.

Högström,U., and Smedman,A.-S., 2004. Accuracy of sonic anemometers: Laminar wind-tunnel calibrations compared to atmospheric in situ calibrations against a reference instrument. *Boundary-Layer Meteor.*, **111**, 33-54.

Kaimal,J.C., Finnigan,J.J., 1994. Atmospheric Boundary Layer Flows. Oxford University Press, New York.

Lee, X., 1998. On micrometeorological observations of surface-air exchange over tall vegetation. *Agric. Forest Meteor.* **91**, 39 -49 .

Pattey,E., Strachan,I.B., Desjardins,R.L., and Massheder,J., 2002. Measuring nighttime carbon dioxde flux over terrestrial ecosystems using eddy covariance and nocturnal boundary layer methods. *Agric. Forest Meteor.* **113**, 145-158.

Paw U,K.T., Baldocchi,D., Meyers,T.P., and Wilson,K.B., 2000. Correction of eddy-covariance measurements incorporating both advective effects and density fluxes. *Boundary-Layer Meteor.* **97**, 487-511.

Staebler,R.M., and Fitzjarrald,D.R., 2004. Observing subcanopy CO2 advection. *Agric. Forest Meteor.* **122**, 139-156.

Vickers,D., and Mahrt,L., 2003. The cospectral gap and turbulent flux calculations. *J. Atmos. Oceanic Technol.* **20**, 660-672.

Wilczak,J.M., Oncley,S.P., and Stage,S.A., 2001. Sonic anemometer tilt correction algorithms. *Boundary-Layer Meteor.* **99**, 127-150.

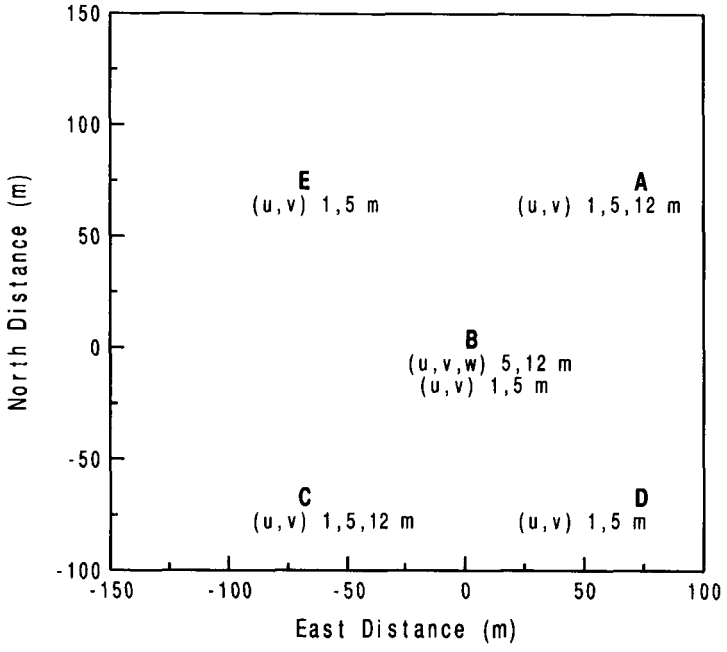

Figure 1: Schematic of young pine site with locations of five towers (A-E) and variables measured at different heights. The site is surrounded on all sides by taller pine trees.

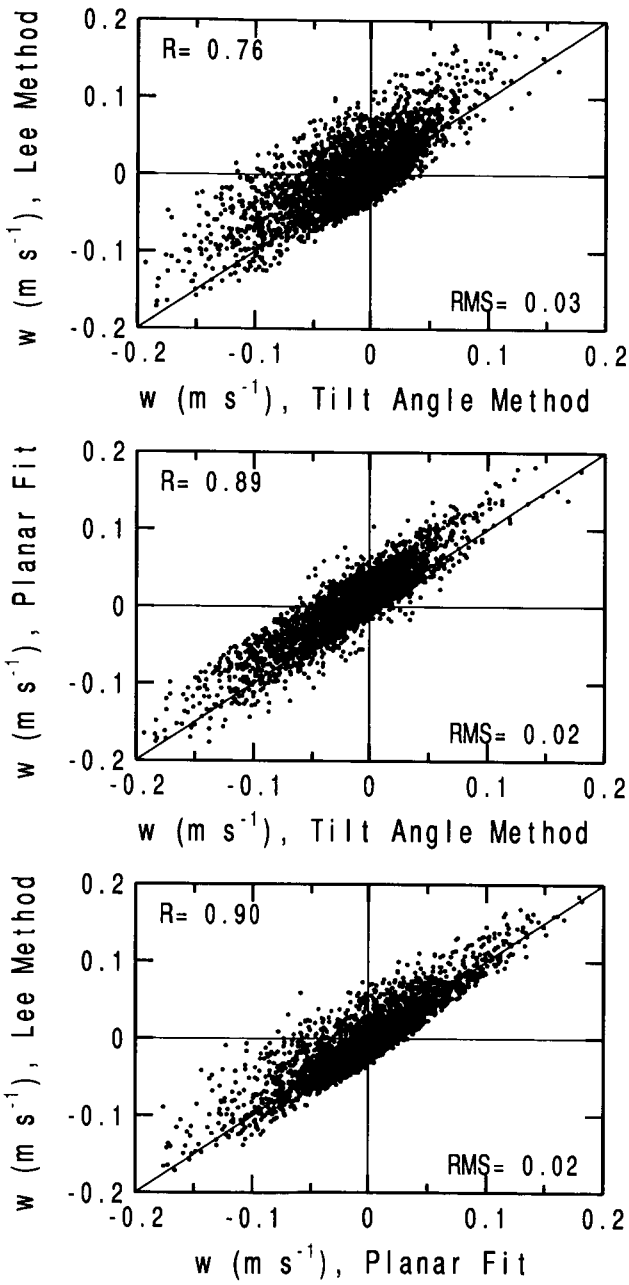

Figure 2: Comparison of 30-minute mean vertical motion at 12 m for three different tilt correction methods.

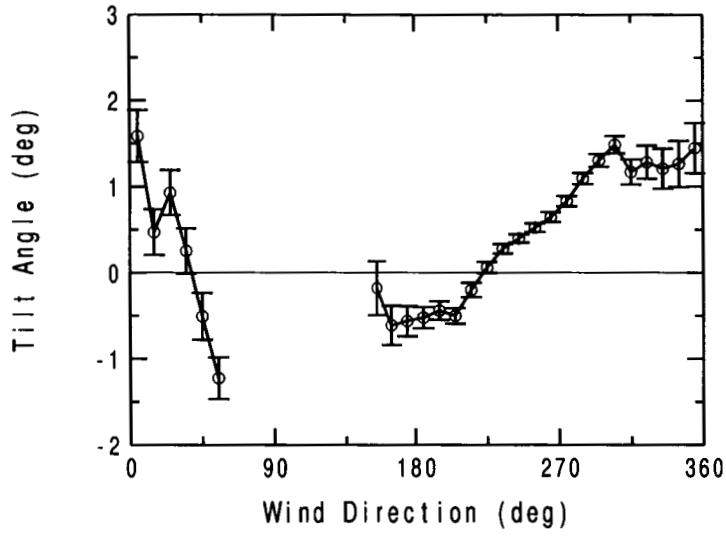

Figure 3: Mean and standard error of the tilt angle vs wind direction (100-s average data at 12 m).

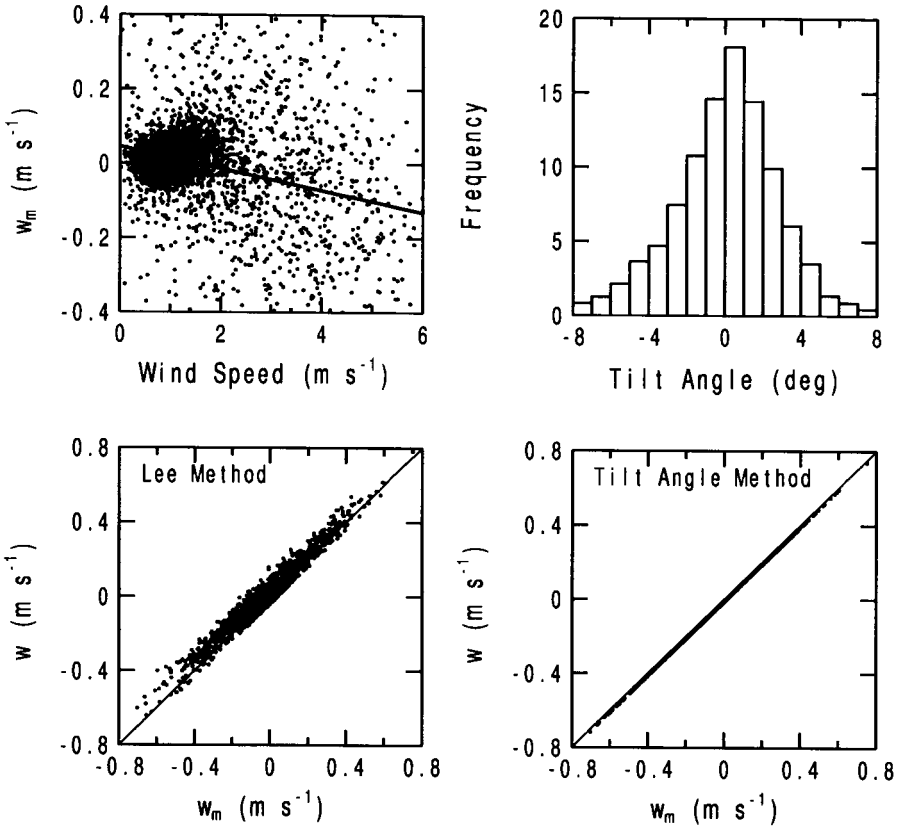

Figure 4: Comparison of the Lee and tilt angle methods for wind direction category $220 < \phi < 230$ deg. (100-s average data at 12 m).

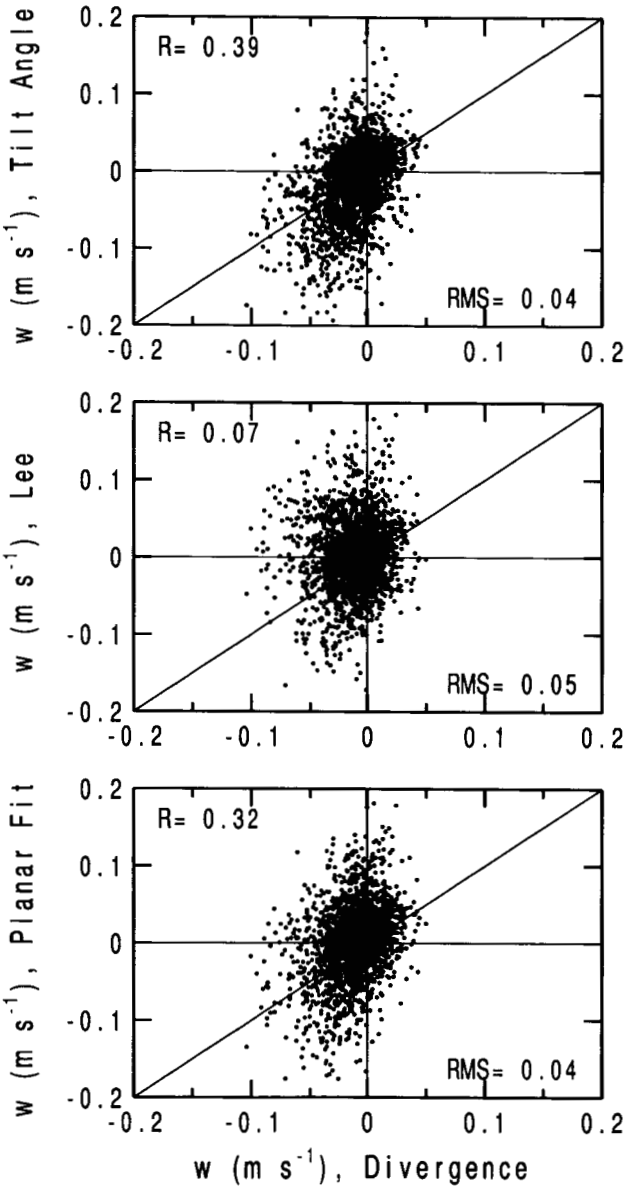

Figure 5: 30-minute mean vertical motion at 12 m for the a) tilt angle, b) Lee, and c) planar fit methods vs the estimate based on the horizontal divergence.

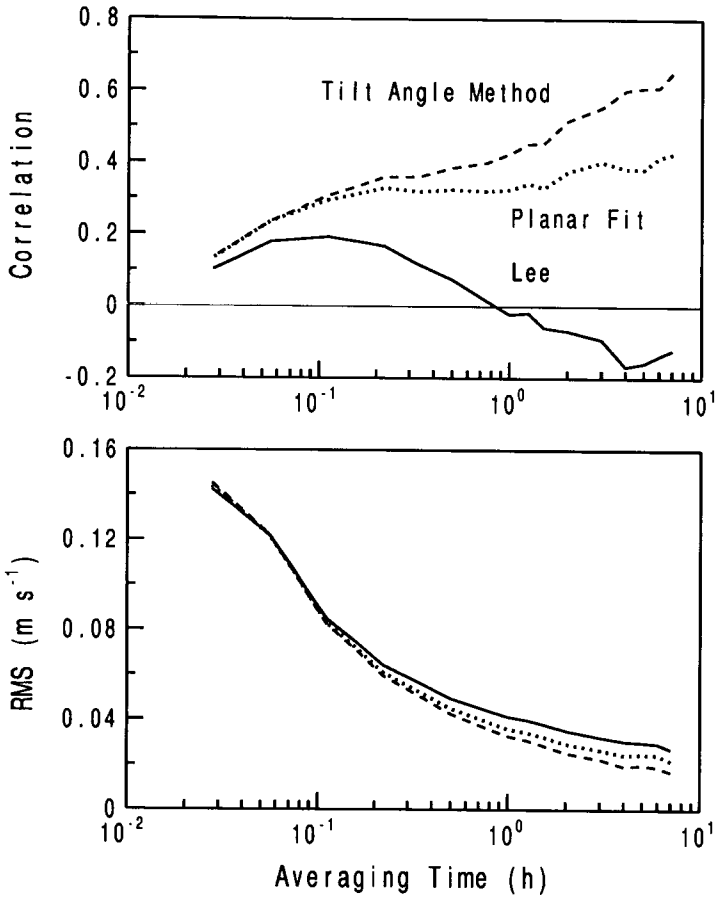

Figure 6: Averaging time dependence of the correlation and root mean square error for contrasting the three direct methods with the divergence method of estimating $\overline{w}$.

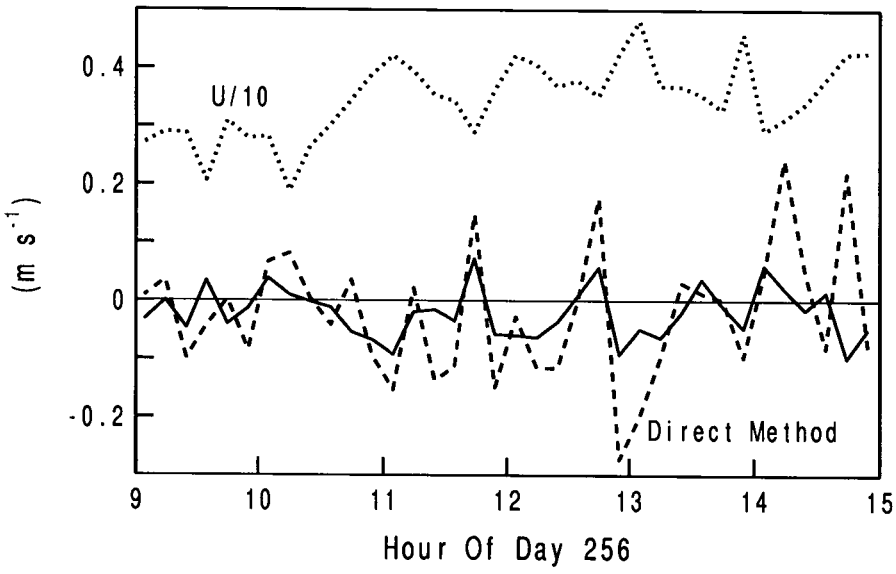

Figure 7: Time series of 10-minute average mean wind speed divided by 10 (dotted), $\overline{w}$ from direct tilt angle method (dashed), and $\overline{w}$ from divergence method (solid).

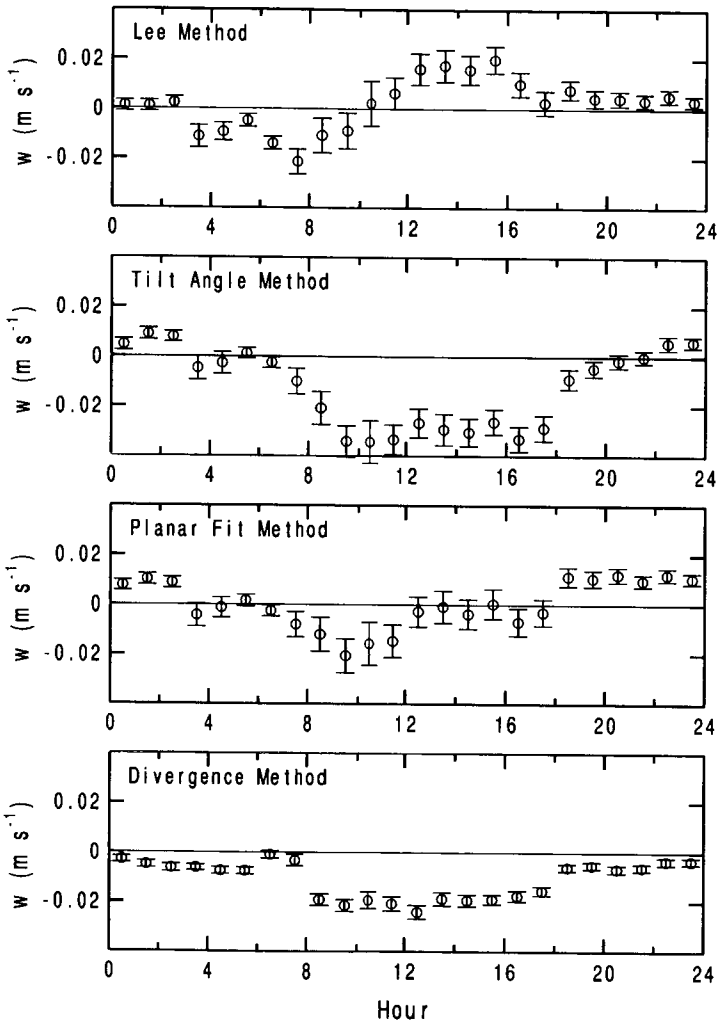

Figure 8: Mean and standard error of the three month composite diurnal cycle of mean vertical motion from four different methods.

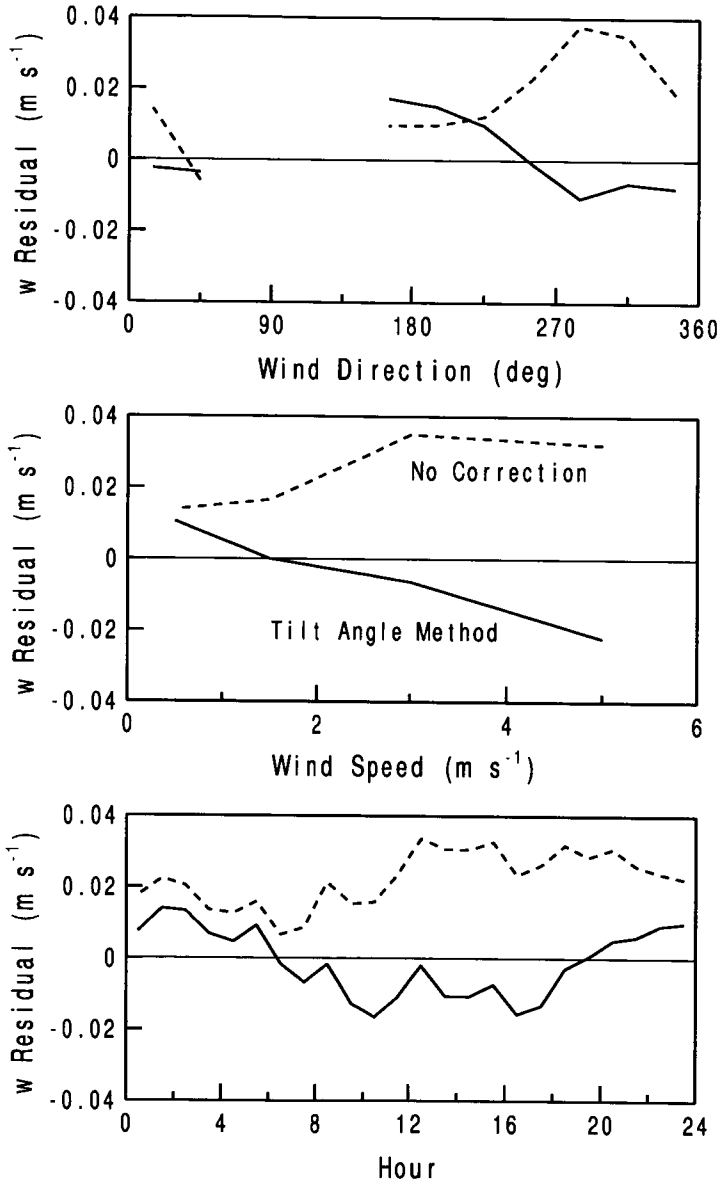

Figure 9: Dependence of the composite $\overline{w}$ residual for the tilt angle method (solid), and for the uncorrected $\overline{w}_m$ (dash), on wind direction, wind speed and time of day.

REPORT DOCUMENTATION PAGE

Form Approved
OMB No. 0704-0188

1. AGENCY USE ONLY (Leave blank)	2. REPORT DATE	3. REPORT TYPE AND DATES COVERED
	9-21-05	Final 8-15-01 to 8-14-05

4. TITLE AND SUBTITLE
Regional Carbon Dioxide Fluxes over Heterogeneous Terrain

5. FUNDING NUMBERS
NAG-11231

6. AUTHOR(S)
Larry J. Mahrt

7. PERFORMING ORGANIZATION NAME(S) AND ADDRESS(ES)
Oregon State University
Corvallis, OR 97331

8. PERFORMING ORGANIZATION REPORT NUMBER
NS1260

9. SPONSORING/MONITORING AGENCY NAME(S) AND ADDRESS(ES)
ONR

10. SPONSORING/MONITORING AGENCY REPORT NUMBER

11. SUPPLEMENTARY NOTES

12a. DISTRIBUTION/AVAILABILITY STATEMENT
Unlimited Public Access

12b. DISTRIBUTION CODE

13. ABSTRACT *(Maximum 200 words)*

In spite of setbacks due to forest fires, eviction after a change of landowners and unanticipated need to upgrade and replace much of the instrumentation, substantial progress has been made during the past three years, resulting in major new findings. Although most of the results are in manuscript form, three papers have been published and a fourth was recently submitted.

The data has been subjected to extensive quality control. Extra attention has been devoted to the influence of tilt rotation and flux-calculation method, particularly with respect to nocturnal fluxes.

A relatively complete canopy model (SPA) used in a data assimilation mode can successfully predict the CO2 budget and NEE by iteratively adjusting the data and model parameters (Chapter 1). To reduce uncertainty in data assimilation methods, long-term flux data are needed (both CO2 and water vapor exchange). The version of the data assimilation method that includes fluxes and state variables is suitable for application in a coupled vegetation-atmosphere regional model.

14. SUBJECT TERMS			15. NUMBER OF PAGES
			16. PRICE CODE
17. SECURITY CLASSIFICATION OF REPORT	18. SECURITY CLASSIFICATION OF THIS PAGE	19. SECURITY CLASSIFICATION OF ABSTRACT	20. LIMITATION OF ABSTRACT